JOINT SOURCE-CHANNEL-NETWORK CODING IN WIRELESS MESH NETWORKS WITH TEMPORAL REUSE

by

Francois Pierre Sarel Luus

Submitted in partial fulfilment of the requirements for the degree

Master of Engineering (Electronic Engineering)

in the

Faculty of Engineering, Built Environment and Information Technology

Department of Electrical, Electronic and Computer Engineering

UNIVERSITY OF PRETORIA

May 2011

SUMMARY

JOINT SOURCE-CHANNEL-NETWORK CODING IN WIRELESS MESH NETWORKS WITH TEMPORAL REUSE

by

Francois Pierre Sarel Luus

Promoter:	Dr. B.T.J. Maharaj
Department:	Electrical, Electronic and Computer Engineering
University:	University of Pretoria
Degree:	Master of Engineering (Electronic Engineering)

Keywords:	Temporal reuse, packet depletion, network coding, joint coding, fountain code

Technological innovation that empowers tiny low-cost transceivers to operate with a high degree of utilisation efficiency in multihop wireless mesh networks is contributed in this dissertation. Transmission scheduling and joint source-channel-network coding are two of the main aspects that are addressed. This work focuses on integrating recent enhancements such as wireless network coding and temporal reuse into a cross-layer optimisation framework, and to design a joint coding scheme that allows for space-optimal transceiver implementations. Link-assigned transmission schedules with timeslot reuse by multiple links in both the space and time domains are investigated for quasi-stationary multihop wireless mesh networks with both rate and power adaptivity. Specifically, predefined cross-layer optimised schedules with proportionally fair end-to-end flow rates and network coding capability are constructed for networks operating under the physical interference model with single-path minimum hop routing. Extending transmission rights in a link-assigned schedule allows for network coding and temporal reuse, which increases timeslot usage efficiency when a scheduled link experiences packet depletion. The schedules that suffer from packet depletion are characterised and a generic temporal reuse-aware achievable rate region is derived. Extensive computational experiments show

improved schedule capacity, quality of service, power efficiency and benefit from opportunistic bidirectional network coding accrued with schedules optimised in the proposed temporal reuse-aware convex capacity region. The application of joint source-channel coding, based on fountain codes, in the broadcast timeslot of wireless two-way network coding is also investigated. A computationally efficient subroutine is contributed to the implementation of the fountain compressor, and an error analysis is done. Motivated to develop a true joint source-channel-network code that compresses, adds robustness against channel noise and network codes two packets on a single bipartite graph and iteratively decodes the intended packet on the same Tanner graph, an adaptation of the fountain compressor is presented. The proposed code is shown to outperform a separated joint source-channel and network code in high source entropy and high channel noise regions, in anticipated support of dense networks that employ intelligent signalling.

OPSOMMING

GESAMENTLIKE BRON-KANAAL-NETWERK KODERING IN DRAADLOSE ROOSTER NETWERKE MET TEMPORÊRE HERWINNING

deur

Francois Pierre Sarel Luus

Promotor:	Dr. B.T.J. Maharaj
Departement:	Elektriese, Elektroniese en Rekenaaringenieurswese
Universiteit:	Universiteit van Pretoria
Graad:	Magister in Ingenieurswese (Elektroniese Ingenieurswese)
Sleutelwoorde:	Temporêre herwinning, pakkie-uitputting, netwerk kodering, gesamentlike kodering, fontein kode

Tegnologiese innovasie wat klein lae-koste kommunikasie toestelle bemagtig om met ’n hoë mate van benuttings doeltreffendheid te werk word bygedra in hierdie proefskrif. Transmissie-skedulering en gesamentlike bron-kanaal-netwerk kodering is twee van die belangrike aspekte wat aangespreek word. Hierdie werk fokus op die integrasie van onlangse verbeteringe soos draadlose netwerk kodering en temporêre herwinning in ’n tussen-laag optimaliserings raamwerk, en om ’n gesamentlike kodering skema te ontwerp wat voorsiening maak vir spasie-optimale toestel implementerings. Skakel-toegekende transmissie skedules met tydgleuf herwinning deur veelvuldige skakels in beide die ruimte en tyd domeine word ondersoek vir kwasi-stilstaande, veelvuldige-sprong draadlose rooster netwerke met beide transmissie-spoed en krag aanpassings. Om spesifiek te wees, word vooraf bepaalde tussen-laag geoptimiseerde skedules met verhoudings-regverdige punt-tot-punt vloei tempo’s en netwerk kodering vermoë saamgestel vir netwerke wat bedryf word onder die fisiese inmengings-model met enkel-pad minimale sprong roetering. Die uitbreiding van transmissie-regte in ’n skakel-toegekende skedule maak voorsiening vir netwerk kodering en temporêre herwinning, wat tydgleuf gebruiks-doeltreffendheid verhoog wanneer ’n

geskeduleerde skakel pakkie-uitputting ervaar. Die skedules wat ly aan pakkie-uitputting word gekenmerk en ’n generiese temporêre herwinnings-bewuste haalbare transmissie-spoed gebied word afgelei. Omvattende berekenings-eksperimente toon verbeterde skedulerings kapasiteit, diensgehalte, krag doeltreffendheid asook verbeterde voordeel wat getrek word uit opportunistiese tweerigting netwerk kodering met die skedules wat geoptimiseer word in die temporêre herwinnings-bewuste konvekse transmissie-spoed gebied. Die toepassing van gesamentlike bron-kanaal kodering, gebaseer op fontein kodes, in die uitsaai-tydgleuf van draadlose tweerigting netwerk kodering word ook ondersoek. ’n Berekenings-effektiewe subroetine word bygedra in die implementering van die fontein kompressor, en ’n foutanalise word gedoen. Gemotiveer om ’n ware gesamentlike bron-kanaal-netwerk kode te ontwikkel, wat robuustheid byvoeg teen kanaal geraas en twee pakkies netwerk kodeer op ’n enkele bipartiete grafiek en die beoogde pakkie iteratief dekodeer op dieselfde Tanner grafiek, word ’n aanpassing van die fontein kompressor aangebied. Dit word getoon dat die voorgestelde kode ’n geskeide gesamentlike bron-kanaal en netwerk kode in hoë bron-entropie en hoë kanaal-geraas gebiede oortref in verwagte ondersteuning van digte netwerke wat van intelligente sein-metodes gebruik maak.

I dedicate this work to my grandmother, who taught me the true meaning of selflessness.

ACKNOWLEDGEMENTS

I would like to thank the following people and institutions.

- My Creator, for every breath.
- My parents and brothers, for their continuous support and encouragement.
- My study leader Dr. B.T.J. Maharaj, for his sage advice and support throughout the course of my studies.
- My fellow students at the Sentech Chair in Broadband Wireless Communication (BWMC) at the University of Pretoria.
- Mr. Hans Grobler, for his diligent administration of the Advance Computing Cluster at the University of Pretoria.
- Credit goes to the University of Pretoria (UP) and the Sentech Chair in Broadband Wireless Communication (BWMC) for the financial sponsorship of my Masters degree.

CONTENTS

CHAPTER 1 INTRODUCTION 1
1.1 BACKGROUND 3
1.1.1 Wireless mesh networking and network coding 3
1.1.2 Predetermined transmission scheduling 4
1.1.3 Link-assignment and temporal reuse 5
1.1.4 High-noise region channel coding 5
1.1.5 High-entropy source coding 7
1.1.6 True joint source-channel-network coding 8
1.2 MOTIVATION AND OBJECTIVE OF DISSERTATION 8
1.3 AUTHOR'S CONTRIBUTION 10
1.3.1 Temporal reuse 10
1.3.2 Temporal reuse-aware rate region 11
1.3.3 Cross-layer optimised scheduling 11
1.3.4 Joint source-channel-network coding 11
1.4 PUBLICATIONS 12
1.4.1 Conference proceedings 12
1.4.2 Journal publications 12
1.4.3 Other publications 13
1.5 OUTLINE OF DISSERTATION 13

CHAPTER 2 WIRELESS MESH NETWORKING 15
2.1 NETWORK TOPOLOGY 16
2.1.1 Node positioning 17
2.1.2 Link formation 17
2.2 ROUTING 19
2.2.1 Shortest path routing 19

2.2.2 Dijkstra's algorithm . . . 19
2.3 TRAFFIC MODEL . . . 20

CHAPTER 3 NETWORK CODING . . . 23
3.1 WIRED NETWORK CODING . . . 24
3.1.1 The butterfly example . . . 24
3.1.2 Max-flow min-cut theorem . . . 26
3.1.3 Linear network coding . . . 27
3.2 WIRELESS NETWORK CODING . . . 28
3.2.1 COPE . . . 29
3.2.2 Opportunistic coding . . . 30
3.2.3 Opportunistic listening . . . 30
3.2.4 Reception reporting . . . 31
3.2.5 Learning neighbour state . . . 31
3.2.6 Coding gain . . . 32
3.2.7 Coding+MAC gain . . . 33
3.2.8 Opportunistic bidirectional wireless network coding . . . 35
3.3 THE RELATIONSHIP OF NC TO THE OSI NETWORK MODEL . . . 36
3.3.1 Application layer network coding . . . 38
3.3.2 Network layer . . . 39
3.3.3 Data link layer . . . 39
3.3.4 Physical layer network coding . . . 39

CHAPTER 4 SCHEDULE ASSIGNMENT . . . 41
4.1 MEDIUM ACCESS CONTROL . . . 42
4.1.1 Dynamic medium access control difficulties . . . 43
4.1.2 Time division multiple access . . . 45
4.1.3 Space-time division multiple access . . . 46
4.1.4 Scheduling and the OSI model . . . 46
4.2 SCHEDULE ASSIGNMENT METHODS . . . 47
4.2.1 Link assignment . . . 48
4.2.2 Node assignment . . . 50
4.2.3 Initial scheduling . . . 53
4.3 TEMPORAL REUSE . . . 55

4.3.1 Motivation . . . 56
4.3.2 Schedule utilisation efficiency . . . 57
4.3.3 Link-assigned TDMA with temporal reuse . . . 59
4.3.4 Link-assigned STDMA with temporal reuse . . . 59

CHAPTER 5 SCHEDULE CAPACITY . . . 61
5.1 LINK-ASSIGNED STDMA CAPACITY . . . 62
5.2 CAPACITY WITH TEMPORAL REUSE . . . 63
5.2.1 Temporal reuse-aware rate region . . . 63
5.2.2 Rate region estimation . . . 64
5.2.3 Ordering policy . . . 66

CHAPTER 6 SCHEDULE OPTIMISATION . . . 68
6.1 LINK-ASSIGNED STDMA OPTIMISATION . . . 69
6.2 COLUMN GENERATION APPROACH . . . 70
6.2.1 Main algorithm . . . 71
6.2.2 Scheduling subproblem . . . 72

CHAPTER 7 SCHEDULE PERFORMANCE . . . 75
7.1 SIMULATION MODEL . . . 76
7.2 IMPROVEMENTS WITH TEMPORAL REUSE . . . 77
7.3 ESTIMATION OF USAGE EFFICIENCY . . . 79
7.4 CONVERGENCE OF THE MASTER PROBLEM . . . 80
7.5 SCHEDULE PERFORMANCE COMPARISON . . . 80
7.5.1 Schedule capacity . . . 81
7.5.2 Flow rate fairness . . . 84
7.5.3 Transmit power efficiency . . . 85
7.6 SPATIAL AND TEMPORAL REUSE . . . 86
7.7 RESULTS SUMMARY . . . 86

CHAPTER 8 FOUNTAIN CODES . . . 88
8.1 CHANNEL MODELLING . . . 89
8.1.1 Binary erasure channel . . . 90
8.1.2 Binary symmetric channel . . . 90

8.2 SPARSE GRAPH CODES . . . 90
8.2.1 Random codes . . . 91
8.2.2 Low-density parity-check codes . . . 92
8.2.3 Fountain codes . . . 94
8.2.4 Comparison between LDPC and fountain codes . . . 95
8.3 BELIEF PROPAGATION DECODING . . . 97
8.3.1 Message node update . . . 98
8.3.2 Check node update . . . 99
8.3.3 Message-passing algorithm . . . 100
8.4 DENSITY EVOLUTION . . . 102
8.4.1 Message node updates . . . 102
8.4.2 Check node updates . . . 103
8.4.3 Degree distribution optimisation . . . 104

CHAPTER 9 JOINT SOURCE -CHANNEL CODING . . . 107
9.1 COMPRESSION WITH ERROR-CORRECTION CODES . . . 108
9.2 SOURCE COMPRESSION WITH FOUNTAIN CODES . . . 109
9.2.1 LT-code compressor with decremental redundancy . . . 110
9.2.2 LT-code compressor with incremental redundancy . . . 112
9.2.3 Performance comparison of compression methods . . . 113
9.3 JOINT SOURCE-CHANNEL CODING WITH FOUNTAIN CODES . . . 114

CHAPTER 10 JOINT SOURCE -CHANNEL -NETWORK CODING . 117
10.1 SYSTEM MODEL . . . 118
10.2 FOUNTAIN CODE COMPRESSOR . . . 120
10.3 JOINT SOURCE-CHANNEL-NETWORK CODING . . . 122
10.4 NUMERICAL ANALYSIS . . . 123

CHAPTER 11 CONCLUSIONS AND FUTURE RESEARCH . . . 126
11.1 CONCLUSION . . . 126
11.1.1 Cross-layer optimisation of wireless networks with temporal reuse . . . 126
11.1.2 Joint source-channel-network coding . . . 127
11.2 FUTURE RESEARCH . . . 128
11.2.1 Cross-layer optimisation of wireless networks with temporal reuse . . . 128

11.2.2 Joint source-channel-network coding 129

LIST OF FIGURES

1.1 Cross-layer optimised scheduling, and separated source, channel and network coding components in the OSI model. 9
1.2 Joint source-channel-network coding and separated joint source-channel and network coding in relation to the OSI model. 10
1.3 An outline of the topics that are addressed in this dissertation. 14

2.1 An outline of the topics addressed in this chapter. 16
2.2 A linked multihop wireless mesh network with $N = 100$ nodes, a maximum transmit power of $P_{\max} = 0.1$ W, a thermal noise of $\sigma = 3.34 \times 10^{-12}$, a normalisation constant of $K = 0.0001$ and a path loss exponent of $\chi = 3$. A sample flow with shortest path route is shown in bold. 18
2.3 Flow load distribution in a 100-node wireless mesh network with equal flow meshing, clearly indicating the central tendency of higher loaded pathways, ideal for network coding without opportunistic listening. 20
2.4 The traffic model and flow pattern as it relates to the OSI model. 21

3.1 Chapter outline for the topics addressed regarding network coding. 24
3.2 A butterfly network with traditional routing used to relay packet AF in the three timeslots a) b) and c). 25
3.3 A butterfly network with network coded routing used to relay packets AF and BE in the three timeslots a) b) and c). 26
3.4 All the possible group splittings for a butterfly network. 27
3.5 The flow cuts for a butterfly network. 28

3.6 Opportunistic two-way wireless network coding, where relay B transmits AC+CA and both receivers A and C can recover their respective intended packets. Opportunistic listening and reception reports are not necessary in this instance. Another possibility is for node E to send the AC+CA packet if node B has other, higher priority packets to transmit. 29
3.7 Two-way NC requiring opportunistic listening and accurate reception reports to sink two partial flows in one timeslot. This can be accomplished if the relay node B transmits AD+CA, since both receivers A and D will be able to extract their intended packets from the NC sum. 30
3.8 Forwarding three dual-hop flows in one timeslot, using $n = 3$-way NC at relay B. The packet BC cannot be supported in the network coding operation, although the other packets can when node B transmits CA+ED+FC. Receivers A, C and D can then recover their respective intended packets. 31
3.9 Cross topology with inadequate information at nodes A (needs packet DE) and D (needs packet AC). A two-way NC packet AC+DE must first be broadcast by node F, then relay B can broadcast AC+CA+DE+ED and all receivers will then be able to recover their respective packets. 32
3.10 Conventional routing without network coding, using an unequal schedule that gives twice the transmission opportunities to the relay B. Timeslots 1-4 are given in subfigures a) to d) respectively. 33
3.11 Only three timeslots are required to relay two packets over two dual-hop paths with network coding. Timeslots 1-4 are given in subfigures a) to d) respectively. 34
3.12 Flow load distribution in a 100-node wireless mesh network with equal flow meshing, clearly indicating the central tendency of higher loaded pathways, ideal for network coding without opportunistic listening. 36
3.13 Various network coding opportunities in relation to the supporting OSI layers. . 38

4.1 The chapter outline of schedule assignment topics discussed. 42
4.2 The hidden terminal effect. Sender A is busy transmitting to receiver R, but because sender C is too far from A it falsely believes it has a transmission opportunity. 43
4.3 Multiple access collision avoidance for wireless (MACAW) where candidate senders contend for a data transmission opportunity using RTS/CTS handshaking. 44

4.4 Receiver initialised MAC, where receiver R grants a data transmission opportunity to sender C and receiver P to sender B. Since receiver R is out of range of sender P, and receiver P out of range of sender C, sender B can transmit to P whilst C is communicating with R. 45
4.5 Transmission scheduling in relation to the OSI layers. 47
4.6 The first eight timeslots in a simplex TDMA scheduling frame of length 14, for a sample multihop mesh network. 49
4.7 Non-optimal link-assigned STDMA seven-slot frame satisfying critical capacity demand. 50
4.8 A node-assigned TDMA equivalent of the example in Figure 4.6. 51
4.9 A more compact node-assigned STDMA schedule with spatial reuse. 53
4.10 Link-assignment with extended transmission rights, or link-assigned TDMA with temporal reuse. 59
4.11 Link-assigned STDMA with prioritised extended transmission rights, higher utilisation efficiency and network coding support. 60
4.12 Compacted link-assigned STDMA with LET, catering for the critical link-set. . 60

5.1 An outline of the topics discussed in this chapter. 62

6.1 The schedule optimisation topics covered in this chapter. 69

7.1 Chapter outline for the schedule performance study. 76
7.2 Schedule capacity (a) with extended transmission rights and corresponding mean end-to-end packet delays (b). 78
7.3 Convergence of the column generation approach to schedule optimisation. . . . 81
7.4 Schedule capacity (a) and corresponding end-to-end packet delay (b) comparisons. 82
7.5 Schedule capacity comparison with (b) and without (a) NC. 83
7.6 Mean flow rate (a) and fairness (b) comparison. 83
7.7 Mean flow rate (a) and fairness (b) comparison with variable rate and power control. 84
7.8 Mean transmit power comparison with (b) and without (a) NC. 85
7.9 Spatial reuse (a) and temporal reuse capacity (b) comparison. 86

8.1 The fountain code outline covered in this chapter. 89
8.2 The (a) BEC(ε) and (b) BSC(p) models indicating the transition probabilities. . 91

8.3 A bipartite graph representation of a linear code with parity-check equations. . 92
8.4 Belief propagation message (a) and check node (b) updates. 98

9.1 An outline of the chapter content and topics on joint coding. 108
9.2 Universal compression with fountain codes. 110
9.3 Comparative memoryless source compression performance comparison. 114
9.4 A noise robustness comparison on the BSC. 115
9.5 Noise robustness comparison on a flat fading BI-AWGN channel. 116

10.1 The chapter outline showing the topics that are covered. 118
10.2 Two-way wireless network coding, and separate and joint source-channel and network coding. 119
10.3 Two-stage approach to joint source-channel coding with an LT-code. 120
10.4 System error rate upper bound comparison. 121
10.5 Joint source-channel-network coding with a two-stage LT-code. 122
10.6 System error rates δ vs. source entropy p for different channel noises ε. 124
10.7 System error rates δ vs. channel noise ε for different source entropies p. 124

LIST OF TABLES

3.1 The coding+MAC gain for a two-component relay chain, with and without network coding for equal and unequal scheduling. The equal schedule, in the subgraph at least, allows the same resources for nodes B, E and F, which for uncoded routing consumes six timeslots to relay two packets. 35

7.1 Prioritised usage probabilities for power-rate adaptive networks. 79

8.1 A comparison of key characteristics between LDPC and fountain codes. 96

LIST OF ABBREVIATIONS

ACK	Acknowledge
AWGN	Additive White Gaussian Noise
BCH	Bose Chaudhuri Hocquenghem
BEC	Binary Erasure Channel
BER	Bit Error Rate
BI-AWGN	Binary Additive White Gaussian Noise
BP	Belief Propagation
BPSK	Binary Phase Shift Keying
BSC	Binary Symmetric Channel
BWT	Burrows-Wheeler Transform
CLID	Closed-Loop Iterative Doping
COPE	Coding Opportunistically
CSMA	Carrier Sense Multiple Access
CTS	Clear to Send
EOI	Entropy Ordered Indices
FAMA	Floor Acquisition Multiple Access
FDMA	Frequency Division Multiple Access
FFT	Fast Fourier Transform
FIFO	First-In-First-Out
ID	Identification
IDP	Incremental Degree Puncturing
IGW	Internet Gateway Router
IS-IS	Intermediate System to Intermediate System
ISM	Industrial, Scientific and Medical
JSCNC	Joint Source-Channel-Network Code
LAN	Local Area Network
LDPC	Low-Density Parity-Check

LET	Link-assignment with Extended Transmission rights
LLR	Log-Likelihood Ratio
LT	Luby Transform
MAC	Medium Access Control
MACA	Multiple Access Collision Avoidance
MACA-BI	Multiple Access Collision Avoidance by Invitation
MACAW	Multiple Access Collision Avoidance for Wireless
MANET	Mobile Ad Hoc Network
MTF	Move-to-Front
NC	Network Coding
NP	Nondeterministic Polynomial
NTR	No-Transmission-Request
OFDM	Orthogonal Frequency Division Multiplexing
OSI	Open Systems Interconnect
OSPF	Open Shortest Path First
PDF	Probability Density Function
RIMA-DP	Receiver Initialised Multiple Access - Dual Polling
RTS	Request to Send
SINR	Signal-to-Interference-and-Noise Ratio
SNR	Signal-to-Noise Ratio
SSCNC	Separate Source-Channel and Network Code
STDMA	Space-Time Division Multiple Access
TCP	Transmission Control Protocol
TDMA	Time Division Multiple Access
WAN	Wide Area Network
WMN	Wireless Mesh Network
XOR	Exclusive Or

NOTATION

$\star$	Convolution
$\odot$	The Hadamard (Schur) product
$(.)'$	The first derivative
$(.)^T$	The transpose operation
$\lvert . \rvert$	The determinant of a matrix, or cardinality of a set, or the magnitude of an element
$\lceil x \rceil$	The smallest integer larger than x
$\lfloor x \rfloor$	The largest integer smaller than x
I_N	The $N \times N$ identity matrix
$\mathbb{R}^{a \times b}$	A two-dimensional a-by-b space with real valued entries
$\mathbb{F}_2^n$	An n-dimensional vector space in GF(2)
log(.)	The natural logarithm
$\log_2(.)$	The binary logarithm
$H_2(.)$	The binary entropy function
conv(.)	The convex hull
$O(.)$	Bachmann-Landau notation for growth complexity
sup(.)	The supremum
min(.)	The minimum
max(.)	The maximum

COMMONLY USED SYMBOLS

W	The system bandwidth of a given channel
$\emptyset$	An empty set
$\mathcal{N}$	The set of wireless network nodes
$\mathcal{L}$	The set of wireless network links
$\mathcal{Y}_D$	The uniform probability distribution
P_n	The transmission power of a certain node n
$P_{\max}$	The maximum instantaneous transmit power
$\gamma_{\text{tgt}}^{(r)}$	The target SINR for transmission at a discrete r-multiple of the base rate
γ_l	The SINR experienced by link l
$c_{\text{tgt}}^{(r)}$	The maximum link capacity for transmission at a discrete r-multiple of the base rate
c_l	The capacity or rate of a link l
$\text{tr}(l)$	The transmitter node associated with a link l
$\text{re}(l)$	The receiver node associated with a link l
σ_n	The thermal noise variance experienced at receiver node n
Q_{nm}	The effective large-scale power gain between transmitter n and receiver m
Q	The effective large-scale power gain matrix
d_{nm}	The Euclidean distance between network nodes n and m
χ	A constant path loss exponent
$\mathcal{F}$	The set of network transport flows
R	The link-flow incidence matrix for a given wireless mesh network
C	The temporal reuse-unaware network link rate region
J_{ij}	The received power at node j when only node i transmits at $P_{\max}$
J	The network interference matrix
T	A schedule frame length

π_l	The maximum global flow load that can be routed by link l per timeslot
T_l	The average number of timeslots between the start of successive scheduled timeslots for link l with continual repetitions of the scheduling frame
c_l	The link rate for link l
c	The vector of link rates for all network links
$\widehat{\pi}$	The maximum global packet load per timeslot
$\mathcal{V}$	The set of all possible link rate vectors
$\mathcal{K}$	The set of link vector indices $[1, K]$
v_k	A link vector with index k
α_k	The scheduling time fraction for link vector with index k
C_e	The temporal reuse-aware network link rate region
$\widetilde{C}_e$	The estimated temporal reuse-aware network link rate region
s_f	The transmission rate for flow f
s	The the vector of transmission rates for all network flows
ξ	A Lagrangian multiplier
H	A linear code adjacency or parity-check matrix
G	A linear code generator matrix
λ_i	The fraction of graph edges that are connected to bipartite graph message nodes that have degree i
ρ_i	The fraction of graph edges that are connected to bipartite graph check nodes that have degree i
Ω_i	The fraction of fountain code bipartite graph output nodes that have degree i
Ψ_i	The fraction of fountain code bipartite graph input nodes that have degree i
ω_i	The fraction of graph edges that are connected to fountain code bipartite graph output nodes that have degree i
ψ_i	The fraction of graph edges that are connected to fountain code bipartite graph input nodes that have degree i
Γ	An intermediate transform matrix for the two-stage fountain joint code approach

CHAPTER 1
INTRODUCTION

Our built environment is evolving into a seemingly sentient organism, sensing and reacting to changes in temperature, humidity, wind, weather, earth-crust activity, incident solar luminosity, socio-political patterns and other events that shift the optimal point of operation. The future is outsourcing the administration and governance of the processes responsible for maintaining an acceptable standard of human living to technological forces that employ automated intelligence gathering. The globally evident socio-economic disparity necessitates the transition to a resource-based economy, where transparent and judicious distribution of goods can alleviate perceived scarcities. Human nature, however, compels first a high level of automation to dispel the need for monetary incentive. A key aspect of the mechanisation of our world is effective communication between the sense-actuators that drive the global automaton.

Swiftly our technological endeavours are projecting our future toward the awesome technological singularity, and progressively our ability to follow the global optimum with information of matching entropy, limited by the Bekenstein bound[1], is improving. Meaning that every hour entered into the great unknown we become even more subject to a chaos theory[2] of our own making, due to the burden of sensitised utility. A butterfly flaps its wings over Tokyo and the result is a tidal wave on the other side of the world. This begs the question: Do we have a sensor in place to detect the flight of the butterfly, and an actuator to prevent the resulting tidal wave or stock market crash in Manhattan? Like an intricate shock absorber, the world wide automaton will react as a unified entity to safely bear the human race

[1] The Bekenstein bound is an upper limit on the information that can be contained within a given finite region of space which has a finite amount of energy.
[2] Chaos theory studies the behaviour of dynamical systems that are highly sensitive to initial conditions.

within its green bosom.

Dubai, the glistening sketchpad for ideas and habitats of the future, already boasts a skyscraper that morphs and rotates its floors independently to suit the living preferences of its inhabitants. Likewise, the buildings of the future will take on a life of their own, sensing and changing continuously to uphold the global optimum. Critical to all this, is inter-node communication on a global scale. Three hundred and forty undecillion appliances, transport vehicles, clothing and even paint particles will plug into the global web, each having a unique IPv6 address. An organism with a life of its own, indeed, having more nodes than the total number of cells in three septillion human bodies. The desire for small and inexpensive communication solutions for home- and body area networks is apparent, as are the operational strategies that can extract maximum benefit from the available hardware, spectrum and communication resources.

Today social interaction platforms, such as Twitter, are being harnessed to attempt economic prediction by measuring public opinion and supported trends. Tomorrow wetware will plug human brains into the grid, where with a thought an election vote can be cast or information downloaded directly for instantaneous consumption. DARPA (Defense Advanced Research Projects Agency) issued a new, daring challenge for our age, namely the mastering of the cognitive cloud. Using wetware, difficult problems that elude answers can be rapidly posed to billions of minds. The diversity advantage will produce a result that bears greater utility than that of any expert in the relevant field. Non-invasive and pseudo-invisible (read minuscule) wetware modules will integrate the peak of technology into the fabric of society.

This dissertation outlines technological innovation that empowers tiny low-cost transceivers to connect to the world wide automaton, in a fashion that ensures a high degree of utilisation efficiency. Recent enhancements such as opportunistic bidirectional network coding are incorporated into predefined cross-layer optimised transmission schedules for multihop wireless mesh networks. Combining important knowledge and advances in this field, an optimal solution independent of OSI layer segregation is found.

Link-assigned scheduling is employed for greater spatial reuse and finer optimisation granularity, and newly defined temporal reuse allows for network coding support and improved utilisation under this assignment strategy. An accurate network link rate region is derived to

determine the achievable capacity for networks with temporal reuse, and a computationally feasible suboptimal estimation is used in a convex optimisation problem, with a utility that supports proportionally fair end-to-end flow rates.

A true joint source-channel-network code is created that allows for both encoding and decoding on a singular bipartite graph, to allow for space-optimal transceiver implementations in silicon. The property of asymptotical code perfection is harnessed to ensure adequate performance in a high noise-entropy coding region, in anticipated support of dense networks with intelligent signalling.

1.1 BACKGROUND

The interconnection of dimensionally constrained and low power transceivers is feasible with wireless mesh networking, and the increased routing load can be offset, in part, via network coding. Predetermined transmission scheduling shifts the computational processing requirement from worker nodes to more powerful centralised gateway nodes, and reduces network load attributed to scheduling control. Link-assigned transmission scheduling is well suited for fine optimisation control and results in good spatial reuse, and with added temporal reuse the inefficiencies relating to predetermined scheduling can be addressed and support can be given for network coding. By tolerating greater interference and background noise, more channels can be made available to less expensive transceivers, therefore the high noise channel coding region is of concern. Additionally, intelligent change-based sensing and relaying of the state of the automaton points toward operation in the high entropy source coding region. The small size advantage can be obtained with a true joint source-channel-network code that operates on a single graph, which is bespoke for the high entropy-noise coding region.

Detailed discussions on these concepts and design choices, as they relate to the aim of this work, follows.

1.1.1 Wireless mesh networking and network coding

Divide-and-conquer is essential in arriving at a workable infrastructure of the magnitude of the world wide automaton. Hierarchical segmentation, synonymous with the deployment of the internet, remains a fitting means of dealing with an engineering challenge of this scale.

Nodes must be grouped together locally, with data flows both between nodes in the same local segment and between nodes belonging to any part of the global network. This cancels the need for every node to have a direct connection to a global backbone interface. A special gateway node could assume this functionality and provide it to nodes that form part of its localised subnet. Significant reduction in cost and size could be affected when the majority of nodes only require local communication capabilities. The rewards of wireless installation and rollout of nodes in complex environments and situations impels the use of wireless communications, and so wireless mesh networking becomes a natural choice for at least the local interconnect.

Allowing routing through a multihop wireless mesh network, relaxes the requirements for transmit power and receive sensitivity, which reduces node size and prolongs battery life. A weak transmitter causes less interference in the mesh, which provides opportunity for spatial reuse, albeit at the cost of a higher routing load for the network. Network coding can alleviate this issue with highly effective routing decisions that forwards multiple packets in one timeslot. By reducing transmitter power the area segmentations can also be kept separate so that transmission schedules can be calculated and run independently across different mesh networks.

1.1.2 Predetermined transmission scheduling

Centralised optimisation of a transmission schedule, with knowledge of the mesh network topology of quasi-stationary nodes, holds several advantages over distributed scheduling calculation. Delegating the schedule optimisation to a powerful processing node, such as the local gateway, relieves the need for extensive processing capacity in the small, low-cost worker nodes. Much of the automaton will consist of structures and environments containing fully or almost stationary motes. The design choice of predetermined schedules, centrally calculated at deployment time and communicated to the network nodes, will relinquish the need for extensive control packet loads. A dynamic schedule will require either increased node processing capability, or a constant communication of the latest schedule as determined by the centralised organiser node. These difficulties can be avoided by opting for schedule predeterminism.

1.1.3 Link-assignment and temporal reuse

Assigning a node to a transmission timeslot, where it can transmit on any of its links, implies adequate SINR (signal-to-interference-and-noise ratio) at all of its neighbours. Scheduling a single link, however, opens up more possibilities for spatial reuse, owing to a lesser SINR requirement on the network. An enlarged possibility space equates to enhanced optimisation opportunity. Link-assignment is and will remain a popular scheduling choice as it affords finer granularity for optimisation control than node-assignment. Spatial reuse improves under the finesse of link-assignment, but effective network coding cannot be performed at a node where only one of its links is scheduled at a time. Good spatial reuse and network coding support is possible with link-assignment, when its conditions are broadened to allow for extended transmission rights.

Temporal reuse, the time-domain analogue of spatial reuse, is proposed (based on the principle of extended transmission rights [1]) to enable network coding under link-assignment and to combat the usage inefficiencies of predetermined transmission schedules. Transmission on an alternative link, when the relevant node has no packets for the primary scheduled link, avoids wasted timeslots. By extending transmission rights in this manner, packet depletion is addressed in predetermined link-assigned schedules with the reuse of a timeslot in the time-domain. In addition to this temporal reuse, the high spatial reuse provided by link-assignment is maintained. Node-assignment has natural support for the multi-link activations needed for network coding, but link-assignment minds only a unitary receiver's sufficient SINR per timeslot. Extended rights with temporal reuse finds other receivers that also have clear channels and so widens transmission opportunities for network coding.

1.1.4 High-noise region channel coding

Sharing bandwidth between a large number of nodes in the same area has been the obsession of wireless communications research, due to the limited resource of spectrum and the ever-growing user-base. As in all engineering disciplines trade-offs are required, and more user-channels can be bundled into the same spectrum at the cost of increased noise and interference. Cognitive radio promises the more effective use of spectrum, and biological nanonetworks foregoes the need for the electromagnetic resource all together. Science is now dabbling in the possibility of biological means of connectivity, but it seems to be an unreliable

method at best, especially at distances greater than one hundred meters, due to the physical dispersion requirements and diffusion latency. These measures will unfortunately only help up to the point where mass amounts of sense-actuators are deployed, and engineers would again have to resort to the more users - more noise compromise.

In orthogonal frequency multiplexing this compromise would be the equivalent of contracting the guard bandwidth or even allowing channel overlap. In wireless mesh networks that use time division multiplexing, this trade-off can be achieved by adding more links to a spatial reuse group. Certain receivers in the reuse group will suffer increased interference noise, but more packets can be routed in the same time and more nodes serviced. Profuse numbers of transceivers permeating every quoin of our environment will contribute greatly to the ambient electromagnetic noise level, and with smaller and weaker receivers a strong science must rescue the signal-to-interference-and-noise ratio from background energy and surfeited reuse groups.

Enter channel error-correction coding, the fascination of information theorists in the telecoms field the world over. Tolerating transmission errors occurring in unknown symbol places, channel coding has saved wireless communications from the flaming embers of stray electromagnetic waves and unwanted energy. The support of vast wireless node quantities asks for a channel code that performs well in the high noise regions, to combat the high usage interference and ambient noise. A powerful channel code can recover the intended information stream amidst the high levels of rogue energy, and so support the ambitious attempts at packing more users into the same bandwidth.

More so than perhaps any other code, sparse parity-check block codes such as low-density parity-check codes have proven their asymptotic reach of the Shannon (channel) capacity, and their affinity for high quality error-correction. Fountain codes, closely related to LDPC (low-density parity-check) codes, are a natural choice for use in systems of varying noise and entropy, due to their rateless property. Belief propagation decoding of these codes on bipartite graphs are mainly the reason for their eager adoption into the newest wireless telecommunications standards and usage in space technologies, since it provides a computationally feasible means of decoding these potentially huge codes. Pearl's contribution of the belief propagation algorithm has been seminal and is one of the great success stories of artificial intelligence in the telecommunications arena. For these reasons fountain codes

with belief propagation decoding are considered in this dissertation for the purposes of joint source-channel-network coding.

1.1.5 High-entropy source coding

Every reduction in inefficient bandwidth usage must be employed in networks of massive scale, including source compression to minimise network load absolutely. Particularly, the focus should be on information sent from sense-actuator nodes that form the sense-organ of the mechanical cloud. Allowing sensors to send the same unchanged environmental measurement value every timeslot is highly cumbersome. Instead, change-based sensing and update information minimises the information sent periodically from sensor nodes to their gateway, and is effective in keeping packet volume low. Still the change information communicated to the rest of the automaton might be slightly compressible, although mostly the information will be of high entropy. Source compression in the high entropy region is another key component that should be addressed for wireless mesh networks of the future.

Both types of linear codes, namely LDPC and fountain codes, have been successfully re-appropriated for source compression, amongst a few other, and consequently joint source-channel coding, through a lateral reconsideration of the essence of sub-unity entropic information. For an error pattern of weight less than the minimum distance of the code, a unique mapping to its corresponding syndrome can be made, if the original codeword is known. Thus assume that the zero-codeword was sent, and transmit only the syndrome, which is calculated from the input information to be compressed, by modulating that onto the error pattern. By recovering the error pattern, the input data is decompressed from only the received syndrome. Varying the syndrome length can provide added redundancy to combat channel errors, in the case of a joint source-channel code. For this reason the rateless fountain codes are a fitting choice of code, since one has full control over the output length without compromising the performance guarantees.

1.1.6 True joint source-channel-network coding

Nielsen's law[3] projects slower growth of bandwidth than Moore's law[4] for processing, although semiconductor science will soon reach the limits posed by the atomic threshold. Semiconductor real estate becomes increasingly valuable in a world that requires devices and motes of ever-decreasing proportions. There is a strong argument for subsuming modular design into monolithic uniformity, if it can decrease die-size and provide the same functionality. Operating at the limits dictated by physics, Wirth's law[5] must be counteracted by removing every immaterial transistor.

The joint source-channel coding capability of fountain codes has been established and this allows for a significant size reduction, where a source compression module and a channel coding module can be replaced with a singular one. Using one bipartite graph, joint decompression and channel decoding can be done, which is a necessity between nodes of the same local mesh network. Both for reasons of a decode-recode forwarding implementation and to allow nodes concerned with the same part of the automaton to affect action independent of decision-making nodes higher up in the network hierarchy. Furthermore the incorporation of network coding itself into the bipartite graph, which for fountain codes, is used both for encoding and decoding, is desired. Such a true three-way joint source-channel-network code will mean a notable reduction in silicon usage, and will provide an important step toward the making of the pseudo-invisible but capable transceivers of the future. Also, by addressing the high noise-entropy coding region in the design of the joint code, the size advantage would be complemented by support for dense networks.

1.2 MOTIVATION AND OBJECTIVE OF DISSERTATION

Recent enhancements such as network coding must be incorporated into the wireless mesh networks of the future, and the network operation must be specifically optimised to intelligently support these additions. By unifying the optimisation over all active network layers (as in Figure 1.1), the solution efficacy is not hampered by layer segregation. Link-assigned scheduling provides the best granularity for high-control optimisation and a great degree of spatial reuse.

[3] Nielsen's law states that network connection speeds for high-end home users double every 21 months.
[4] Moore's law originally described a long-term trend where the number of transistors that can be placed inexpensively on an integrated circuit doubles approximately every 18 months.
[5] Wirth's law is a computing adage stating that software is getting slower more rapidly than hardware becomes faster.

Therefore this assignment strategy must be opted for in the cross-layer optimisation of the network ensemble. Amendments must be investigated to allow for network coding support under link-assignment, and the schedule inefficiencies relating to predeterminism should be inspected.

The achievable network capacity with temporal reuse has to be calculated, and the new link rate region has to be used in the optimisation problem. The schedules have to provide proportionally fair end-to-end flow rates, to ensure an agreeable service quality. In evaluating the goodness of the various schedules, the schedule capacity, packet delay, flow-rate fairness and power efficiency must to be considered. A thorough comparison of these measures has to be done with extensive computational experiments, to highlight the improvements with the unique contributions in this study.

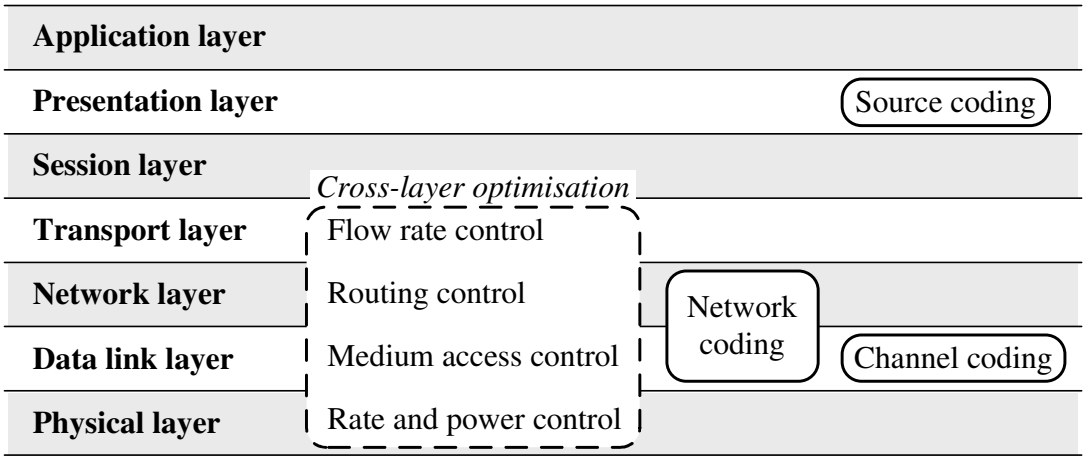

Figure 1.1: Cross-layer optimised scheduling, and separated source, channel and network coding components in the OSI model.

As a continuation of the cross-layer focus on optimal network behaviour, a joint source-channel-network code must be designed. The joint code must allow for encoding and decoding on one low-density bipartite graph, with the aim to realise the small size advantage required by future hardware. Data compression, channel error-correction coding and network coding should be performed by the code, in both directions of encoding and decoding. Specifically, the joint source-channel-network code should outperform a separated

source-channel and network code in the high noise-entropy region of the system channel. This bespoke coding region defines the conditions of dense wireless mesh networks (high noise) that employ change-based signalling (high entropy). The graph-based code should be based on degree distributions that perform well in the intended coding region. The manner in which the separate codes are combined in the OSI model is displayed in Figure 1.2.

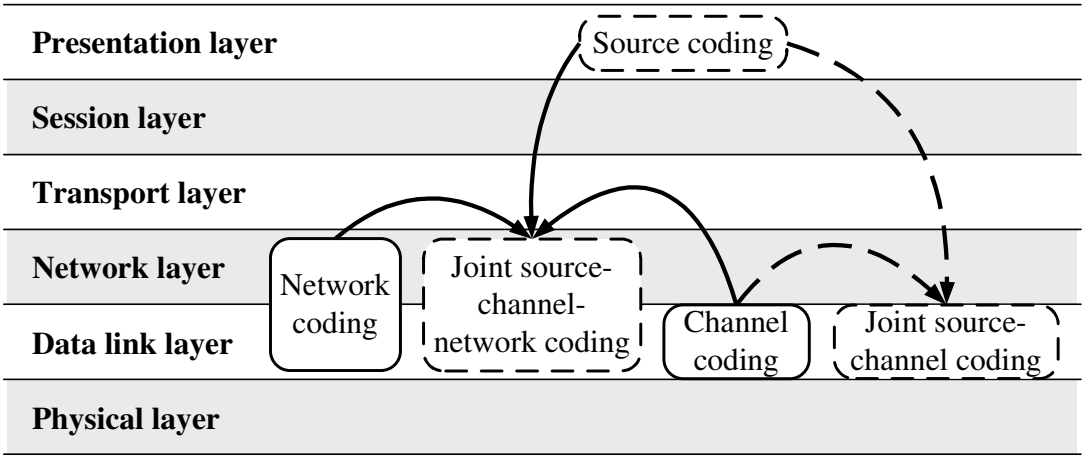

Figure 1.2: Joint source-channel-network coding and separated joint source-channel and network coding in relation to the OSI model.

1.3 AUTHOR'S CONTRIBUTION

A unique investigation of temporal reuse is done in this dissertation and novel advancements, such as network coding, are incorporated into a new cross-layer optimisation of wireless mesh networks. All aspects of the implementation of temporal reuse-aware cross-layer optimisation are considered and concrete contributions are made in this area. A truly joint source-channel-network code, designed for the high entropy-noise coding region, is another of the important research outputs achieved in this study. More specific details on these contributions are elaborated on in this section.

1.3.1 Temporal reuse

Link-assignment with extended transmission rights is redefined in terms of a new term that is coined in this dissertation, namely temporal reuse, which is recognised as the time-domain analogue of spatial reuse. This scheduling enhancement is used to good effect, by addressing

the usage inefficiencies that arise from scheduling predeterminism. Packet depletion is a phenomenon newly introduced in this work, and the reason it causes usage sub-optimalities in networks operating under predetermined link-assigned schedules is discussed. The conditions of these inefficiencies are investigated and the networks that suffer from packet depletion, and consequently the networks that benefit from temporal reuse, are characterised. In addition to improved bandwidth usage and the maintenance of high spatial reuse, the utility of temporal reuse, to allow for network coding, is demonstrated.

1.3.2 Temporal reuse-aware rate region

The achievable wireless mesh network capacity is formulated for scheduling with reuse in both the space and time domains, which gives the first accurate link rate region for networks with temporal reuse. A computationally feasible calculation of the temporal reuse-aware rate region is derived, and its assumptions are challenged and the suboptimum is shown to provide a good approximation of the optimal capacity. The generalness of the rate region derivation is established, which states that the actual achievable capacity can be determined without having to observe or simulate the network in question.

1.3.3 Cross-layer optimised scheduling

Link-assigned schedules with proportionally fair end-to-end flow rates are cross-layer optimised using the new temporal reuse-aware rate region, and extensive simulation confirms greater schedule capacity, better flow-rate fairness and higher power efficiency than with the temporal reuse-unaware rate region. The enhanced convex optimisation algorithm is explained and several complexity reductions are provided, as these are warranted by the enlarged search space owing to fully variable power and rate control assumed for all nodes. In addition to various implementations of cross-layer optimised schedules that were implemented, several more modified schedulers, based on popular methods, are contributed that newly incorporates temporal reuse.

1.3.4 Joint source-channel-network coding

The first truly joint source-channel-network code, that performs three-way encoding and decoding on one Tanner graph, is proposed. The system capacity of the joint

source-channel-network code is formulated for use in the code design. The improvised re-appropriated two-stage bipartite graph structure on which the joint code is based is revisited, and the modifications that allow for the added network coding is explained. A low-complexity construction component is contributed for the design of the two-stage Tanner graph, and the system error rate is derived and verified. The intelligent design of the joint code is demonstrated to rely on the asymptotic reach of the Shannon bound by good linear error-correction codes. A numerical analysis is done to validate the performance increases of the joint source-channel-network code, due to its design, over a separated source-channel and network coding scheme.

A structural comparison between LDPC and fountain codes is made, and the knowledge is used in the proposition of density evolution for joint source-channel-network coding. The use of density evolution to optimise the degree distributions for the unique joint code is discussed.

1.4 PUBLICATIONS

The advances made in cross-layer optimised link-assigned scheduling with temporal reuse, and joint source-channel-network coding were published in the following peer reviewed and accredited conference proceedings and journals.

1.4.1 Conference proceedings

Part of the contributions made during the undertaking of this degree, were published in the following peer reviewed and accredited conference proceedings:

1. F.P.S. Luus and B.T. Maharaj, “Cross-layer optimization of wireless networks with extended transmission rights,” IEEE GlobeCom 2010, Miami, USA, Dec. 2010.

2. F.P.S. Luus and B.T. Maharaj, “Joint source-channel-network coding for bidirectional wireless relays,” IEEE ICASSP 2011, Prague, May 2011.

1.4.2 Journal publications

The following article submission was made to a peer reviewed and accredited journal, as part of the research activities for this degree:

1. F.P.S. Luus and B.T. Maharaj, "Transmission scheduling for wireless mesh networks with temporal reuse," EURASIP Journal on Wireless Communications and Networking, accepted for publication.

1.4.3 Other publications

The research as reflected in this dissertation was partially based on the following conference paper and journal article, previously published by the author.

1. F.P.S. Luus and B.T. Maharaj, "Decremental redundancy compression with fountain codes," IEEE International Conference on Wireless and Mobile Computing (WiMob 2008), pp. 328-332, 12-14 Oct. 2008.

2. F.P.S. Luus, A. McDonald, and B.T. Maharaj, "Universal decremental redundancy compression with fountain codes," SAIEE Africa Research Journal, Vol. 101(2), pp. 68-77, June 2010.

1.5 OUTLINE OF DISSERTATION

Realistic simulation of a complete wireless mesh network is one of the key contributions in this dissertation, and a numerical analysis is used to verify that the various design goals have been met. An outline of the dissertation is shown in Figure 1.3. The dissertation explains exactly how the networks are constructed and how they operate to form the network simulation environment. In Chapter 2 the network layout and topology formation are defined, and in Chapter 3 it is shown how network coding is performed in the wireless mesh networks. Transmission scheduling is examined in Chapter 4, and the concepts of temporal reuse and schedule assignment are investigated. The network capacity with certain scheduling algorithms is derived in Chapter 5, especially the rate region of link-assigned scheduling with extended transmission rights. This newly derived rate region is used in Chapter 6 to perform a more accurate cross-layer optimisation, which is shown in Chapter 7 to outperform the temporal reuse-unaware approach by measuring various performance metrics through extensive simulation.

In the first part of the study schedules that support network coding were optimised, and it then becomes the focus of the remainder of the document to analyse the benefits of

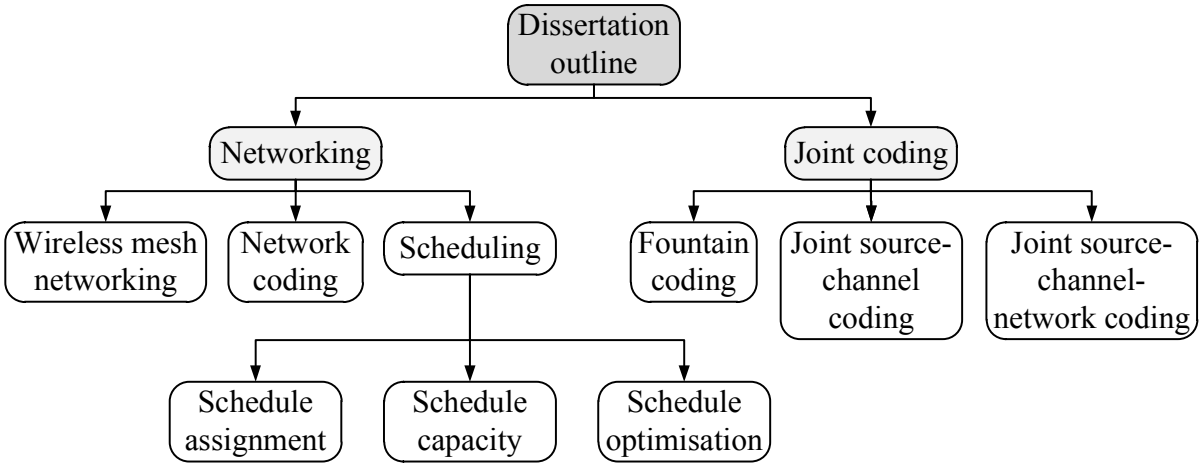

Figure 1.3: An outline of the topics that are addressed in this dissertation.

the integration of channel and network coding. Sparse graph codes and their decoding are introduced in Chapter 8, and details are given regarding the encoding, decoding and optimisation of fountain codes. In Chapter 9 it is shown how fountain codes can be harnessed to compress data in a noise-robust manner, and specific implementation details are reviewed. The preceding demonstration of joint source-channel coding serves as an introduction to the use of fountain codes in a truly three-way joint source-channel-network code. The specifics of the joint coding scheme are discussed in Chapter 10, and performance results display the effectiveness of truly joint coding. Finally, the dissertation is concluded with a summary of the research questions and the associated contributions. Recommendations are also given for future research in the areas addressed in this study.

CHAPTER 2

WIRELESS MESH NETWORKING

Three decades ago mobile ad hoc networks (MANET [2]) originated from a need for wireless networking on the battlefield. This DARPA initiative had questionable security, low throughput, and advancements were driven by military-specific requirements. Thus MANETs were deemed unfit for civilian uses such as broadband internet connectivity and WAN (wide area network) access, so WMNs (wireless mesh networks) recently emerged to address the weak points, but maintain the self-organisation, self-configuration, self-discovery and self-healing properties of MANETs. Specifically WMNs have a hierarchical structure with both mesh clients and a stable mesh backbone, which is not present with MANETs. The mesh backbone consists of wireless routers (forming a wireless network of their own), with either wired or wireless direct internet access, which interconnect different groups of wireless mesh clients. A subset of the backbone routers with direct internet access become the internet gateway routers (IGW) for the network. This provides cost-effective access to internet and WAN services by reducing the dependence on a local loop infrastructure, through the use of multihop networking.

Focusing on buildings, structures, habitats and environments that need to react as single entities to environmental or other changes, a very specific WMN is envisioned. One where mesh clients need to communicate with other clients in the mesh network, in addition to IGW access, to allow for a dynamic coherence of the entity in question. In this scenario, the mesh clients are sense-actuators that communicate measurements, and receive instructions for action to and from all or a select subset of other mesh clients. Thus, in this dissertation, transport-layer data flows between every mesh client pair contribute to the network load,

which is also called client meshing. The schedule optimisation utility is formulated to support any network flow pattern, including that of a normal WMN, but the focus in this study is on inter-client connectivity. A definition of the traffic flow patterns used for this work is one of the topics covered in this chapter, as shown in the outline of Figure 2.1.

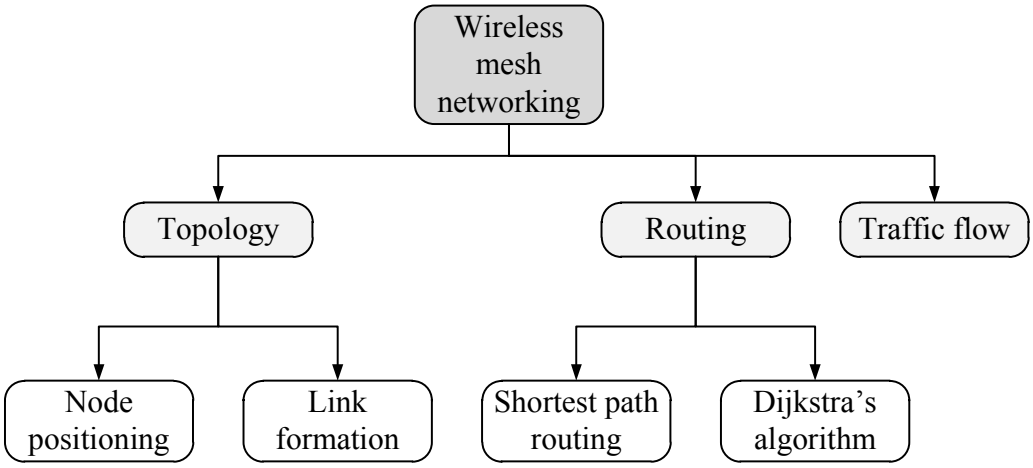

Figure 2.1: An outline of the topics addressed in this chapter.

For example, when a residential skyscraper is threatened during an earthquake, then the advanced central columns throughout the building can shorten or lengthen to absorb the resulting shock. A large number of accelerometers distributed in and around the building, and at the central columns, can provide the information needed by the central column actuators to counteract the earth's movement. In particular, for the study of centrally calculated scheduling, low-mobility is assumed, where a mesh network can successfully operate on a schedule for a reasonable amount of time. A potentially significant control overhead is experienced when a new schedule has to be sent to all the wireless mesh clients, which necessitates the condition of quasi-stationarity. Under these conditions, the goal of this exercise is to predetermine the optimal transmission schedule for a utility that supports proportionally fair end-to-end flow rates.

2.1 NETWORK TOPOLOGY

Relative node positioning and the conditions for link formation are defined in this section, for the class of networks considered in this work. Nodes are randomly distributed, with isotropic antennas, and unidirectional links are formed when a link has a sufficient SINR value. The

physical interference model is used, and only networks with a path between every node pair are considered. The specifics of the network topology model follows.

2.1.1 Node positioning

Multihop wireless mesh networks with N nodes $n \in \mathcal{N}$, and L links $l \in \mathcal{L}$ are investigated, where L depends partly on the node density of the network. A quasi-stationary condition requires the alteration of scheduling to maintain optimal performance. Thus, for the duration of the predetermined schedule usage, the nodes are assumed to have fixed locations. The network nodes are randomly distributed on a two-dimensional plane, according to a uniform distribution $\mathcal{Y}_D$. Each dimension value forms a uniform distribution, so independent Mersenne twisters [3] $x(n), y(n) \in \mathcal{Y}_D$ are employed to generate separately the x- and y-axis values of a newly added transceiver n.

2.1.2 Link formation

Every node has one isotropic (omni-directional) antenna, with mutually exclusive transmit and receive functionality. The transmission power of a certain node n is set as P_n, and the maximum instantaneous transmit power is limited to $0 \geq P_n \geq P_{\max}, \ n \in \mathcal{N}$. The receive sensitivity is only defined in terms of an SINR threshold requirement $\gamma_{\text{tgt}}^{(1)}$, as it pertains to a specific link on which a node receives signalling. A link SINR value of $\gamma_l(P)$ is a function of the global power assignment (possibly multiple transmitters due to spatial reuse), which is denoted by $P = (P_n : n \in \mathcal{N})$. The target SINR for transmission at a discrete r-multiple of the base rate is given by $\gamma_{\text{tgt}}^{(r)}$, where $r = 1$ refers to the base transmission rate and $r = 0$ a zero transmission rate. In practice the transmission rate of link l is limited to $c_l = c_{\text{tgt}}^{(r)} = rW \log(1 + \gamma_{\text{tgt}}^{(1)})$ when $\gamma_{\text{tgt}}^{(r)} \leq \gamma_l(P) < \gamma_{\text{tgt}}^{(r+1)}$, where W is the system bandwidth in the Shannon capacity formulation.

The wireless physical interference model [4] is adhered to, for accurate accumulative SINR accounting, as opposed to protocol interference model which does not consider cumulative interference. With the protocol interference model, communication between nodes u and v are successful if no other node within a certain interference range of from v (the receiver) is simultaneously transmitting. The physical interference model is more practical, since it takes into account all interference experienced by a node. A wireless communication link l is directed from transmitter $\text{tr}(l)$ to receiver $\text{re}(l)$, and is formed when the link SINR

$\gamma_l(P) \geq \gamma_{\text{tgt}}^{(1)}$ at least equals the threshold SINR, according to the physical interference model. The link formation requirement is given as in Equation 2.1.

$$\frac{Q_{\text{tr}(l)\text{re}(l)} P_{\text{tr}(l)}}{\sigma_{\text{re}(l)} + \sum_{n \neq \text{tr}(l)} Q_{n\text{re}(l)} P_n} = \gamma_l(P) \geq \gamma_{\text{tgt}}^{(1)}. \tag{2.1}$$

The unidirectional wireless link is modeled as a single-user Gaussian channel, with a thermal noise of σ_m at a receiver m. The effective power gain between transmitter n and receiver m is given by Q_{nm}. This gain is calculated according to a deterministic fading model $Q_{nm} = K_{nm} d_{nm}^{-\chi}$, where K_{nm} is a normalisation constant, d_{nm} is the Euclidean distance between n and m, and χ is a constant path loss exponent. Thus, when a receiver has sufficient SINR greater than the threshold SINR required for base rate transmission, then a link is formed. Only network instances with a path between every node pair are considered, and the SINR requirements are correctly re-evaluated for higher rate links. An example of a conforming network instance is shown in Figure 2.2, with a sample shortest path route between two nodes in bold.

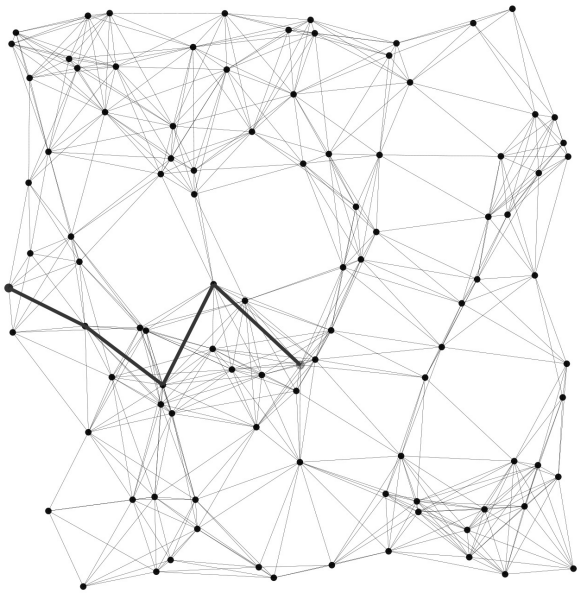

Figure 2.2: A linked multihop wireless mesh network with $N = 100$ nodes, a maximum transmit power of $P_{\max} = 0.1$ W, a thermal noise of $\sigma = 3.34 \times 10^{-12}$, a normalisation constant of $K = 0.0001$ and a path loss exponent of $\chi = 3$. A sample flow with shortest path route is shown in bold.

2.2 ROUTING

The network layer of the OSI is concerned with data transmission on a network, and in particular it defines how packets are routed in a network. In multihop wireless mesh networks, nodes have the responsibility to forward data for specific flows. The forwarding duties are dictated by the network routing, which specifies the paths that packets must traverse in delivering the data flows. Recalling that a data flow is a connection between a specific sender and a different receiver, the flow packets can follow only a single path or multiple paths, dynamically. The key focus of this dissertation is to investigate the network performance gains with temporal reuse in a cross-layer optimised predefined schedule, so single-path routing is used instead of dynamic multipath routing. This allows for predetermination of the schedule and better focus on the performance aspects of cross-layer optimisation with temporal reuse.

2.2.1 Shortest path routing

Routing algorithms rely on metrics, which gives relative path utility that assists in choosing the best route for a flow. The minimum-hop routing metric prefers, of all possible paths between a sender and receiver, the single-path route with the least number of hops. Also termed shortest-path routing, Dijkstra's algorithm [5] can be used to find the shortest-path tree for every node, which gives the shortest path to every other node. This shortest path algorithm is widely used in network routing protocols such as IS-IS (intermediate system to intermediate system) and OSPF (open shortest path first).

2.2.2 Dijkstra's algorithm

Dijkstra's algorithm operates on a graph with non-negative edge (link) costs, and functions according to Bellman's famous principle of optimality [6]. This principle states that if a node o is on the shortest path from node m to n, then it can be implied that the path-segment between m and o is also the shortest path between m and o. For this reason the collection of shortest paths from a node origin form a tree, as depicted in Figure 2.3. The worst case complexity for this algorithm is $O(|L| + |N| \log |N|)$, where L is the number of network links and N is the number of nodes. Construction of the shortest path tree progresses hop-by-hop from an initial root node, specifically the sender. Setting the current node as the root node, the path cost to each unvisited neighbour is calculated. The hop metric adds one hop to the distance of a path

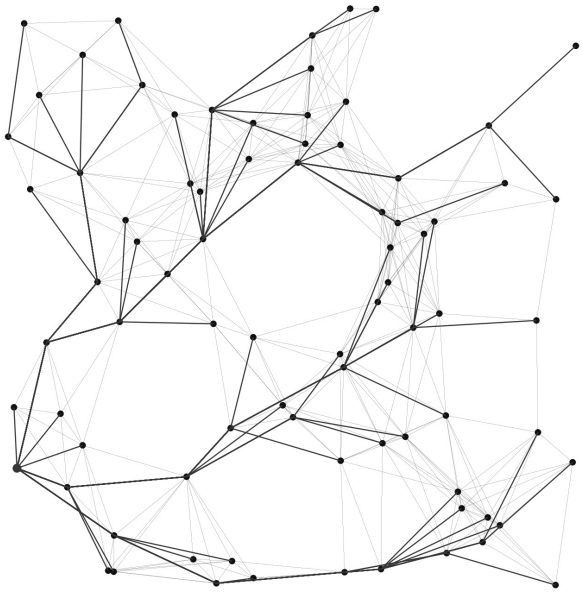

Figure 2.3: Flow load distribution in a 100-node wireless mesh network with equal flow meshing, clearly indicating the central tendency of higher loaded pathways, ideal for network coding without opportunistic listening.

extended to a neighbouring node. The minimum value of this tentative cost or distance indicates which neighbour gives the shortest path option, and this visited neighbouring node is then set as the current node. The procedure is repeated until all nodes have been visited, and then the resulting shortest path tree defines in part the routing duties of the network nodes. Calculating the trees for every node in the network will give the full routing tables for every mesh client, as shown in Algorithm 1.

2.3 TRAFFIC MODEL

Scheduling will be investigated for the traffic pattern arising from wireless meshing, where nodes communicate with each other in the same network. When a sender (source) node communicates with a receiver (sink) node, the data transmission is referred to as a transport flow. The flow pattern largely determines the node loads in the network, owing to multihop routing, and affects how optimal scheduling should be done. The transport layer of the OSI model is tasked with ensuring the reliable delivery of a flow segment, although the network layer has to send the packets of the segment from source to sink, as shown in Figure 2.4.

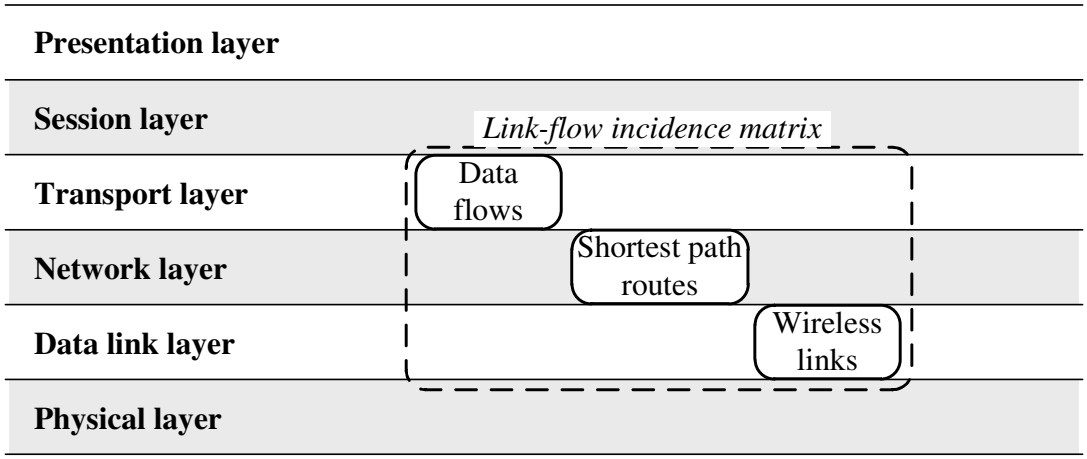

Figure 2.4: The traffic model and flow pattern as it relates to the OSI model.

Data traffic is modelled as $F = N(N-1)$ transport flows $f \in \mathcal{F}$ between every possible source-sink node pair in the network, where data is generated at the source and delivered to the sink at flow rates $s = (s_f : f \in \mathcal{F})$. The flow rate specifies the average number of packets sent by the source that successfully reaches the sink in one timeslot. The predetermined scheduling frame and the specific traffic model determine what flow rates can be achieved for the network, and so as a schedule performance measure the flow rates are an important indicator. Only single-path routing is considered in this study and the link-flow incidence matrix $R \in \mathbb{R}^{L \times F}$ couples the links with the flows so that

$$R_{lf} = \begin{cases} 1 & \text{if flow } f \text{ uses link } l \\ 0 & \text{otherwise} \end{cases} . \tag{2.2}$$

Algorithm 1 Dijkstra's algorithm with the minimum-hop metric.

```
1:  procedure DIJKSTRA(𝒩)
2:      𝒩 = Network                                   ▷ Set of nodes in the network
3:      trees=∅                                       ▷ To store shortest path trees
4:      for i ∈ 𝒩 do                                  ▷ For all nodes
5:          prev= 0          ▷ Shortest path tree stores previous hop for each node
6:          cost= ∞                                   ▷ Tentative cost to node in tree
7:          cost(i) = 0                               ▷ Start at root
8:          current= i                                ▷ Set root as current
9:          unvisited= 𝒩                              ▷ Tree yet to be created
10:         while unvisited≠ ∅ do                     ▷ Tree not complete
11:             for j ∈ neighbours(current) do        ▷ For all neighbours of current
12:                 if j ∈ unvisited then
13:                     cost(j) =cost(current)+1      ▷ Add one hop
14:                     prev(j) =current              ▷ Link node to tree
15:                 end if
16:             end for
17:             unvisited.remove(current)             ▷ Current becomes visited
18:             current=minimumcost_neighbour(i)      ▷ Advance current to nearest neighbour
19:         end while
20:         trees=[trees,prev]                        ▷ Add tree map to trees
21:     end for
22: end procedure
```

CHAPTER 3
NETWORK CODING

By regarding information flow on a network as 'fluid', nodes are limited to only routing and forwarding operations. However, when permitting nodes to intelligently code packets together before a multicast, significant gains in capacity can be achieved [7]. Network coding was initially studied as it applied to wired networks, and the key concepts were adapted later for use in wireless networks [8]. A wired network can activate all of its links simultaneously in a full-duplex manner, which provides complex network coding opportunities. In general, network coding in wireless networks is simpler to analyse, owing to shared medium access. It is, however, also the shared medium that provides the network coding opportunities in wireless networks, which rely on the broadcasting of an NC packet, and opportunistic coding and listening.

The use of network coding in wired networks is explained in this chapter, and it is shown how network usage efficiency can be increased with network coding. The throughput bounds that limit the flow in networks are discussed, as well as the role of network coding in reaching those bounds. Network coding for wireless networks is looked at, specifically opportunistic coding or COPE. The implementation aspects of wireless network coding is considered, and a coding scheme is chosen for use in the wireless mesh networks further considered in this dissertation. The expected gains with network coding in wireless networks are analysed, and the results are employed in deciding on the coding scheme. Finally, the operations of network coding are classified according to their involvement in the OSI network model. An outline of the chapter content is given in Figure 3.1, indicating the subjects that are covered.

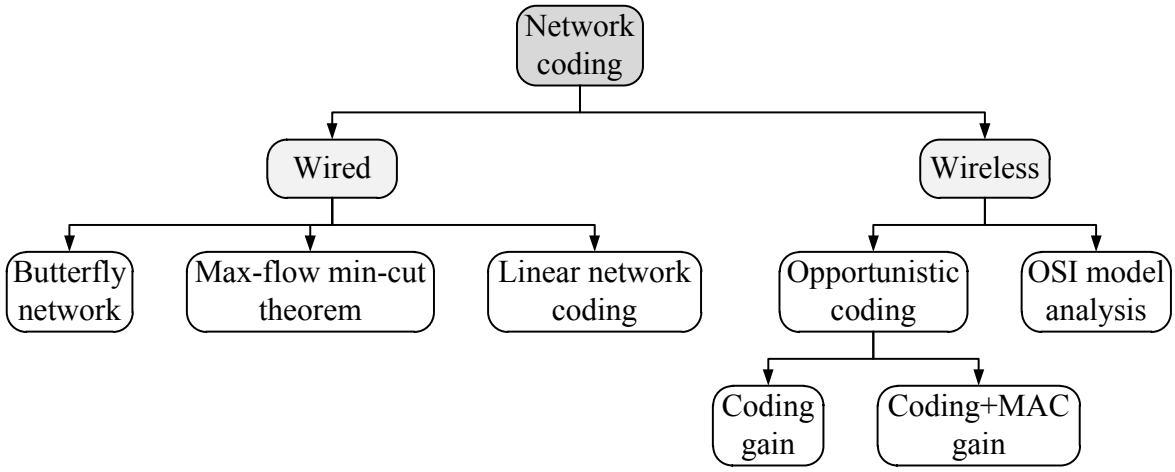

Figure 3.1: Chapter outline for the topics addressed regarding network coding.

3.1 WIRED NETWORK CODING

Networks have always been implemented such that the information flowing through the network is separated from the coding and transmission mechanisms. This is a restriction which is removed through the use of network coding. Network coding increases the throughput of a network by coding on the network level at intermediate nodes. Traditional network operation involves routing where intermediate nodes only forward received packets and do no combinations or coding, in contrast to network coded operation.

3.1.1 The butterfly example

A node in a wired network could have one or more separate directed (half-duplex) wired links to other nodes, and is able to transmit simultaneously and independently on each link. A directed wireless link can only transmit data in the particular direction of the link, unless the link is indicated as bidirectional. For the purposes of demonstrating network coding, a packet transmission is assumed to take one timeslot to be sent and stored in the receiving node buffer. Copy-based forwarding is employed to route a packet between two nodes that are not directly connected, unless network coding is specifically done. Network nodes can only transmit or forward a packet once the packet is fully available in its buffer.

The wired and directed network in Figure 3.2 consists of six nodes (A to F) and seven directed links, and in the portrayed scenario the objective is to transmit two packets AF (from

A to F) and BE (from B to E). The network topology resembles the image of a butterfly, and is normally used to explain the concept of wired network coding [9]. Three timeslots are depicted in the subfigures a) b) and c) of Figure 3.2, where only one forwarding objective is met, namely the forwarding of packet AF from node A to F. The packet buffer of each node is shown in a box near the node, and the packets available to the buffer is indicated. If a link is actively engaged in a timeslot, then the link is emphasised in black and the packet transmitted is noted on the link. Similarly, if the buffer of a node is accessed in a timeslot, then it is also emphasised in black.

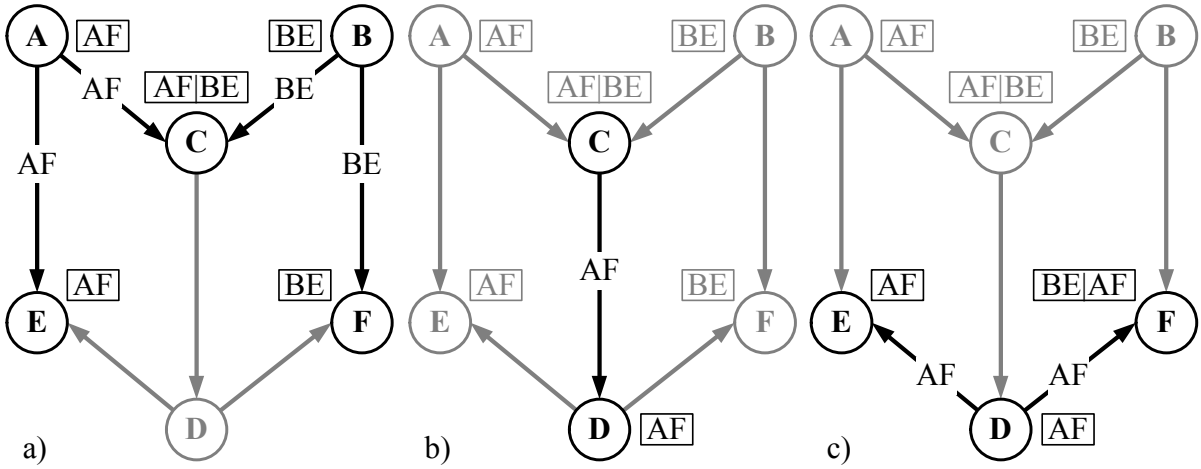

Figure 3.2: A butterfly network with traditional routing used to relay packet AF in the three timeslots a) b) and c).

The directed nature of the network in Figure 3.2 makes A-C-D-F the only available path for the packet AF to be delivered from node A to node F. In the same manner the path B-C-D-E is the only available path for the forwarding of packet BE. The two nodes C and D along paths A-C-D-F and B-C-D-E are shared, which causes a congestion, since only one path can use the contested nodes C and D at any one time. In the first timeslot in Figure 3.2 a) the node C can receive packets AF and BE at the same time on its two directed links. During the second timeslot in Figure 3.2 b) the node D receives the packet AF from node C, and in the third timeslot in Figure 3.2 c) the node F receives its intended packet AF from node D. Thus, with traditional routing, only one packet can be delivered in three timeslots.

There is congestion at nodes C and D, due to both the paths A-C-D-F and B-C-D-E required for meeting the delivery objective. A routing mechanism is required to allow the simultaneous usage of nodes C and D by both routes, in order for both packets AF and BE to

be delivered in three timeslots. Network coding is such a routing mechanism, and it can be employed when certain conditions are met. Consider the same network and objectives in Figure 3.3, but this time with network coding being used to deliver packet BE as well as packet AF.

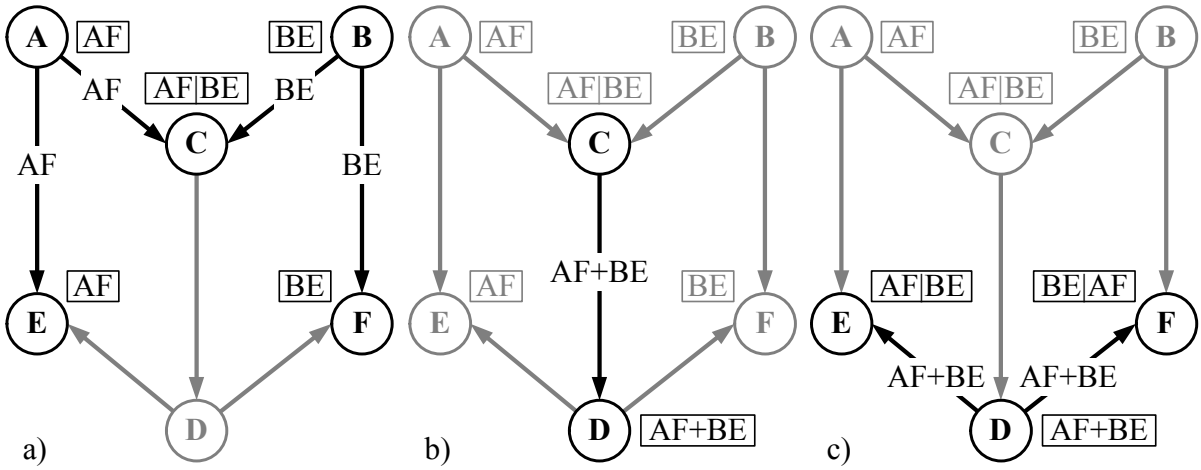

Figure 3.3: A butterfly network with network coded routing used to relay packets AF and BE in the three timeslots a) b) and c).

The important observation is that nodes E and F each has one of the packets received by node C, and if these sink nodes E and F receive the sum AF+BE then they can recover the packet they don't have. For example, if node E has packet AF and receives AF+BE then it can perform the operation AF+(AF+BE)=BE to recover BE. This operation is true when the packet is processed as a symbol string in GF(2), where a sum and minus produces the same answer so that AF+AF=AF-AF=0 and thus (AF+BE)-AF=(AF+BE)+AF=BE. The opportunity is available at node F, where the node can recover its intended packet AF by performing the operation BE+(AF+BE)=AF at the end of timeslot three in Figure 3.3 c). In this manner network coding is used to deliver both packets AF and BE in three timeslots, as opposed to the normal four timeslots required by traditional routing means.

3.1.2 Max-flow min-cut theorem

Wired networks in particular can be analysed to determine the maximum flow that can be maintained between a source and sink node. The max-flow min-cut theorem, first proposed in [10], states that the maximum network throughput between a source and destination node is bounded by the least throughput en route to the destination. In the butterfly network example of Figures 3.2 and 3.3 the minimum cut between nodes A and F is one. All the different cut

groupings for the butterfly network are shown in Figure 3.4.

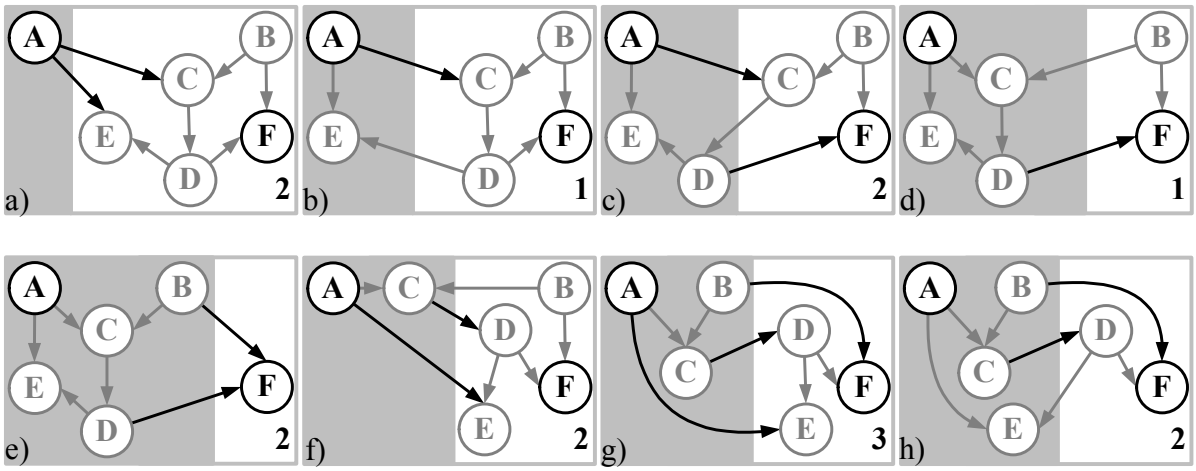

Figure 3.4: All the possible group splittings for a butterfly network.

By splitting the network into two groups, such that the source and sink nodes always belong to different groups, the cut can be determined as the number of links directed from the source group to the sink group. The maximum cut in the butterfly network in Figure 3.5 is three, but this does not mean that a throughput of three packets from node A to node F can be sustained. The sustainable throughput is limited by the minimum cut, which is one, represented by the link between node D and node F.

This analysis gives the maximum possible flow between two nodes, but it is the task of network coding to attempt to achieve that flow. Since traditional routing can only ensure a throughput of a half, as in the case of Figure 3.2, network coding must be employed to achieve the full maximum flow. This done by sharing the minimum cut link between the packets AF and BE. This analysis pertains only to wired networks, where a node can use all of its links simultaneously.

3.1.3 Linear network coding

In the butterfly network scenario a linear combination of packets forms the network coded packet, which is effective in relaying the necessary information. It has been constructively proven in [11] and [12] that linear coding can achieve the max-flow bound between any source and sink in a directed wired network. Thus the most popular network coding techniques produce packets which are linear combinations of received packets, since the linearity eases

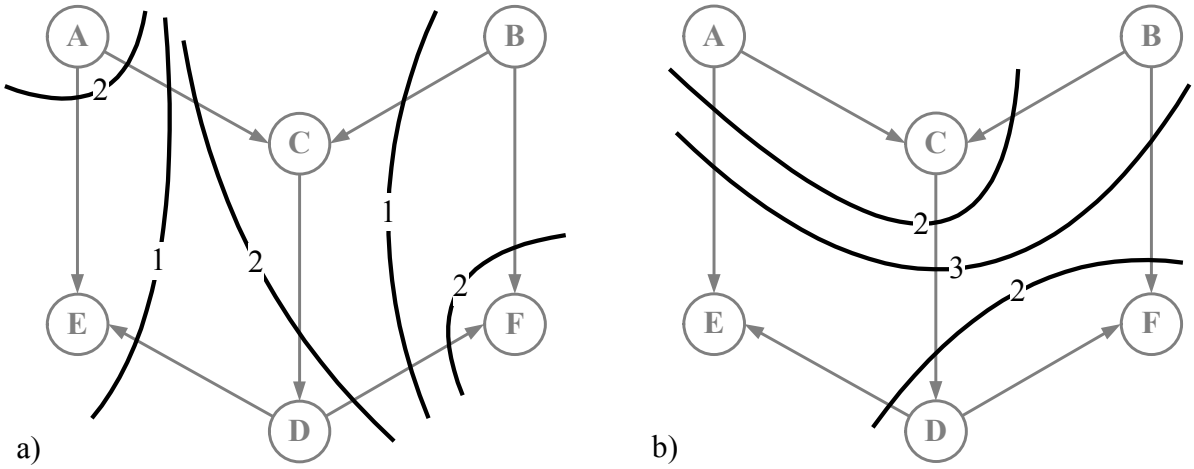

Figure 3.5: The flow cuts for a butterfly network.

practical implementations [13].

If a node has received n packets $M_1, \ldots, M_n$, which might be linear combinations done at a previous node, then linear network coding combines the packets such that the transmitted packet or information vector is given by $\sum_{i=1}^{n} g_i M_i$. The coefficients $g_1, \ldots, g_n$, called the encoding coefficients, are randomly chosen over the same field $\mathbb{F}_2^k$ as the packets M_i, where each packet contains k bits. This allows for distributed operation of network coding. An efficient distributed randomised approach was proposed in [13] that asymptotically achieves the multicast capacity given by the max-flow min-cut bound. Random linear network coding can be used in general multi-source multicast networks with possible correlated sources [14].

3.2 WIRELESS NETWORK CODING

As an introductory example of basic network coding in wireless networks, consider the mesh subnetwork in Figure 3.6. In this particular instance, a centralised relay node has to forward two packets in support of the two opposing flows-indicated between nodes A and C. Since A and C are out of range, the multihop facilities of mesh networks must be employed for their interconnect. Typically a node in range of both A and C, namely B in this case (alternatively node E), will serve as a relay that forwards packets between A and C. Therefore A will transmit a packet (AC), as part of a flow intended for C, which relay B will receive. The packet AC is received by the neighbours of A, as indicated in the node buffers. In the same way B receives packet (CA) from sender C, so that the relay is now tasked with the forwarding of both packets

AC and CA. Normal routing dictates that two separate transmissions, and thus two separate timeslots are needed to fulfil the relaying duty. However, with network coding, the two packets can be combined and transmitted in one timeslot, with the intended receivers A and C still able to resolve their respective intended packets CA and AC.

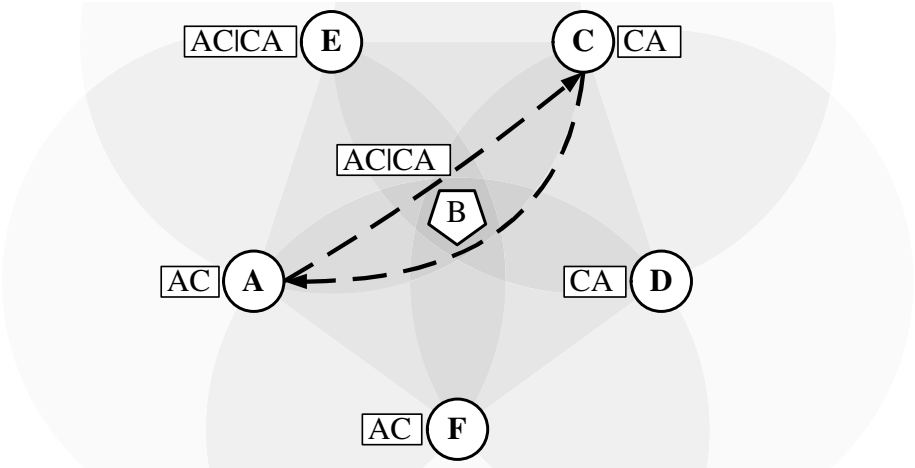

Figure 3.6: Opportunistic two-way wireless network coding, where relay B transmits AC+CA and both receivers A and C can recover their respective intended packets. Opportunistic listening and reception reports are not necessary in this instance. Another possibility is for node E to send the AC+CA packet if node B has other, higher priority packets to transmit.

3.2.1 COPE

COPE (coding opportunistically) is one of the primary examples of network coding in wireless networks, which relies on opportunistic listening, coding and neighbour state updates to identify and exploit network coding opportunities [8]. As a wireless forwarding architecture, COPE operates on a coding layer between the network and data link layers of the OSI model. It assumes that network nodes forward packets according to an underlying routing protocol. Opportunistic listening places nodes in promiscuous mode which fills their buffers with overheard packets, so that the number of network coding opportunities are maximised. Reception reports and estimation of neighbour buffer content helps a relay in determining which packets it can potentially code together for a network coded broadcast, as the successful decoding of the transmission relies on the packets each neighbour has available.

3.2.2 Opportunistic coding

The first condition for a coding opportunity is that a relay should have $n > 1$ packets that have to be forwarded to n specific neighbours. Secondly, through reception reports and/or routing intelligence, the relay must be relatively certain that all n participating neighbours already have at least $n-1$ of the n packets. This is a necessary condition; otherwise some receivers might not be able to decode their packets. To avoid network coding becoming disruptive, a packet must never be delayed for the sake of network coding it later. This is especially true for prioritised buffers, where the reshuffling of packets is interpreted by TCP as a congestion signal.

3.2.3 Opportunistic listening

The broadcast nature of wireless networks is advantageous, since it allows for opportunistic listening. The result is a network with more information at hand, which provides more network coding opportunities. When the neighbours of a relay possess more overheard packets, then there are more coding possibilities. While packet snooping creates higher-order network coding opportunities, it complicates the architecture in an attempt to validate the feasibility of the opportunities. Integrating reception reporting into a working network, to enable network coding with opportunistic listening, adds bandwidth and processing overhead as well. For these reasons, opportunistic listening is not used for the network coding done in this dissertation.

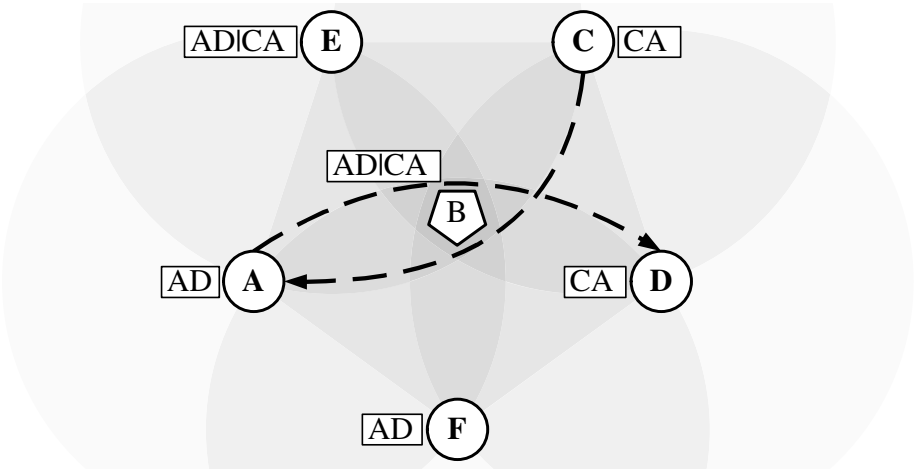

Figure 3.7: Two-way NC requiring opportunistic listening and accurate reception reports to sink two partial flows in one timeslot. This can be accomplished if the relay node B transmits AD+CA, since both receivers A and D will be able to extract their intended packets from the NC sum.

3.2.4 Reception reporting

In the case of network coding without opportunistic listening shown in Figure 3.6, the relay knows that the two participating transceivers each have sufficient packets to recover their respective intended packets, since the relay has received the packets from those transceivers. In this unique case opportunistic listening is not required, as the relay need only inspect the packets to see where it came from.

In more complex scenarios, as in Figure 3.7, the relay B could not be certain if node D has successfully overheard packet CA. To support complex network coding instances, nodes need to communicate their buffer content (packet IDs) to their immediate neighbourhood. In this direct manner, a relay can learn what packets are available at a neighbouring node, and network code accordingly.

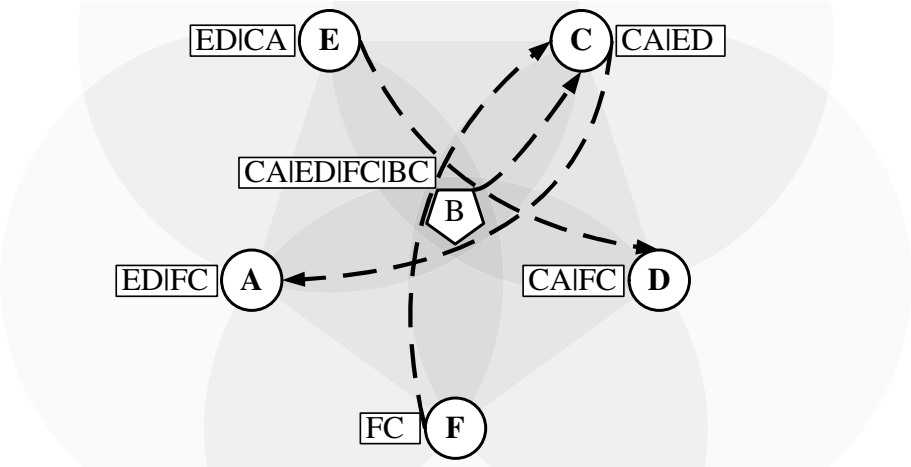

Figure 3.8: Forwarding three dual-hop flows in one timeslot, using $n = 3$-way NC at relay B. The packet BC cannot be supported in the network coding operation, although the other packets can when node B transmits CA+ED+FC. Receivers A, C and D can then recover their respective intended packets.

3.2.5 Learning neighbour state

Excessive network congestion may cause reception reports to collide, and during light network load the updates may reach a coding node too late, due to a minimum threshold update length. For these reasons, a relay must estimate the probabilities of neighbouring nodes possessing

certain packets, in addition to the perusal of reception reports. Network routing information allows a relay to estimate the probability that a neighbouring node overheard a packet that was transmitted to the relay. By performing this investigative analysis, the relay can learn the buffer content of its neighbours. In the case of an incorrect assumption of neighbour packet availability, the relay can just retransmit a newly coded packet to the neighbour with insufficient information. The decision-making process at the relay is illustrated in Figure 3.8.

3.2.6 Coding gain

Network coding gain is defined as the ratio of the number of transmissions required without network coding, to the number of transmissions needed with network coding to deliver the same set of involved packets. In the examples of Figures 3.6 and 3.7, the last network coded transmission consumes one timeslot, instead of the uncoded two. Then, for a total of four transmissions in the uncoded case, a coding gain of four out of three is achieved. When opportunistic listening is omitted in Figure 3.7, then no coding gain will be possible.

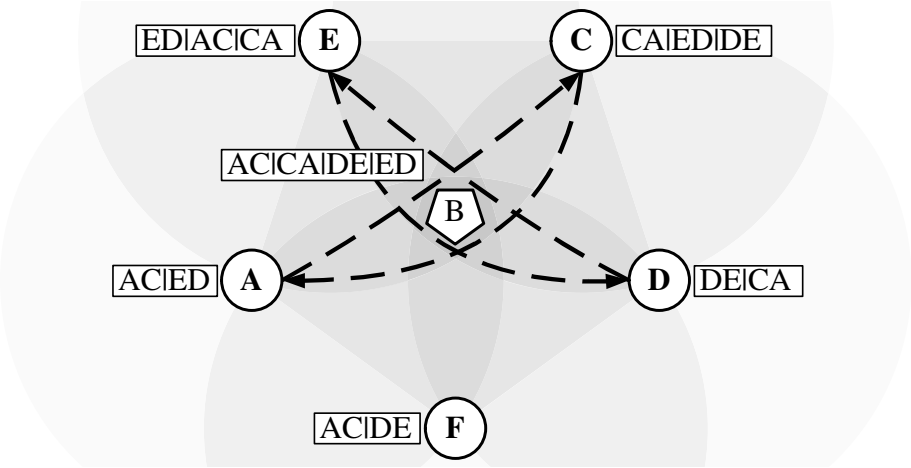

Figure 3.9: Cross topology with inadequate information at nodes A (needs packet DE) and D (needs packet AC). A two-way NC packet AC+DE must first be broadcast by node F, then relay B can broadcast AC+CA+DE+ED and all receivers will then be able to recover their respective packets.

One of the key topologies for analysing the coding gain of COPE, is the cross topology [8]. A modified cross topology is shown in Figure 3.9. Normally, if nodes A and D were in direct contact, a coding gain of eight out of five could be achieved. Uncoded, two transmissions would be required for each of the four opposing flows, and with network coding the last four

packets forwarded by relay B can be done in one timeslot, to give eight out of five. However, since A and D are out of range, an extra network coded packet must be broadcast by node F to give A and D sufficient information to decode the network coded packet to be sent by relay B. In this case, a smaller coding gain of eight out of six can be achieved.

The assumption is made that all the involved flows have infinite load, and the gain is determined without regard for the potential coding overhead, loss of coding opportunities, or packet loss due to medium difficulties. Wireless network coding increases the information rate above the bit rate, and is able to sustain the capacity increase even during full medium utilisation. This contrasts with opportunistic routing [15], which only improves utilisation efficiency when there is little congestion, but does not increase the network capacity.

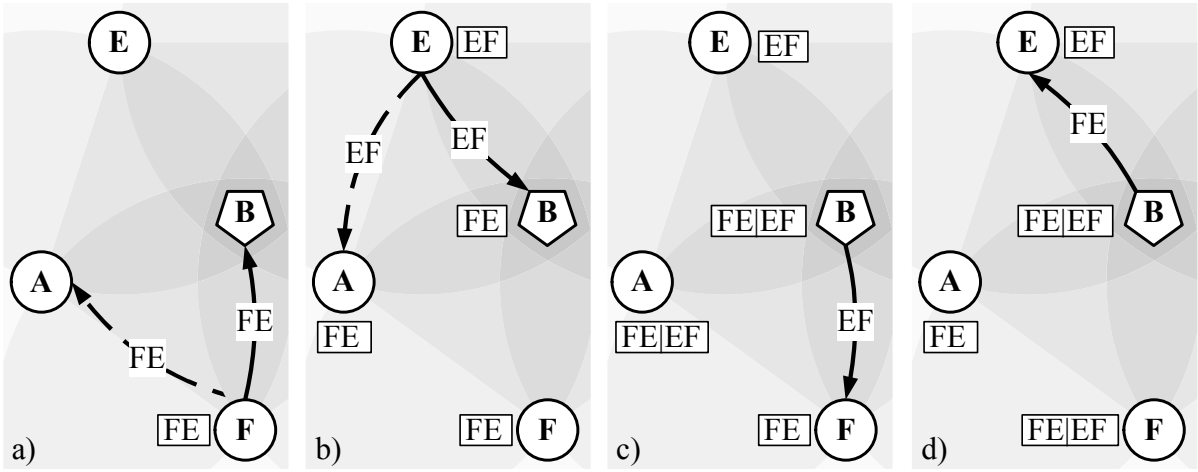

Figure 3.10: Conventional routing without network coding, using an unequal schedule that gives twice the transmission opportunities to the relay B. Timeslots 1-4 are given in subfigures a) to d) respectively.

3.2.7 Coding+MAC gain

In the previous analysis of coding gain, the relay node was afforded all the consecutive timeslots needed to relay its load, as shown in Figure 3.10. In an equal transmission schedule, where each node receives the same number of timeslots per frame, the relay would quickly become backlogged as it is unable to forward the same number of packets it receives per frame. This is where network coding excels in increasing the capacity of the network, since it allows the relay to sink its acquired load in one timeslot, as shown in Figure 3.11. The network coded packet

multicast in the third timeslot in Figure 3.11 c) contains both of the two packets that required two separate timeslots to be transmitted without network coding (Figure 3.10). When these two packets are sent in one timeslot, the limitations of the equal opportunity schedule does not affect the relay any more. Network coding is then effectively able to double the number of packets a relay can forward in a scheduling frame, which in turn doubles the capacity, in the case of Figures 3.6 and 3.7. This gain is termed the coding+MAC (medium access control) gain, which reflects the actual improvement that is experienced by the network.

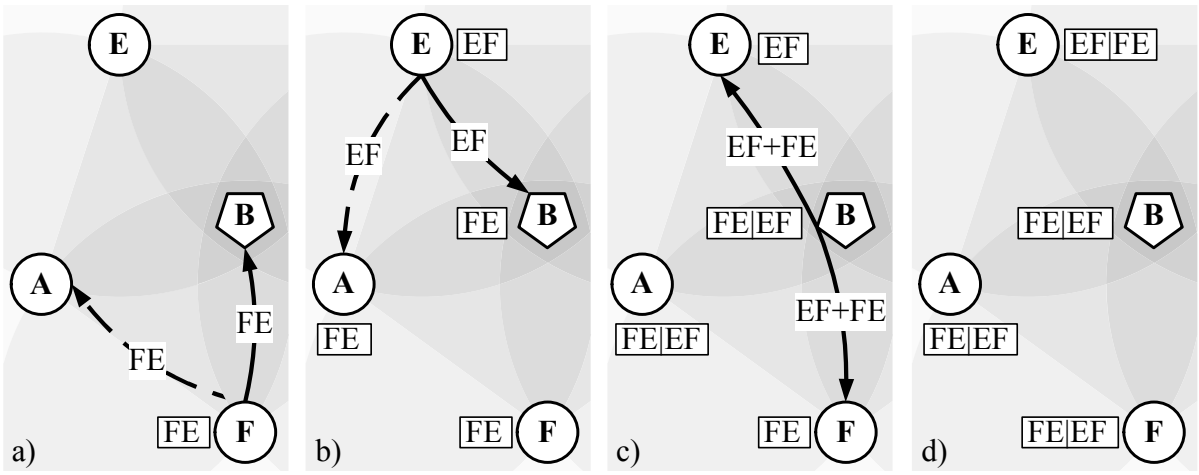

Figure 3.11: Only three timeslots are required to relay two packets over two dual-hop paths with network coding. Timeslots 1-4 are given in subfigures a) to d) respectively.

The Coding+MAC gain is the ratio of the number of transmissions needed without network coding, to the number of transmissions required with network coding, to sink the same set of involved packets, in a network that gives equal scheduled transmission time to every participating node. As a continuation of the example shown in Figures 3.10 and 3.11, the transmissions for the equal schedule without network coding is listed in Table 3.1. Since relay B can only transmit for one timeslot in the scheduling frame, it is unable to unload the two packets it acquires each frame. Six timeslots are needed then, as opposed to the case with network coding, where the relay can unload the two packets it gained in one timeslot.

For proportionally fair schedules, that tend to give greater apparent bandwidth to the more centralised nodes, the coding+MAC gain is reduced. Relays have more transmission opportunities, and are able to sink more of the acquired load, reducing the number of transmissions required. Without opportunistic listening, the maximum possible coding+MAC gain is two, as evidenced in an analysis of the chain topology discussed in [8]. This gain is also

Table 3.1: The coding+MAC gain for a two-component relay chain, with and without network coding for equal and unequal scheduling. The equal schedule, in the subgraph at least, allows the same resources for nodes B, E and F, which for uncoded routing consumes six timeslots to relay two packets.

Timeslot	NC	Uncoded	Uncoded-equal
1	F-(FE)→B	F-(FE)→B	F-(FE)→B
2	E-(EF)→B	E-(EF)→B	E-(EF)→B
3	B-(EF+FE)→F	B-(EF)→F	B-(EF)→F
4		B-(FE)→E	F→B
5			E→B
6			B-(FE)→E
Coding+ MAC gain	6/3 = 2	6/4 = 1.5	6/6 = 1

achievable, as shown in Table 3.1.

3.2.8 Opportunistic bidirectional wireless network coding

Network coding that can be integrated into wireless mesh network functionality can increase capacity in the absence of opportunistic listening or reporting overhead, without the need for control messaging additions. This eases the upgrade of existing networks, and simplifies the operation of new networks, which is beneficial. For these reasons, network coding without opportunistic listening, reception reports or learning of the neighbour states will be employed in this dissertation.

Wireless mesh networks with opposing data flows provide frequent network coding opportunities, where opportunistic listening is not needed for network coding to visibly improve network throughput. In this respect, the term bidirectional is used in terms of data flows and not as a statement of the directionality of a single wireless link. Two flows that traverse the same three nodes, but in opposite directions, present a network coding opportunity where opportunistic listening is not necessary. These network coding opportunities occur especially in the more central parts of the mesh network, where there is a higher density of opposing flows as indicated in Figure 3.12.

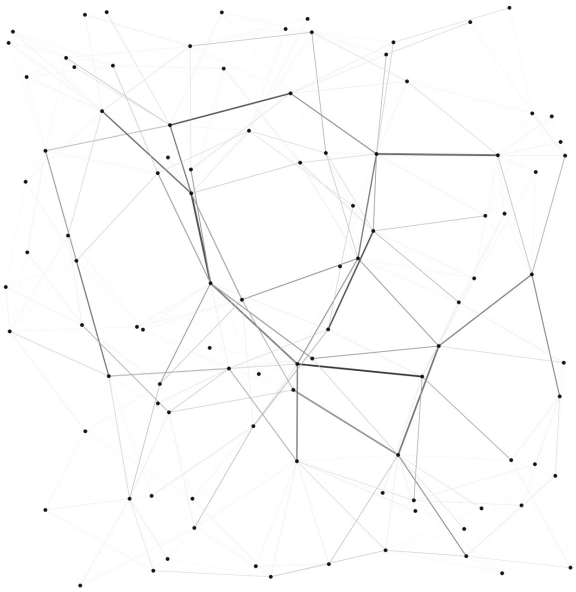

Figure 3.12: Flow load distribution in a 100-node wireless mesh network with equal flow meshing, clearly indicating the central tendency of higher loaded pathways, ideal for network coding without opportunistic listening.

Since the specific scenario depicted in Figure 3.11 achieves the maximum possible coding+MAC gain of two (no opportunistic listening), network coding will be limited to opportunities of only this instance. In the case of wireless meshing, the multihop network moves most of its traffic on centralised 'arteries', much like highways in a metropolitan street system. For equal flow load, this traffic pattern creates ample cross-flow coding opportunities, which will significantly increase throughput if the network coding of Figure 3.11 is harnessed. The specific algorithm for opportunistic bidirectional wireless network coding is given in Algorithm 2.

3.3 THE RELATIONSHIP OF NC TO THE OSI NETWORK MODEL

Cross-layer optimisation is a central theme in this dissertation, and therefore the focus on network coding, which is a very specific coding policy involving multiple OSI layers. Essentially, network coding has only been introduced in the last decade, and it requires an unorthodox integration of decisions on different network layers. There are different types of network coding that involve different OSI layers, as depicted in Figure 3.13. The relationship of network coding to the OSI network model is discussed in this section, where reference is made

Algorithm 2 Opportunistic bidirectional wireless network coding algorithm.

1: **procedure** NetworkCoding(T, **L**)
2: T = Transmitter ▷ A node part of active spatial reuse set
3: **L** = Available links ▷ Temporal reuse set for T, links on which T may transmit
4: **B** = TransmitBuffer(T) ▷ Buffer of packets to be transmitted by T
5: $F_a = \emptyset$ ▷ To store the first packet that can be forwarded
6: **repeat**($l \in$ **L**) ▷ For every usable link in temporal reuse set
7: R = Receiver(l) ▷ Receiver node of link l
8: a = FirstPacket(**B**) ▷ First packet in transmit buffer
9: **while** NextHop(a)$\neq R$ **do** ▷ Compare the next hop of packet a with receiver
10: Advance(a) ▷ Use next packet, until entire buffer is checked
11: **end while**
12: **if** NextHop(a)$= R$ **then** ▷ Suitable packet has been found
13: $F_a = a$ ▷ Store for future use
14: **end if**
15: **until** $F_a \neq \emptyset$
16: **if** PrevHop(F_a)$\in$ **L then** ▷ Temporal reuse set allows for NC
17: F_b = FirstPacket(**B**) ▷ First packet in transmit buffer
18: **while** NextHop(F_b)$\neq$PrevHop(F_a) or NextHop(F_a)$\neq$PrevHop(F_b) **do**
19: Advance(F_b) ▷ Use next packet, until entire buffer is checked
20: **end while**
21: **if** NextHop(F_b)=PrevHop(F_a) and NextHop(F_a)=PrevHop(F_b) **then**
22: $F_{NC} = F_a + F_b$ ▷ Network coded packet
23: **end if**
24: **end if**
25: **end procedure**

to specific kinds of coding approaches and how the network layers are involved.

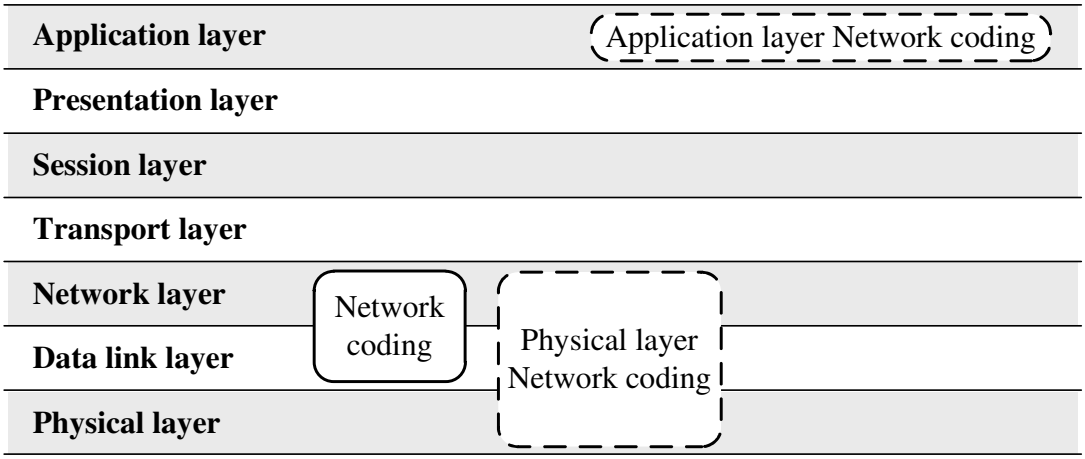

Figure 3.13: Various network coding opportunities in relation to the supporting OSI layers.

3.3.1 Application layer network coding

Random linear network coding is used in Avalanche [16], a peer-to-peer content distribution application by Microsoft. Operating only on the application layer, this type of network coding transmits random linear combinations of packets, together with the encoding vector values, from the server and between the peers. A distribution server divides a file into blocks and network codes blocks together in this manner, so that when a peer has enough randomly coded blocks, the peer can reconstruct the original file. Diversity is afforded through the linear combinations, which make the solution robust against servers leaving early or peers connecting only for the download duration.

As another example of network coding for peer-to-peer content distribution, R-squared was implemented in [17]. Suitable for live peer-to-peer streaming, this protocol takes full advantage of random network coding. A randomised push algorithm is used to relieve peers from having to explicitly request segments. Random network coding is used for each segment, so that multiple peers can serve a client without incurring a messaging overhead. The decoding complexity is reduced with dense linear codes, and priority to segments close to the playback point is given, so that new peers enjoy short buffering delays. These examples serve only to illustrate network coding as it relates to the application layer, and will not be considered further in this dissertation.

3.3.2 Network layer

At the network layer, a relay node has to evaluate its packet buffer in the context of its routing table to recognise network coding opportunities. When opportunistic listening is involved, it even has to take into consideration the buffers of neighbouring nodes. Also, in the absence of opportunistic listening, a relay node can inspect a set of packets to infer the buffer content of the original senders of that packet. When taking into account the intended receivers of those packets, a relay can decide whether neighbours have sufficient information to process a network coded packet.

3.3.3 Data link layer

The data link layer is concerned with transmission over a direct link, and since a relay activates two direct virtual links (multicast), the network coding operation have aspects in this layer as well. Indeed, we show in this work, that channel forward error-correction coding and network coding can become one coding operation. Still, routing decision and intelligence at the network layer is involved for successful network coding, as shown in Figure 3.13.

3.3.4 Physical layer network coding

Even more efficient than conventional wireless network coding is physical layer NC [18], although from a signal processing perspective it is more complex. Understanding that the relay typically does not need the individual packets itself, from which the NC packet is formed, one can go one step further and subsume the communication of the two packets into one timeslot instead of two. So in the example of Figure 3.6, physical network coding allows nodes A and C to transmit their packets AC and CA to relay B at exactly the same time. Here receiver B records the superposition of packets AC and CA, which is in fact a physical layer NC packet. Relay B does not need to separate the two packets; instead it only needs to transmit their sum. Since receivers A and C know the waveform they originally transmitted to B, they can just subtract it from the sum broadcast by relay B to recover their intended packets.

The complication of physical layer network coding is due to wide scope of optimisation spread over three OSI layers. Intricate scheduling decisions now have to be made by not just the relay, but all nodes involved in the network coding operation. This requires network layer and data link layer knowledge about routing and medium access control. Fitting

forward error-correction coding has to be chosen that complements the unique superpositions experienced on the physical layer. For the best performance, the implementation of physical network coding requires a cross-layer optimised design, across the base OSI layers. This type of network coding will, however, not be used in this work.

CHAPTER 4
SCHEDULE ASSIGNMENT

The methodology of sharing the capacity of one medium between a network of nodes is considered in this chapter. Regulating access to the wireless communication medium is one of the key aspects of wireless scheduling, and the different means of access control are discussed. The problems of dynamic medium access and scheduling are explained, and the use of predetermined scheduling is further motivated. Definitions and examples are used to illustrate time and space-time division multiple access, which are used in particular for this study. The relation of scheduling to the OSI model is explained and used to indicate the importance of scheduling in the operation of wireless mesh networks. An algorithm for initial wireless mesh network scheduling is proposed, which is crucial for schedule optimisation and the relaying of new improved schedules in ad hoc networks.

The different manners in which a scheduling frame is populated are explored in this chapter, in particular link and node-assignment. The best situations for and the benefits of each schedule assignment method are discussed, and the results are used to explain the superiority of link-assignment with extended transmission rights. The different schedule assignment methods are analysed in terms of the two concepts of packet depletion and temporal reuse, which are newly defined in this work. It is shown that link-assignment with extended transmission rights can achieve higher schedule usage efficiency and allow for network coding, owing to the added measure of temporal reuse. Figure 4.1 shows the main topics that are covered in this chapter.

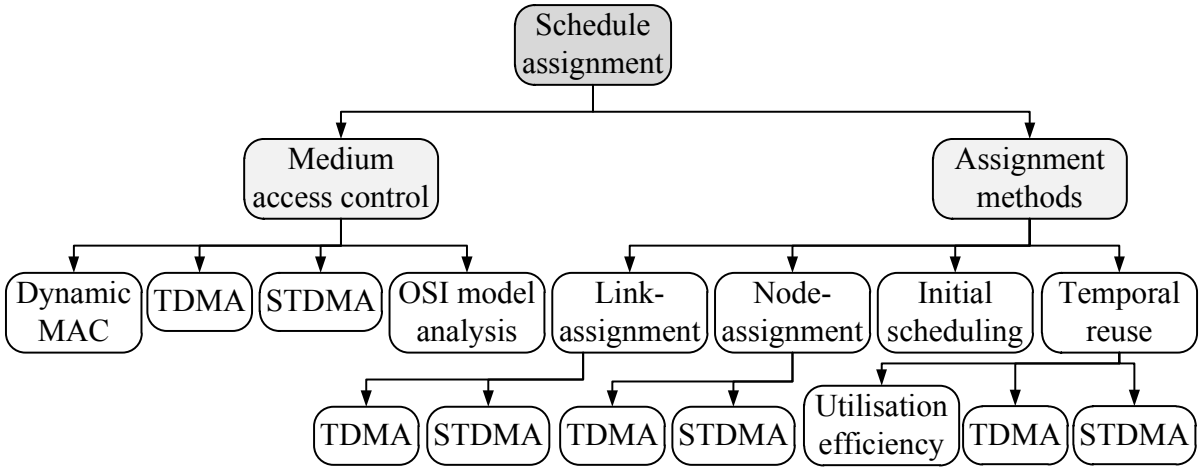

Figure 4.1: The chapter outline of schedule assignment topics discussed.

4.1 MEDIUM ACCESS CONTROL

The network topology defines the usable wireless links in a mesh network, but transmission over those channels has to be coordinated for successful network operation. Local mesh clients have access to the same medium, which has to be shared to provide a transmission opportunity for all links. The communication resource of limited bandwidth has to be rationed in a manner that maintains the threshold SINR of activated links.

Two of the primary methods of bandwidth sharing is frequency division multiple access (FDMA) and time division multiple access (TDMA), where either the frequency band or a time period is divided into segments which are assigned to certain links. Frequency or time segments can be made equal, or unequal, but equality is preferable since it is more amenable to the use of synchronisation. For improved bandwidth management even both multiplexing methods can be employed together, where, for example, an FDMA bandwidth segment is utilised by multiple links through TDMA division of the sub-band. This study will focus on scheduling under the TDMA regime with equal-length timeslots, since time division multiplexing is instrumental in the cross-layer optimisation undertaken in this dissertation.

A distinction is made between predetermined and dynamic scheduling, for either fixed or variable-length timeslots under TDMA. Network nodes that transmit according to the same deterministic network scheduling algorithm, or preset pattern, are not plagued by dynamic MAC issues such as the hidden terminal problem. Predetermined schedules have an affinity for

centralised optimisation, whereas dynamic scheduling involves primarily ad hoc decentralised node operation which is difficult to incorporate in a global optimum. Dynamic scheduling requires more complicated control signalling to manage medium contention, which is not required with predetermined scheduling under synchronisation. The difficulties of dynamic scheduling are explained in greater detail in the following subsection.

4.1.1 Dynamic medium access control difficulties

Medium access control in wireless mesh networks is a difficult problem due to the hidden terminal effect, and for dynamic schedules only non-perfect solutions can be achieved. Two potential transmitters want to communicate with a specific receiver, but if the transmitters are out of sensing range of each other then the second transmitter will interrupt a transmission from the first. Multiple access collision avoidance (MACA [19]) RTS/CTS (request to send/clear to send) handshaking improves the chances for successful data transmission, where the receiver transmits a CTS message to only one of possibly several senders who transmitted contending RTS messages to the receiver. When a sender requires a transmission opportunity it transmits an

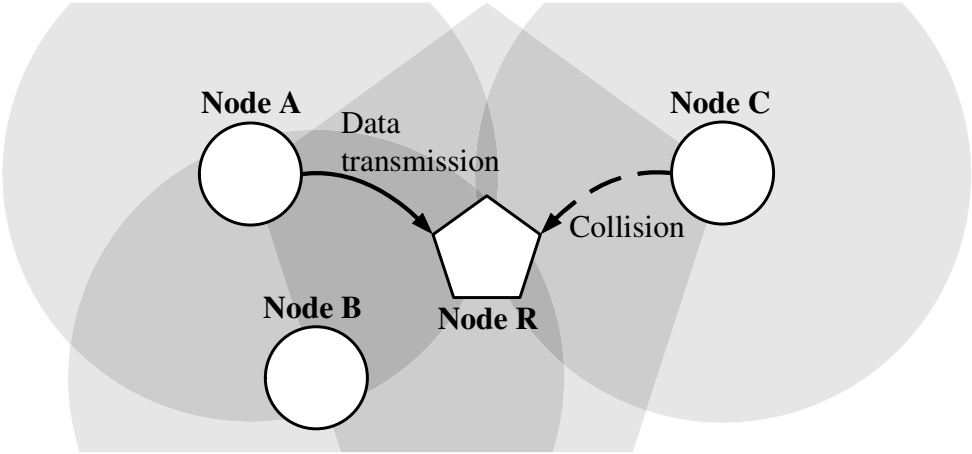

Figure 4.2: The hidden terminal effect. Sender A is busy transmitting to receiver R, but because sender C is too far from A it falsely believes it has a transmission opportunity.

RTS message declaring its need for access to the receiver, as shown in Figure 4.2. The receiver then processes all the RTS messages and with fair access in mind, broadcasts a CTS message stating which sender has the right for data transmission. The RTS/CTS messages contain the sender and receiver addresses, the required length of transmission time et cetera in order for the mesh neighbourhood is aware of the planned medium usage.

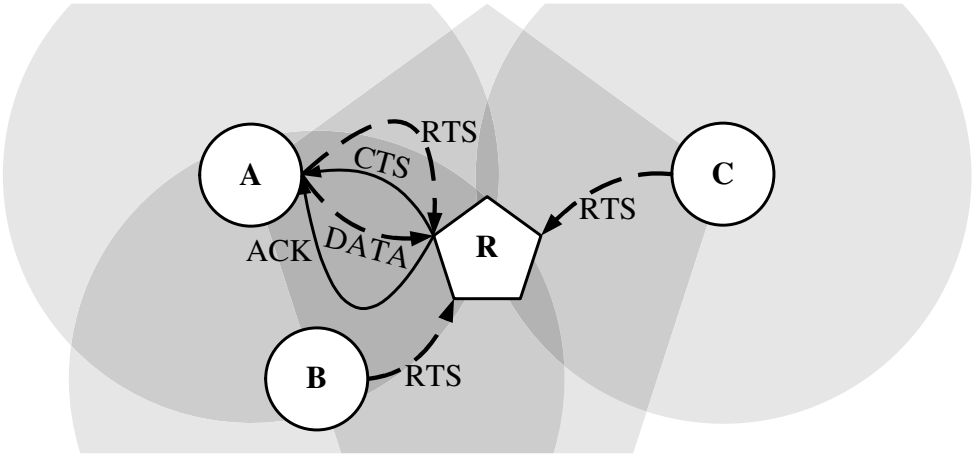

Figure 4.3: Multiple access collision avoidance for wireless (MACAW) where candidate senders contend for a data transmission opportunity using RTS/CTS handshaking.

By acknowledging the correct receipt of the sender's data, the receiver can improve reliability. This is done in multiple access collision avoidance wireless (MACAW [20]), which operates according to the handshake RTS-CTS-DATA-ACK indicated in Figure 4.3. The difficulty of MAC persists since collisions can occur during the RTS message contention phase. Floor acquisition multiple access (FAMA [21]) addresses this issue in part, by requiring that candidate senders sense the channel before broadcasting the RTS, in other words CSMA-RTS-CTS-DATA-ACK. The separation of the control messaging and data transmission is effective in alleviating the hidden terminal problem, although it cannot completely ensure RTS-phase non-collision. Another approach is to have receiver initialised MAC, where transmission authorisation is given to a potential sender by the receiver via a ready-to-receive RTR message. In this manner the receiver polls all of its neighbours to give them a transmission opportunity, as shown in Figure 4.4, and to inform non-intended senders that the sanctioned sender will communicate with the receiver. The RTR-DATA-ACK handshake is employed in multiple access collision avoidance by invitation (MACA-BI [22]) for its ability to avoid collisions during the DATA phase. Control collisions, particularly RTR clashes, can still occur due to the hidden terminal effect. When an RTR collision occurs, a no-transmission-request (NTR) is broadcast to forbid the data transmission. Receiver initialised multiple access - dual polling (RIMA-DP [23]) improves on MACA-BI by allowing a reverse data transmission from the receiver to the sender, in an attempt to minimise control messaging. An RTR-DATA-DATA-ACK handshake is used by RIMA-DP for this purpose.

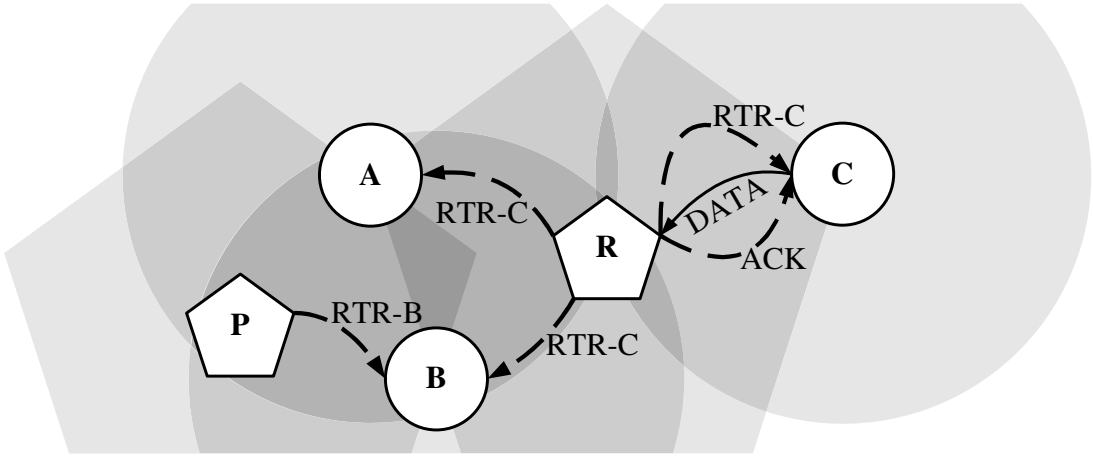

Figure 4.4: Receiver initialised MAC, where receiver R grants a data transmission opportunity to sender C and receiver P to sender B. Since receiver R is out of range of sender P, and receiver P out of range of sender C, sender B can transmit to P whilst C is communicating with R.

4.1.2 Time division multiple access

Networks operating under a predetermined TDMA schedule with fixed-length time divisions, enjoy a number of benefits over dynamic scheduling. Coordinating medium access centrally via a shared schedule for the entire network, allows for integrated optimisation, whereas dynamic scheduling relies on decentralised operation. In addition, with the predetermined schedules, complex control signalling is not needed to regulate medium access as with dynamic scheduling. Simple TDMA scheduling can eliminate the hidden terminal problem completely since it does not employ spatial reuse, and being predetermined it provides perfect medium control.

A predetermined TDMA schedule can be represented as a frame of a limited number of consecutive timeslots, with one network element active per timeslot to prevent the hidden terminal problem. Network elements are referred to here as single network components, physical or conceptual, that interfaces with the communication medium, like nodes or links. For successful network function, the entire frame has to provide transmission opportunities for every essential network element. An essential element is part of a set of critical elements, without which some flows will not be routable. Thus, if the cardinality of the critical set of network elements is K, then the frame of basic TDMA must have at least length K for adequate capacity. The network nodes then operate according to the frame, and repeat the frame when

its end is reached to give continued transmission capacity for the wireless mesh network.

4.1.3 Space-time division multiple access

Nodes in wireless multihop mesh networks generally have a significant transmit radius smaller than the mesh radius, such that multiple hops are required to deliver the longest flows (in terms of hops). This creates a scenario where possibly multiple transmissions can be active in the same timeslot, without the particular receivers experiencing interruption. The opportunity for multiple active links at the same time is termed spatial reuse, since there is a significant spatial distance between the activated links. The necessary condition for a valid spatial reuse set, is for each receiver in the link-set to have sufficient SINR, given the set of activated transmitters. Space-time division multiple access (STDMA) and TDMA are equivalent when all spatial reuse groups in STDMA have only one transmitter. Otherwise, STDMA provides a more efficient schedule, packing more network elements into each timeslot than TDMA.

When the mesh network has a larger average flow hop-count, then the links are more removed in space, and the spatial reuse potential is higher. As the spatial reuse set grows larger, the interference increases from the larger number of transmitters. For denser networks, the threshold SINR may be reduced in order to increase spatial reuse, so that the network can service greater numbers of mesh clients. This is the trade-off that makes the high-noise channel coding region relevant to STDMA networks, since lower SINR means stronger coding is required to combat the high interference. Later in this dissertation, this coding region will be addressed to allow for dense mesh deployments of the future.

4.1.4 Scheduling and the OSI model

Transmission scheduling, whether fixed or dynamic, defines most operational and functional aspects of the wireless mesh network. The timing of a link transmission, the power used, the listening receivers and the achievable flow rates, are all subject to the active schedule. The power limits and transmission rates of each scheduled link is part of the physical layer definition, which sets the power and modulation scheme a link should use when transmitting in a particular timeslot. Regulating access to the communication medium is one of the schedule's most important tasks, to permit transmission rights to all links in spite of the limited bandwidth. This functionality resides in the MAC sub-layer of the data-link OSI layer, and it ensures that

each intended receiver has a sufficient SINR.

The links defined in the data-link layer are related to the network flows, defined in the network layer, via the link-flow incidence matrix R given in Chapter 3. The schedule should use the link-flow incidence matrix as an optimisation tool, since R gives the relative routing loads of the links, which are important utility measures. In the transport layer the flow rates are regulated, and here the design of a schedule affects the achievable rates. The higher OSI layers are thus concerned with flow fairness and rates, and the transmission scheduling can be set up so that certain flow objectives can be realised. The relation of transmission scheduling to the OSI model is indicated in Figure 4.5.

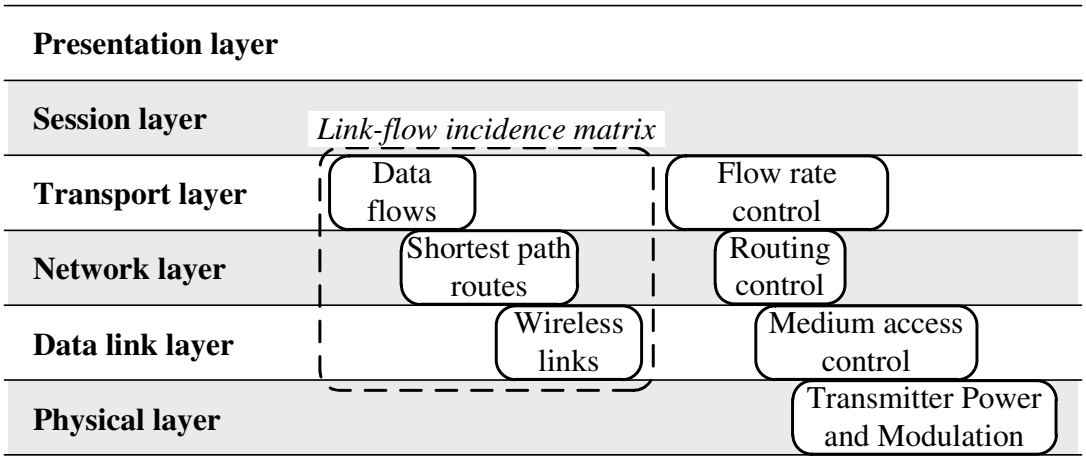

Figure 4.5: Transmission scheduling in relation to the OSI layers.

4.2 SCHEDULE ASSIGNMENT METHODS

Given the user multiplexing method of TDMA, with or without spatial reuse, a schedule assignment strategy has to be formulated to actually assign capacity for the network. If only a transmitter or receiver is scheduled, then the bandwidth sharing becomes dynamic and the hidden terminal problem becomes an issue. Thus, the smallest network element that can be scheduled is a single directed link. A transmitter node can also be scheduled, or at least the set of outgoing links pertaining to a certain node, to clearly control medium access.

The two predominant transmission schedule assignment methods are thus node- and link-assignment, and while node-assigned schedules [24, 25] can perform NC and have better

usage efficiency, they lack the higher spatial reuse and finer granularity for optimisation achieved by link-assigned schedules [26–28]. Preference is given to link-assignment since it is more amenable to cross-layer optimisation and it can achieve greater capacity owing to better spatial reuse. In this subsection illustrations of the workings of these two assignment methods are given, both with and without spatial reuse, and their properties are discussed.

Initial schedule assignment is discussed in this section, to address how a newly formed or changed mesh network communicates topology information for centrally optimising a schedule. This first schedule assignment is crucial to obtain an optimised schedule, and to update mesh clients with new schedules. The schedule, as a form of medium access control, is required for the control signalling and information gathering that can allow for more refined schedules to be calculated and advertised.

4.2.1 Link assignment

The most basic network element that can be scheduled in a timeslot is a directed wireless link from one transmitter node to another single receiving node. A complete and valid TDMA scheduling frame must provide capacity for the critical link set, so that all network flows can be routed. Whether for simplex TDMA or when the spatial domain is reused, the active spatial reuse set must allow for adequate receiver SINR as formulated in Equation 2.1.

Since links are not grouped together as in node-assigned scheduling, greater assignment variation is possible with spatial reuse, which gives better optimisation results. Another benefit owing to the finer granularity is improved spatial reuse, although the resultant temporal reuse is non-existent. Network coding is not possible with a link-assigned schedule, unless transmission rights are extended. Typically, link-assigned schedules have longer frames, but no node-based scheduling algorithm is required as with node-assigned scheduling. A link-assigned schedule contains a complete MAC definition, as opposed to node-assigned scheduling where each node needs to manage the transmissions on its various links.

4.2.1.1 Link-assigned TDMA

An example of link-assigned TDMA network operation is shown in Figure 4.6. The arrays of short vertical lines represent the links in the network and indicate in bold lining the currently

activated link for the particular timeslot. Only one link is permitted to transmit in any timeslot for link-assigned TDMA, and this is the case for the specific schedule in Figure 4.6. For L links, it is then clear that the most basic TDMA schedule will require also L timeslots to satisfy the critical link demand. Since no spatial reuse is utilised, the original link definitions still hold, so all links are assumed to have sufficient SINR by design.

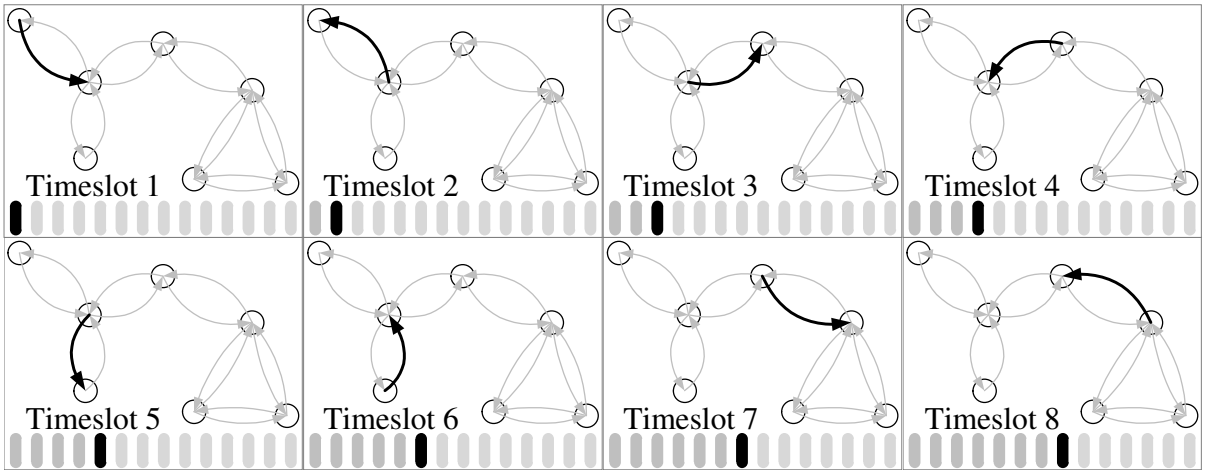

Figure 4.6: The first eight timeslots in a simplex TDMA scheduling frame of length 14, for a sample multihop mesh network.

4.2.1.2 Link-assigned STDMA

When a set of links are sufficiently removed in space, such that their receivers do not receive significant interference, then that set can be scheduled in one timeslot. The SINR requirement formulated in Equation 2.1 will be met by a valid spatial reuse group. In Figure 4.7 an example of link-assigned STDMA is shown, where in some timeslots multiple links are scheduled simultaneously. In the first timeslot the two indicated links may transmit at the same time for the duration of the timeslot, since each receiver has sufficient SINR. The schedule is set up so that each network link has at least one timeslot available for transmission, but the specific schedule will not necessarily give the best performance. This is the case since the single link in timeslot seven allows for other links to transmit simultaneously, but the example serves only to illustrate the concept of link-assigned STDMA. The result is a schedule that has half the size of a plain TDMA schedule, due to an average spatial reuse of two links per timeslot.

The link-assigned STDMA schedule employed in the simulations of this dissertation,

uses a packing heuristic [29], which packs as many links as have not yet transmitted into a timeslot. The scheduling program is shown in Algorithm 3, where spatial reuse groups are formed with maximum link inclusion, first satisfying links with positive demand. An urgency value assigned to each link gives preference to links which were included a longer time ago. When the unsatisfied links have been checked for possible inclusion, the satisfied links are checked as well to maximise spatial reuse. The procedure `SimultaneousLinkValid()` checks if the threshold SINR values are met for all receivers in the expanded spatial reuse clique, if a link addition is made. Since some links carry more traversing flows, like the more centrally located ones, a traffic-adaptive version of this algorithm can also be used as in [30]. The traffic-adaptive version will give higher demands for links routing more flows, to create a fairer schedule.

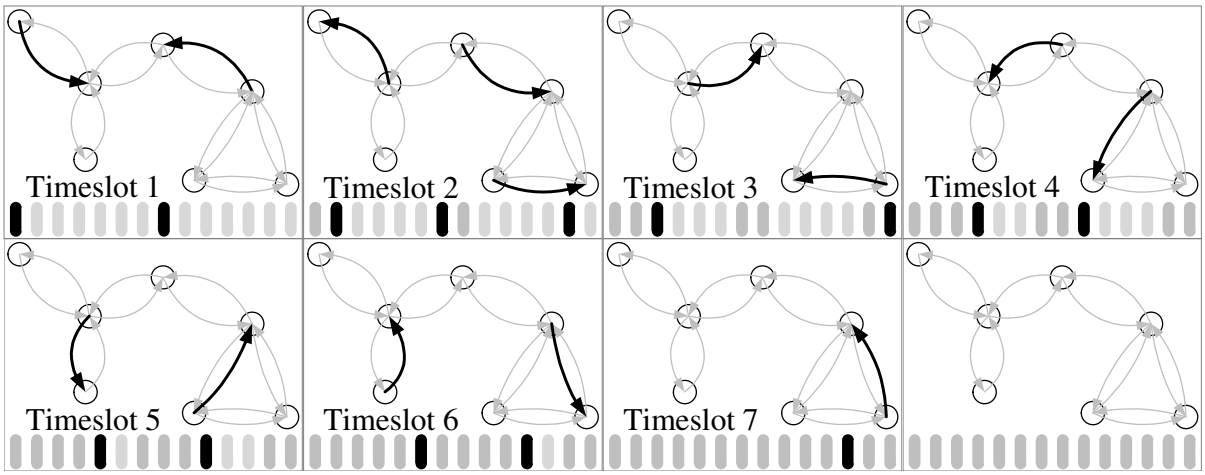

Figure 4.7: Non-optimal link-assigned STDMA seven-slot frame satisfying critical capacity demand.

4.2.2 Node assignment

Instead of scheduling single links, single nodes can be assigned to timeslots in a TDMA schedule. The nodes that are assigned serve the role of transmitter, but successful medium access is guaranteed, unlike with dynamic MAC such as MACAW where collisions can still occur during the RTS message contention phase. This is achieved by ensuring adequate SINR for the receivers of each outgoing link of the scheduled node, especially when spatial reuse is considered. However, since a collection of links pertaining to a certain node has to contend for the same timeslot, each scheduled node has to execute a scheduling algorithm of its own to

share a timeslot between multiple links. So, while node-assigned schedule frames tend to be shorter than link-assigned frames, extra control and definition is required at the nodes, which reduces optimality. Since all the outgoing links of a node is scheduled in one timeslot, such a schedule enjoys full temporal reuse. Node-assigned schedules do, however, not in general achieve the spatial reuse of link-assigned schedules. The simultaneous grouping of the links of a node also gives less optimisation control.

4.2.2.1 Node-assigned TDMA

Assigning one transmitter node to a timeslot is a very basic way to create a TDMA schedule, as displayed in Figure 4.8. The default link SINR values are maintained, since only one transmitter is active, and so no SINR adequacy checking is required. Seeing that all outgoing links of a node is scheduled in the same timeslot, the resulting schedule frame is shorter than with link-assigned TDMA. It should be noted that the set of scheduled links do not simultaneously transmit in one timeslot, but the timeslot is rather reused over successive frame repetitions to serve all the links. Due to this extra node-based scheduling requirement, a node-assigned schedule is not necessarily more efficient (in terms of throughput) than a link-assigned one.

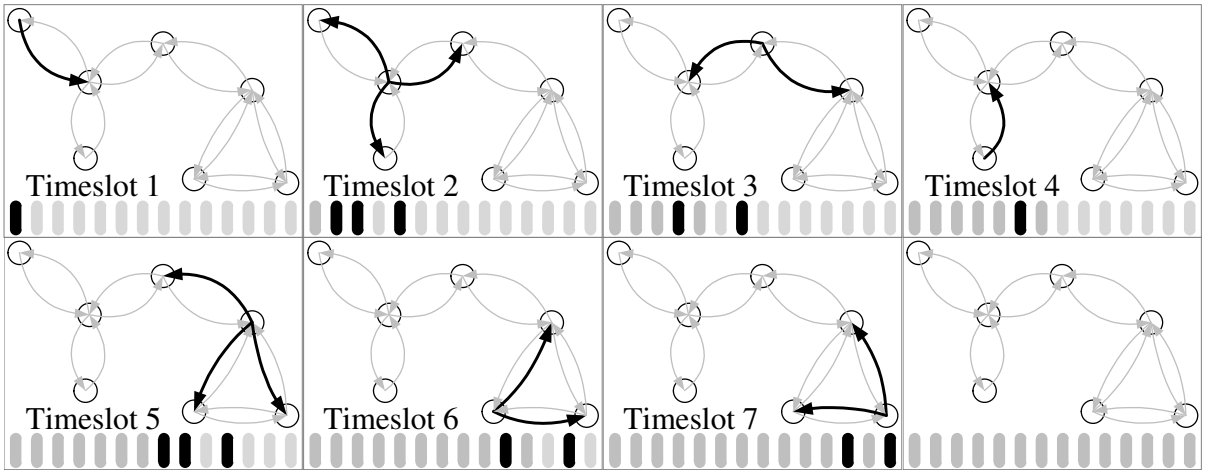

Figure 4.8: A node-assigned TDMA equivalent of the example in Figure 4.6.

4.2.2.2 Node-assigned STDMA

Multiple nodes can also be scheduled simultaneously, although the spatial reuse tends to be less than with link-assigned scheduling. This is due to the fact that more links at each node should have sufficient SINR, which increases the areas of influence in the network. The reduced

Algorithm 3 Link-assigned STDMA schedule assignment algorithm.

procedure LINKSTDMA($\mathcal{L}$)
  D= (**D**(l) = 1, l $\forall\mathcal{L}$) ▷ Demand: Link once or the number of flows using the link
  U= (**U**(l) = 1, l $\forall\mathcal{L}$) ▷ Urgency: When last was a link included?
  A= $\mathcal{L}$; **B**= $\emptyset$; **S**= $\emptyset$ ▷ Unsatisfied links; Satisfied links; Empty schedule
  repeat ▷ Until all links satisfied
    Atemp=**A**; **Btemp**=**B**; **L**= $\emptyset$ ▷ Temporary arrays; Empty spatial reuse linkset
    repeat ▷ Until all unsatisfied links checked
      $l = \arg_{m\in\mathbf{Atemp}}\max(\mathbf{D}(m)\cdot\mathbf{U}(m))$ ▷ Link with maximum demand×urgency
      if SimultaneousLinkValid(**L**, l) **then** ▷ Can add link to set
        L.add(l); **D**(l)=**D**(l)-1; **U**(l)=0 ▷ Extend linkset; Reduce demand, urgency
        if **D**(l)= 0 **then** ▷ Satisfied
          B.add(l); **A**.remove(l) ▷ Not unsatisfied
        end if
      end if
      Atemp.remove(l) ▷ Link already checked
    until **Atemp**= $\emptyset$ ▷ Check all unsatisfied links
    repeat ▷ Until all satisfied links checked
      $l = \arg_{m\in\mathbf{Btemp}}\max(\mathbf{D}(m)\cdot\mathbf{U}(m))$ ▷ Link with maximum demand×urgency
      if SimultaneousLinkValid(**L**, l) **then** ▷ Can add link to set
        L.add(l); **U**(l)=0 ▷ Extend linkset, null urgency
      end if
      Btemp.remove(l) ▷ Link already checked
    until **Btemp**= $\emptyset$ ▷ Check all satisfied links
    S=[**S**, **L**] ▷ Add spatial reuse linkset to schedule
  until (**B**= $\mathcal{L}$) ▷ Is there an unsatisfied link?
end procedure

spatial reuse can be seen in Figure 4.9, where an average spatial reuse of $7/4 < 2$ is achieved, which is less than with link-assigned STDMA. Temporal reuse is increased with node-assigned STDMA however, and a temporal reuse of $8/4 = 2$ is achieved here. This schedule frame is even shorter than link-assigned STDMA, owing to the high temporal reuse and spatial reuse, but its efficiency is not necessarily greater.

Similar to the link-assigned STDMA scheduling Algorithm 3, node packing is done to maximise spatial reuse in node-assigned STDMA scheduling shown in Algorithm 4. Unsatisfied nodes are first checked if they can be successfully included into a spatial reuse node group, then satisfied links are checked, with the goal of spatial reuse maximisation. The function `SimultaneousNodeValid()` establishes whether the inclusion of a new node will cause the involved link SINR values to decrease below the threshold. When a node can be added such that all the links of all the included nodes have sufficient SINR values, then the clique is extended. The traffic-adaptive version assigns node demands according to the collective flow load experienced by the links of a certain node, to deliver a more fair transmission schedule.

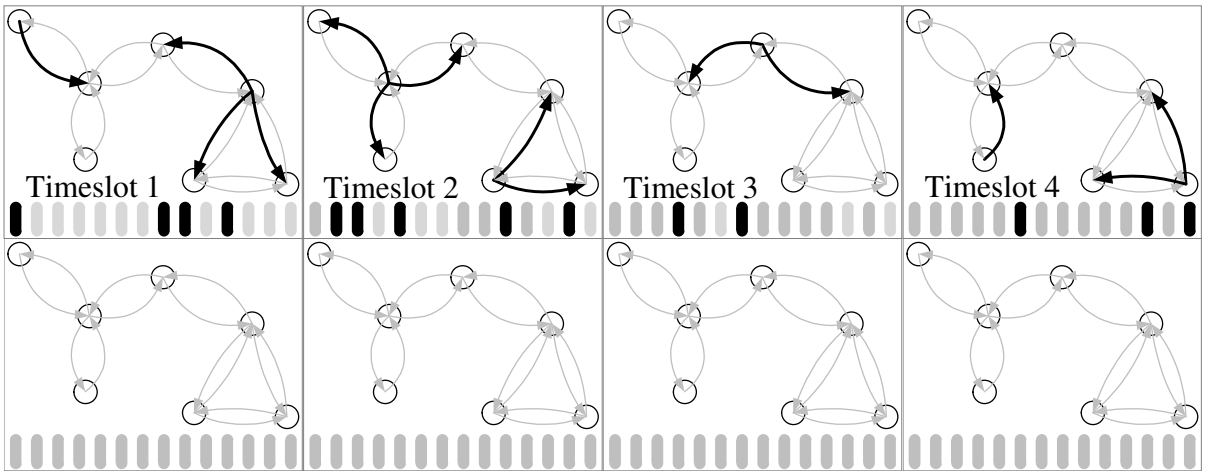

Figure 4.9: A more compact node-assigned STDMA schedule with spatial reuse.

4.2.3 Initial scheduling

During mesh network deployment, each node n gets a unique timeslot assignment $t_n \in [1, T]$, in a TDMA frame of length T. Node clocks are also synchronised, so that each node will transmit during the correct timeslot. A global or local synchronisation pilot signal can be established

Algorithm 4 Node-assigned STDMA schedule assignment algorithm.

procedure NODESTDMA($\mathcal{N}$)
  D= (**D**(n) = 1, n $\forall\mathcal{N}$) ▷ Demand: Node once or the number of flows using the node
  U= (**U**(n) = 1, n $\forall\mathcal{N}$) ▷ Urgency: When last was a node included?
  A= $\mathcal{N}$; **B**= $\emptyset$; **S**= $\emptyset$ ▷ Unsatisfied nodes; Satisfied nodes; Empty schedule
  repeat ▷ Until all nodes satisfied
    Atemp=**A**; **Btemp**=**B**; **N**= $\emptyset$ ▷ Temporary arrays; Empty spatial reuse nodeset
    repeat ▷ Until all unsatisfied nodes checked
      n = arg$_{m\in\mathbf{Atemp}}$max (**D**(m) · **U**(m)) ▷ Node with maximum demand×urgency
      if SimultaneousNodeValid(**N**, n) **then** ▷ Can add node to set
        N.add(n);**D**(n)=**D**(n)-1;**U**(n)=0 ▷ Extend nodeset; Reduce demand, urgency
        if D(n)= 0 **then** ▷ Satisfied
          B.add(n); **A**.remove(n) ▷ Not unsatisfied
        end if
      end if
      Atemp.remove(n) ▷ Node already checked
    until Atemp= $\emptyset$ ▷ Check all unsatisfied nodes
    repeat ▷ Until all satisfied nodes checked
      n = arg$_{m\in\mathbf{Btemp}}$max (**D**(m) · **U**(m)) ▷ Node with maximum demand×urgency
      if SimultaneousNodeValid(**N**, n) **then** ▷ Can add node to set
        N.add(n); **U**(n)=0 ▷ Extend nodeset, null urgency
      end if
      Btemp.remove(n) ▷ Node already checked
    until Btemp= $\emptyset$ ▷ Check all satisfied nodes
    S=[**S**, **N**] ▷ Add spatial reuse nodeset to schedule
  until (**B**= $\mathcal{N}$) ▷ Is there an unsatisfied node?
end procedure

to guide the timings of all nodes. Now, with the simple predetermined TDMA schedule, each node transmits at maximum power $P_{\max}$ during their timeslot. Each node records the power received for each timeslot in the frame, with the purpose of forming a topology image from the resulting interference matrix J. Node j will record received interference power J_{ij} during the timeslot of node i, and from this the gain $Q_{ij} = J_{ij}P_{\max}^{-1}$ can be calculated.

Once an entire frame has been cast, a second frame commences wherein each node i broadcasts its interference vector J_{*i}. Each neighbouring node with sufficient SNR stores the overheard vector, and forward broadcasts it together with its own interference vector and other overheard vectors. This topology broadcast continues until all nodes have forwarded all their own and overheard interference vectors. In this manner, an IGW or other powerful processing node can obtain the interference matrix J and consequently the gain matrix Q. Having these measures, the simple link-assigned TDMA schedule can be replaced throughout the network with a schedule optimised at a central node.

4.3 TEMPORAL REUSE

Spatial reuse is the reuse of a timeslot by simultaneously activated links, with sufficient SINR, in the spatial domain. Likewise, temporal reuse is defined here as the reuse of a timeslot by a group of links in the time domain. A temporal reuse group is the set of outgoing links from a particular node that may transmit in a certain timeslot. Since a transmission schedule is composed of a T-length frame that is repeated in time, every timeslot in the frame is repeated at frequency $1/T$. This means that the links in a temporal reuse group will share the capacity of a timeslot over all the repetitions of the timeslot in which the temporal reuse group appears. The reuse of a timeslot in the time domain thus refers to a timeslot, at a particular location in the scheduling frame, that is reused by a group of links as the specific timeslot reoccurs with the repetition of the frame in time.

Node-assigned schedules enjoy full temporal reuse, at the expense of secondary schedule requirements at transmitting nodes. A measure of temporal reuse can be given to link-assigned schedules, without the need for additional scheduling policies, by assigning priorities to links in the temporal reuse sets. This prioritised temporal reuse for link-assigned scheduling was

first proposed in [1] as link-assignment with extended transmission rights (LET), although the relationship to temporal reuse was not brought to light. This section extends the work in [1] by characterising the networks that can benefit from temporal reuse, in terms of the concepts of packet depletion and temporal reuse that are newly defined in this work.

Packet depletion is defined here (and in [31]) as the condition where a scheduled link does not have packets to transmit, resulting in a wasted timeslot with link-assigned scheduling. When a transmitting node does not have a packet ready for a scheduled link, then the timeslot can be used to transmit on another link instead. In this manner, a timeslot is reused by multiple links over the continuous repetition of the limited-length scheduling frame. Temporal reuse is important in transmission scheduling, as it is a means to share capacity and improve schedule usage efficiency. This term is explained further in this section, and the networks that can have improved efficiency with temporal reuse are also characterised.

4.3.1 Motivation

Node-assigned schedules [24] have to employ a form of temporal reuse to provide capacity for every outgoing link associated with a scheduled node. Here secondary scheduling is involved, where every node has to decide how to divide its available capacity between its outgoing links. Having multiple link options per node results in higher capacity usage efficiency, at the expense of reduced spatial reuse. Due to packet depletion, node-assigned schedules can achieve higher usage efficiency than normal link-assigned schedules. The downside is reduced spatial reuse, since the scheduling of all the links of a node extends the interference.

Alternatively, link-assigned schedules with extended transmission rights can achieve some measure of the same improved efficiency of node-assigned scheduling with better spatial reuse, which results in a higher schedule capacity. A spatial reuse group is first established, as with normal link-assigned STDMA, and then transmission rights are extended to all alternate links, of scheduled nodes, with sufficient SINR. The links in the extended temporal reuse set are prioritised primarily so that secondary scheduling is not required, which would complicate global optimisation. The link prioritisation sets LET apart from temporal reuse in regular node-assigned scheduling, and prioritisation also serves to allow for a more concise network capacity estimation under temporal reuse. The initial spatial reuse group

forms the highest priority linkset, and the additional links are further given lower priorities on a node-centric basis. This means that the reserve links of a node are assigned different priorities, and that links from other nodes are not involved in that particular priority assignment.

In addition, by extending a link assignment to a prioritised group of links, the schedule allows for the implementation of opportunistic network coding, which further improves performance, as in the case of node-assigned scheduling. Normal link-assigned scheduling does not employ temporal reuse, and the fact that only one link per node is sanctioned for transmission, makes network coding impossible, since it requires a multicast on at least two outgoing links of the same node. Node-assignment achieves the highest temporal reuse, and thus has more network coding opportunities given the right secondary scheduling. Link-assignment with temporal reuse can only normally achieve a sub-unity fraction of the temporal reuse and network coding opportunities of node-assigned scheduling. However, with the increased spatial reuse and global optimisation, link-assigned scheduling with temporal reuse can outperform node-assigned scheduling.

4.3.2 Schedule utilisation efficiency

A link must have a packet to transmit every timeslot that it is scheduled, otherwise a usage inefficiency occurs due to packet depletion. The networks that can experience packet depletion and the associate usage inefficiencies are characterised in this subsection. Predefined schedule frames with a limited number of timeslots provide capacity π_l for each link l, where π_l packets per timeslot can be added to a data flow randomly chosen according to a uniform distribution, such that the schedule will be able to handle the resultant load on l.

Let p_l be the probability that a packet added to a random flow will have to be routed on a link l, and let $T_l \approx c_l^{-1}$ be the average number of timeslots between the start of successive scheduled timeslots for link l with continual repetitions of the scheduling frame. The link scheduling period T_l is approximately the inverse of the link rate c_l, if the schedule is composed in a cyclical manner so that multiple schedulings of a link rate vector are as far removed in the scheduling frame as possible. Then the average number of packets that have to be sent in a

scheduled timeslot of link l is given by $\eta_l(\pi)$, for a global flow load π, as in

$$\eta_l(\pi) = \sum_{i=1}^{\lfloor \pi T_l \rfloor} i \prod_{j=0}^{i-1} \frac{(\lfloor \pi T_l \rfloor - j)}{j+1} (p_l)^i (1-p_l)^{\lfloor \pi T_l - i \rfloor} \tag{4.1}$$

Equation (4.1) also represents the efficiency of the schedule in terms of link l, where at most one packet can be transmitted per timeslot. This formulation sums the products of the probability that a certain number of i packets will be added to l in between successive schedulings of l with the number of packets i, to get the average number of added packets for l in each of its scheduled timeslots. This is a monotonically increasing function that relates a global load to a locally resultant load at a specific link l. The full efficiency load for link l is then the solution to $\eta_l(\pi_l) = 1$, which equates to the applied global load that will fully utilise the specific link capacity provided by the schedule. The globally applied flow load is upper bounded by the link capacity that is saturated first, thus the maximum packet load per timeslot is $\widehat{\pi} = \min_{l \in \mathcal{L}} \pi_l$. Thus for every link with $\pi_m > \widehat{\pi}$ the average utilisation efficiency is $\eta_m(\widehat{\pi}) < 1$, which means that the maximum load allowed is too small to make full use of the available capacity for link m.

Full schedule utilisation can thus only be achieved when $\eta_l^{-1}(1) = \eta_m^{-1}(1), \ \forall l, m \in \mathcal{L}$, otherwise for any inequality $\pi_l < \pi_m, \ l \neq m$ it must mean that $\eta_l(\pi_l) < 1$. The global load may not exceed the minimum π_l, because then link l will experience a load greater than its capacity, so only when the full efficiency loads for all the links are equal can every link be saturated without exceeding the capacity of any one link. For networks with spatial reuse and multihop flows it becomes more difficult to calculate schedules that give equal full efficiency load π_l for each link $l \in \mathcal{L}$, and even if it is achieved, there is still no trivial guarantee that the schedule will achieve optimal schedule capacity and fairness. The optimisation problem is thus further constrained by $\eta_l^{-1}(1) = \eta_m^{-1}(1), \ \forall l, m \in \mathcal{L}$, which mainly constrains the link scheduling periods T_l, rather than flow-link probabilities p_l, which are determined by the network topology and routing.

By extending transmission rights to alternative links in the case of packet depletion, the unused timeslots of the unsaturated links can be used to increase the capacity for most of the links in the network to $\pi_m + \varepsilon_m$. Consequently the maximum schedule capacity will be increased to $\widehat{\pi} = \min_{l \in \mathcal{L}}(\pi_l + \varepsilon_l)$ and the schedule will have a higher possible usage efficiency due to the applied temporal reuse.

4.3.3 Link-assigned TDMA with temporal reuse

The simple link-assigned TDMA schedule in Figure 4.6 can be extended with LET, which would increase the usage efficiency and enable network coding, as shown in Figure 4.10. The same number of timeslots is used, but now when the primary link does not have packets the reserve links may be used. This will reduce wasted timeslots, and in addition, network coded packets can be multicast under certain circumstances when there are additional links with transmission rights at a node.

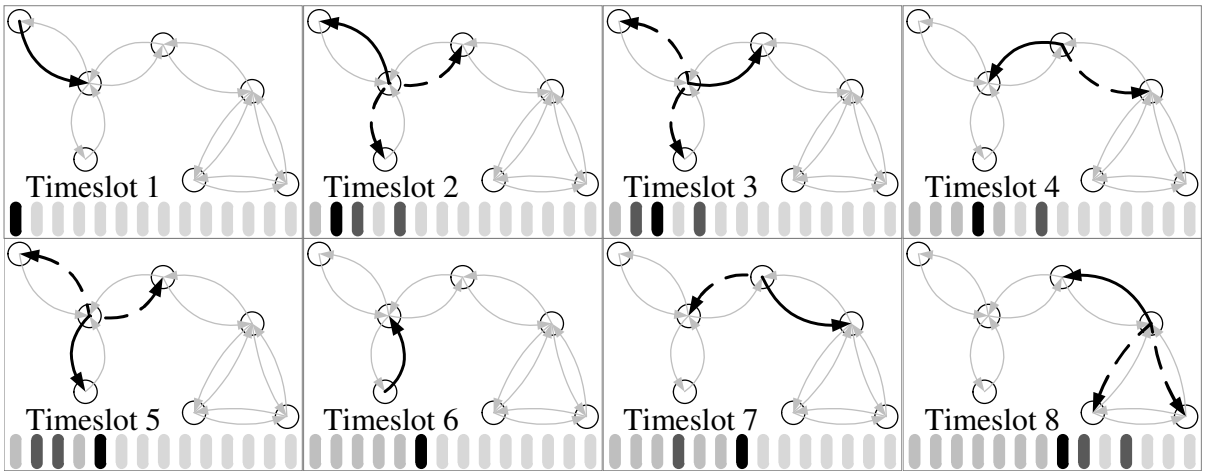

Figure 4.10: Link-assignment with extended transmission rights, or link-assigned TDMA with temporal reuse.

4.3.4 Link-assigned STDMA with temporal reuse

For link-assigned STDMA shown in the example of Figure 4.7, the transmission rights of scheduled nodes can also be extended, but because of the spatial reuse the temporal reuse will be less than with node-assigned scheduling. The schedule with the extended transmission rights is thus depicted in Figure 4.11, where the same number of timeslots are used as in link-assigned STDMA.

An equivalent scenario of critical link-set fulfilment, as with node-assigned STDMA, can be created as indicated in Figure 4.12. Comparing this compacted schedule to node-assigned STDMA in Figure 4.9, it can be seen that the same frame-size is achieved. The spatial reuse for node-assigned STDMA is $7/4$ and the temporal reuse is $14/7 = 2$, while the spatial reuse for link-assigned STDMA with LET is $9/4 > 7/4$ and the temporal reuse here is $15/9 < 2$. As expected, the spatial reuse is greater and the temporal reuse less with LET, but the same

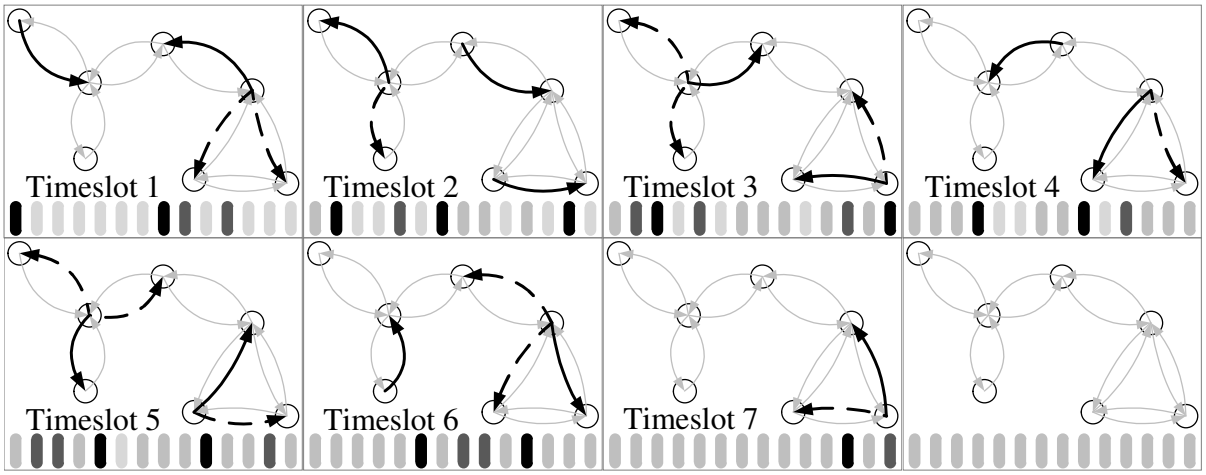

Figure 4.11: Link-assigned STDMA with prioritised extended transmission rights, higher utilisation efficiency and network coding support.

number of timeslots are required.

Additional benefits may be gained with LET however, since it integrates more easily into an optimisation framework. The integrated secondary scheduling with LET also makes capacity estimation easier than with node-assigned scheduling, which makes LET more appropriate for use in optimisation. In practice, the LET schedule frame in Figure 4.12 will not be as short, but a separate timeslot will be dedicated to each link to have first priority. Such a schedule may, or may not perform as well as a node-assigned schedule.

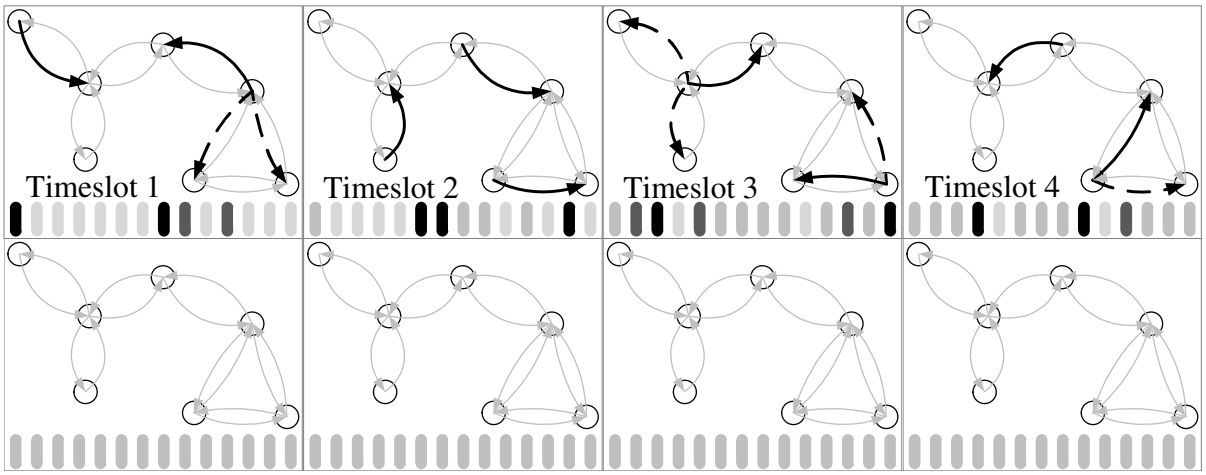

Figure 4.12: Compacted link-assigned STDMA with LET, catering for the critical link-set.

CHAPTER 5
SCHEDULE CAPACITY

One of the most important measures of network performance is schedule capacity, which is calculated in this chapter. Having formed the network topology and the links of the wireless mesh network, and having defined the particulars of medium access control, the transmission scheduling needs to be optimised. The primary utility of schedule performance is the capacity that a network can achieve under the control of the schedule. This utility serves as a metric of comparison to evaluate the goodness of a schedule, and to facilitate in the planning of the wireless network and its usage. Specifically, the capacity is measured as the optimal set of link transmission rates that can be achieved, which is referred to as the link transmission capacity or rate region of the network.

From the viewpoint of optimisation, the link rate region defines the multivariate space that restricts the transmission rates that can be achieved by the wireless links. Since the links of a network share the same communication medium, the achievable transmission rate of a link depends on the transmission rates of the rest of the links, and thus forms a rate possibility space. The rate region is then used to restrict the link transmission rates when optimising the schedule, in terms of its spatial and temporal reuse groups and their duration in the transmission schedule.

The link transmission rate region of link-assigned STDMA is reviewed from [32] in this chapter, and those principles are used to formulate the temporal reuse-aware rate region applicable to link-assigned STDMA with extended transmission rights (LET). The capacity region formulation is then simplified and a feasible sub-optimum is obtained by relying on link

prioritisation. This inherent secondary scheduling in LET makes capacity estimation possible, as opposed to node-assigned scheduling where a separate definition of secondary scheduling is required. The issues and calculations that are covered in this chapter is shown in Figure 5.1.

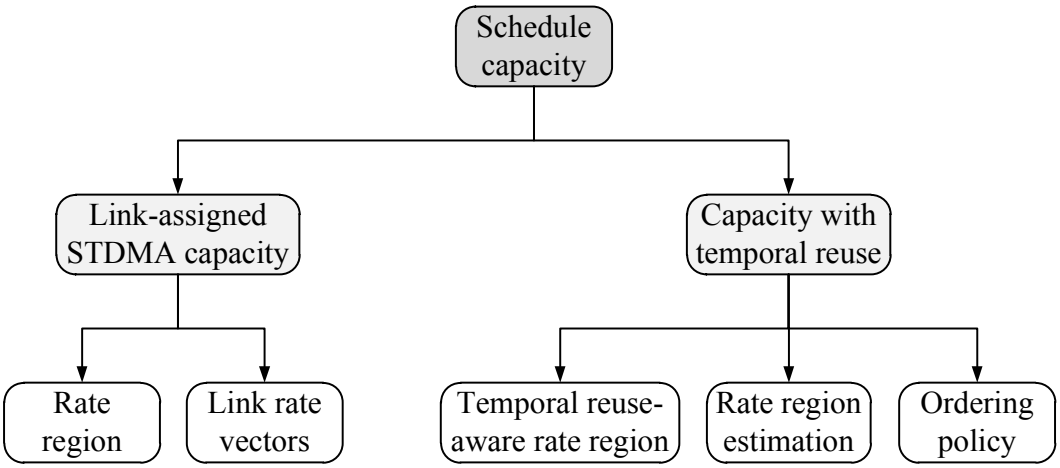

Figure 5.1: An outline of the topics discussed in this chapter.

5.1 LINK-ASSIGNED STDMA CAPACITY

The purpose of a transmission schedule is to control link transmission powers and rates, regulate medium access and provide adequate capacity for all network traffic. Transmission schedules are predetermined for a limited number of timeslots, with the frame being repeated in time. The capacity provided during a specific timeslot is defined by the associated link rate vector, which gives the transmission rate for each active link in the spatial reuse group, or clique. The link rate region for link-assigned STDMA in [32] is partly reviewed in this section, since it forms the basis of the capacity determination for link-assigned STDMA with temporal reuse.

The target SINR for transmission at a discrete r-multiple of the base rate is given by $\gamma_{\text{tgt}}^{(r)}$, where $r = 1$ refers to the base transmission rate and $r = 0$ a zero transmission rate. In practice the transmission rate of link l is limited to $c_l = c_{\text{tgt}}^{(r)} = rW\log(1 + \gamma_{\text{tgt}}^{(1)})$ when $\gamma_{\text{tgt}}^{(r)} \leq \gamma_l(P) < \gamma_{\text{tgt}}^{(r+1)}$, where W is the system bandwidth in the Shannon capacity formulation. Each link can be assigned a total of $r_{l,\max} + 1$ different rates according to the link rate allocation policy $C_l = \left\{c_{\text{tgt}}^{(r_l)} : r_l \in [0, r_{l,\max}]\right\}$, where $r_l = 0$ means an inactive link and $r_l = r_{l,\max}$ the maximum possible multiple of the base rate for the link l. All possible link rate vectors are

given by

$$\mathcal{V} = \{v_k = (c_l \in C_l : l \in \mathcal{L}), \quad k \in [1, K]\}. \tag{5.1}$$

There can be at most $K = |\mathcal{V}| \leq \prod_{l \in \mathcal{L}} (r_{l,\max} + 1)$ unique link rate vectors, but in actuality much less, owing to interference limiting the spatial reuse clique sizes. A schedule allocates a certain number of timeslots to each link rate vector so that the long-term achievable link rate region can be defined as

$$C = \text{conv}(\mathcal{V}) = \left\{ c = \sum_{\substack{k \in [1,K] \\ v_k \in \mathcal{V}}} \alpha_k v_k \;\middle|\; \begin{array}{l} \alpha_k \geq 0, \\ \sum_k \alpha_k = 1, \\ k \in [1, K] \end{array} \right\}. \tag{5.2}$$

This is similar to the capacity region for wireless ad hoc networks defined in [33]. The convex hull conv() of the set $\mathcal{V}$ includes all achievable average link capacities owing to time-sharing of all the link rate vectors. This convex combination of link rate vectors allocates a time fraction of α_k to every link vector v_k to form the polyhedral rate region.

5.2 CAPACITY WITH TEMPORAL REUSE

Given a scheduled link rate vector $v_k \in \mathcal{V}$ that experiences packet depletion for one of the associated links $\mathcal{L}(v_k) = \{l \in \mathcal{L} : v_k(l) > 0\}$, the scheduler can resort to transmission on an alternative link through temporal reuse. In such a timeslot where an alternate link is used, another link rate vector $v_m \neq v_k$ describes the capacity used for the temporal reuse instance. All possible link rate vectors that can describe temporal reuse for the primary vector v_k are defined by the extended set $\mathcal{V}(v_k) = \{v_m \in \mathcal{V} : P(v_k) \geq P(v_m)\}$.

An extended set of link rate vectors can be associated with any one specific link rate vector, such that spatial reuse is maintained but with increased temporal reuse. The node transmission powers for a link rate vector v_k are given by $P(v_k)$, and the power assignment should not be exceeded by any alternate link rate vector.

5.2.1 Temporal reuse-aware rate region

The average link capacities used for a scheduled extended set depend on its ordering policy, the network topology, radio propagation model and traffic load, as these factors influence the prevalence of packet depletion. For all repetitions of a timeslot where an extended set of v_k is scheduled, a certain fraction φ_{km} of repetitions will be represented by every link rate vector

$v_m \in \mathcal{V}(v_k)$ in the extended set. These fractions can only be determined by simulating the network, although the values $\Phi(\mathcal{V}) = \{\{\varphi_{km} : \sum \varphi_{km} \leq 1,\ v_m \in \mathcal{V}(v_k)\} : v_k \in \mathcal{V}\}$ will change when a schedule is used that is optimised using those values in the temporal reuse-aware rate region

$$C_e = \left\{ \sum_{\substack{k \in \mathcal{K} \\ v_k \in \mathcal{V}}} \alpha_k \sum_{v_m \in \mathcal{V}(v_k)} \varphi_{km} v_m \;\middle|\; \begin{array}{l} \alpha_k \geq 0, \\ \sum_k \alpha_k = 1, \\ k \in \mathcal{K} \end{array} \right\}. \tag{5.3}$$

The aware rate region C_e gives the achievable link capacities with the extended temporal reuse sets when taking the inefficiencies due to packet depletion into account. Optimising a schedule with more accurate representations of the link rate vectors leads to improved network performance.

5.2.2 Rate region estimation

A schedule optimisation algorithm should be independent of a specific network topology and radio propagation model, so several assumptions and simplifications are applied to create a generic optimiser:

(i) Each alternative link in the temporal reuse set must operate at the maximum possible transmission rate, within the power constraints.

(ii) The usage probabilities of links in a temporal reuse set are determined only on the basis of the order in which the links are queried for packets in the case of packet depletion, regardless of network topology or radio propagation model.

Since some links in a temporal reuse set could have sufficient SINR to transmit at different rates, only the highest rate (primary criterion) is chosen to maximise the capacity of each extended set. For schedules that use link rate vectors with variable power control, a minimum power criterion (secondary with a small $\epsilon > 0$) could also be used to differentiate between multiple link rate vectors with a maximum rate for a specific link. The temporal reuse set for a clique node $n \in \mathcal{T}(v_k) = \{n \in \mathcal{N} : \mathcal{L}(v_k) \cap O(n) \neq \emptyset\}$, where $O(n)$ are the outgoing links of node n, is thus calculated as $\mathcal{L}_n(v_k) = \{l \in \mathcal{L} : c_l > 0,\ c_l \in C_n(v_k)\}$ where

$$C_n(v_k) = \left\{ \arg_{v_m(l)} \max_{v_m \in \mathcal{V}(v_k)} (v_m(l) - \epsilon P(v_m, n)) : l \in O(n) \right\}. \tag{5.4}$$

To calculate the rate region C_e a very large set of $|\Phi(\mathcal{V})| = \sum_{v_k \in \mathcal{V}} |\mathcal{V}(v_k)|$ values particular to $\mathcal{V}$ is needed. A network-agnostic rate region can be rendered by focusing on the usage

probabilities of alternative links in $\mathcal{L}_n(v_k)$, instead of alternative link rate vectors as in the case of $\Phi(\mathcal{V})$. With temporal reuse, when a primary scheduled link experiences packet depletion the alternative links are queried in a certain order for available packets, according to the ordering policy, until a usable link is found.

Each link l in a temporal reuse set $\mathcal{L}_n(v_k)$ is assigned an ordering value $\Theta_n(v_k, l) \in [0, |\mathcal{L}_n(v_k)| - 1]$, where a smaller value means a higher priority, to establish an ordering policy, so a link $l \in \mathcal{L}_n(v_k)$ with a higher priority $\Theta_n(v_k, l) < \Theta_n(v_k, m)$ than $m \in \mathcal{L}_n(v_k)$ will have a higher usage probability $\mathcal{U}_n(v_k, l) > \mathcal{U}_n(v_k, m)$. The number of usage probabilities are reduced with the assumption that the utilisation probabilities $\mathcal{U}_n(v_k, l) \approx \mathcal{U}_o(v_j, m)$ are approximately equal when the usage priorities $\Theta_n(v_k, l) = \Theta_o(v_j, m)$ are the same, regardless of differences in networks, the extended sets, the particular node temporal reuse sets or links in question. This simplification is made on the basis that it is the order in which links in the temporal reuse set are checked that determines the link usage probabilities. Let U be the simplified priority-based link usage probabilities, where the usage probability for a link with priority θ is U_θ, then

$$U = \left\{ U_\theta \in [0, 1] : \sum_\theta U_\theta \leq 1,\ U_{\theta - i} > U_\theta,\ 0 \leq i \leq \theta,\ \forall \theta \geq 0 \right\}. \tag{5.5}$$

The primary outgoing link for a node, in other words the active link that is originally implicated in v_k, has priority $\theta = 0$, and lower priority reserve links have higher θ values. The simplified usage probabilities of outgoing links in the temporal reuse set for a specific node n active in v_k are given by

$$\mathcal{U}_n(v_k) = \{\beta_l : l \in O(n)\} \subseteq U. \tag{5.6}$$

Although this form does not define a specific ordering policy, one based on relative traffic flow magnitudes is presented in the following subsection. Let I_L be the identity matrix in $\mathbb{R}^{L \times L}$, where $I_L(l)$ is the j^{th} column in I_L so that j is the index of link l in $\mathcal{L}$. Temporal reuse link sets are mutually exclusive, thus for any $v_k \in \mathcal{V}$ the relationship $\cap_{n \in \mathcal{T}(v_k)} \mathcal{L}_n(v_k) = \emptyset$ holds, so the usage probability vector for a v_k with temporal reuse is given by

$$\mathcal{U}(v_k) = \sum_{n \in \mathcal{T}(v_k)} \sum_{l \in O(n)} \mathcal{U}_n(v_k, l) I_L(l). \tag{5.7}$$

The full link rate template for v_k with temporal reuse given by $C(v_k)$ represents the non-achievable capacity before taking the actual usage limits specified by $\mathcal{U}(v_k)$ into account,

as shown in

$$C(v_k) = \sum_{n \in \mathcal{T}(v_k)} \sum_{l \in O(n)} C_n(v_k, l) I_L(l). \tag{5.8}$$

The Hadamard (Schur) product of the usage probability estimates $\mathcal{U}(v_k)$ and the rate template $C(v_k)$ gives the resultant achievable capacity for v_k with full temporal reuse, and so the simplification of C_e gives the estimated achievable rate region $\widetilde{C}_e$ for networks with spatial and temporal reuse, as shown in

$$\widetilde{C}_e = \left\{ \sum_{\substack{k \in \mathcal{K} \\ v_k \in \mathcal{V}}} \alpha_k \Big(\mathcal{U}(v_k) \odot C(v_k) \Big) \;\middle|\; \begin{array}{l} \alpha_k \geq 0, \\ \sum_k \alpha_k = 1, \\ k \in \mathcal{K} \end{array} \right\}. \tag{5.9}$$

Apart from the time-sharing coefficients $\{\alpha_k : k \in \mathcal{K}\}$ and the link rate vector power assignments $\{P(v_k) : v_k \in \mathcal{V}\}$, each schedule has to include the prioritised temporal reuse link rate sets $\{\Theta(v_k), \mathcal{U}(v_k), C(v_k) : v_k \in \mathcal{V}\}$ associated with every active transmitter node n in the spatial reuse node set (clique) $\mathcal{T}(v_k)$ for every $v_k \in \mathcal{V}$. The schedule frame length is set at a minimum of $\delta(L + 1)$ since the optimal solution involves at most $L + 1$ link rate vectors according to Carathéodory's theorem [34] (see [35]). The schedule is composed by cycling between the involved link rate vectors until there are $\lceil \alpha_k \delta(L + 1) \rceil$ occurrences of each vector v_k. A value of $\delta = 3$ has experimentally shown to give good results for various network sizes.

U is independent of a particular network topology or radio propagation model, and can be determined once with the averaged values of simulations of many different networks and used to optimise any network afterward, as done in the numerical analysis of the schedule performance chapter. The number of utilisation probability values needed to calculate $\widetilde{C}_e$ is

$$|U| = \max_{\substack{n \in \mathcal{T}(v_k) \\ v_k \in \mathcal{V}}} |\mathcal{L}_n(v_k)| \ll |\Phi(\mathcal{V})|. \tag{5.10}$$

This estimate $\widetilde{C}_e$ is thus greatly simplified while maintaining the effect of temporal reuse on the usage efficiency and achievable capacity of link-assigned schedules.

5.2.3 Ordering policy

The discriminator that is used to assign priorities $\mathcal{U}_n(v_k, l)$ to the alternative links in a temporal reuse set v_k is taken as the number of data flows $\sum_f R_{lf}$ that traverse a link l. The more flows that have to be routed by a link, the greater the need for capacity, thus preference is given to

links that relay more flows. This traffic flow-based ordering policy assigns higher priority to the higher traffic link as formulated by

$$\operatorname{sgn}(\mathcal{U}_n(v_k, l) - \mathcal{U}_n(v_k, m)) = \begin{cases} +1 & \text{when } \sum_f R_{lf} > \sum_f R_{mf}, \\ 0 & \text{never}, \\ -1 & \text{when } \sum_f R_{lf} \leq \sum_f R_{mf} \end{cases}$$
$$\text{for} \quad l \neq m, \ \forall l, m \in \mathcal{O}(n), \ \forall n \in \mathcal{T}(v_k). \quad (5.11)$$

This policy check is performed for every pair combination of the outgoing links of a scheduled node n in a temporal reuse set v_k.

CHAPTER 6
SCHEDULE OPTIMISATION

Quality of service and the efficient use of communication resources necessitate engineered optimisation of the control processes of the wireless mesh network. The fairness between the flow rates is an important measure of service quality, and a good schedule should give preference to flow rate fairness over total network throughput. Specifically, a global utility of proportional fairness is used in this work to evaluate the fitness of a candidate transmission schedule, with the flow rates limited by the link capacities. In Chapter 5 the capacity of all possible spatial and temporal reuse groups were determined, and those capacities will be used here to help construct an optimal schedule.

The fractional duration of each reuse group is modified to bring about a change in the link rate region of the network, guided by the proportionally fair objective function. Since the fractional durations of all the reuse groups should sum to 1, the rate region is called convex and it limits the total flow loads that can traverse the links. The resulting problem is thus termed convex optimisation, where a linear objective function is subject to a convex constraint. Solving the convex optimisation problem produces the optimal flow rates and perceived link demands, which indicate capacity shortages in some links. The duration of a reuse group that can fulfil the largest sum of demands is then increased, until the maximum utility is reached.

Convex optimisation for link-assigned STDMA is first reviewed, and the computational aspects of the solution are discussed. The optimisation problem is then extended to address link-assigned STDMA with extended transmission rights, by using the modified temporal reuse-aware capacity region calculated in Chapter 5. Complexity reductions are introduced

to make the temporal reuse-aware solution computationally feasible, and the solver is further explained. This chapter then endeavours to derive the complete optimised transmission schedule for networks running LET. An outline of the topics that are discussed in this chapter is given in Figure 6.1.

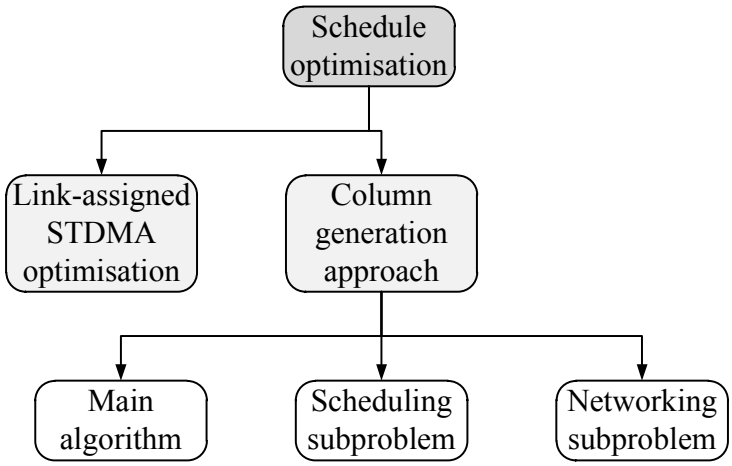

Figure 6.1: The schedule optimisation topics covered in this chapter.

6.1 LINK-ASSIGNED STDMA OPTIMISATION

Link capacities are represented by the transmission schedule, which can be optimised to maximise a global utility function. The level of satisfaction with a flow rate s_f is given by a utility function $u(s_f)$, which is concave and strictly increasing. Maximising the weighted network throughput $\sum_{f\in\mathcal{F}} w_f s_f$ leads to grossly unfair flow rates [36], so a proportionally fair flow utility is decided on where $u \to -\infty$ when $s_f \to 0^+$. The flow rates s are proportionally fair if, and only if, $u(s_f) = \log(s_f)$ (see [37]), and this leads to a higher total network throughput than with maximisation of a uniform flow rate.

Network throughput depends on the available link capacities, which are consumed with relaying potentially multiple flows. The aggregate traffic load on the links is given by the vector Rs, which is due to the point-to-point data flows and the multihop nature of the mesh network. The achievable link rates are given by the capacity vector $c \in C$, so that the flow rates are limited by the primary constraint $Rs \preceq c$, where $\preceq$ denotes a component-wise inequality. The purpose of the optimisation problem is to find the time-sharing coefficients $\{\alpha_k : k \in \mathcal{K}\}$

(let $\mathcal{K} = [1, K]$) for a capacity vector c that maximises the global utility according to

$$\begin{aligned} \text{maximise} \quad & \textstyle\sum_f u\left(s_f\right) \\ \text{subject to} \quad & Rs \preceq c \\ & c \in C, \quad s \succeq 0. \end{aligned} \tag{6.1}$$

The concave global utility proposed in [32] is subject to convex constraints so it can be solved as a convex optimisation problem that produces a cross-layer optimised solution. The resultant schedule consists of link rate vectors $\{v_k : k \in \mathcal{K}\}$ and the associated time-sharing coefficients $\{\alpha_k : k \in \mathcal{K}\}$, which define transmission power and rate control in the physical layer and medium access control in the data link layer, respectively. The delivery route of each data flow is established in the network layer as represented by R, and the flow rates s are regulated in the transport layer.

The optimal solution involves at most $L + 1$ link rate vectors according to Carathéodory's theorem [34] (see [35]), therefore there are at most $L + 1$ non-zero α_k values in the optimal schedule. The exact number of utilised link rate vectors depends on the specific optimal solution for a particular network. The greater the number of links, the more numerous the possible spatial reuse groups, which increases the number of used link rate vectors. For a proper TDMA (time-division multiple access) schedule, it can be seen that L link rate vectors would be needed for a feasible solution. When spatial reuse comes into play, less link rate vectors can describe the same capacity of TDMA, so the limit of the number of involved link rate vectors is not exceeded.

6.2 COLUMN GENERATION APPROACH

The global utility maximisation problem in Equation (6.1) determines the time-sharing coefficients for each link rate vector in $\mathcal{V}$. The number of link rate vectors is exponential in the number of network links, so calculating and storing them in order to solve Equation (6.1) becomes a hurdle as the network grows. The solution also tends to be more inaccurate with computer solvers when more link rate vectors are involved.

For these reasons the mathematical programming technique of column generation [38] is employed, where modifications specific to temporal reuse are made to the algorithm discussed in [32] and [39], which is reconsidered in this section. Optimisation can then be started with

only a small number of link rate vectors, and more vectors that contribute most to increasing the global utility are added through column generation. The process of optimising a schedule with column generation, for networks that employ both spatial and temporal reuse, is explained in this section.

6.2.1 Main algorithm

The utility maximisation problem guides the column generation by providing information pertaining to capacity demands, therefore it is referred to as the master problem. The full master problem in Equation (6.1) contains all $\mathcal{K}$ link rate vectors, but it is restricted to a subset $\mathcal{J} \subseteq \mathcal{K}$ of vectors in the restricted master problem (6.2) used for column generation. The full master problem is described by

$$\begin{aligned} \text{maximize} \quad & \textstyle\sum_f u\left(s_f\right) \\ \text{subject to} \quad & Rs \preceq c, \quad s \succeq 0 \\ & c = \sum_{\substack{k \in \mathcal{J} \subseteq \mathcal{K} \\ v_k \in \mathcal{V}}} \alpha_k \Big(\mathcal{U}(v_k) \odot C(v_k) \Big) \\ & \textstyle\sum_k \alpha_k = 1, \ \alpha_k \geq 0, \ k \in \mathcal{J} \subseteq \mathcal{K}. \end{aligned} \tag{6.2}$$

The link-flow incidence matrix is given by R and the flow rate vector is given by s, so that Rs gives the link flow load vector that needs to be less than the available link capacity vector c. The available capacity is calculated according to the temporal reuse-aware link rate region. When solving the restricted master problem the capacity demand ξ_l for each link l can be determined, which indicates the relative utility improvement for a unit increase in link capacity. For $u(\cdot) = \log(\cdot)$ each link demand also equals the inverse flow rate of the flow that only uses the corresponding link [40]. These capacity demands are given by the Lagrangian duality for (6.2), which is as follows:

$$L(s, c, \xi) = \textstyle\sum_f u\left(s_f\right) - \xi^T \left(c - Rs\right). \tag{6.3}$$

The optimal Lagrangian multipliers ξ^* are used to update $\mathcal{J}$ by maximising the upper bound on the optimum (weak duality, see [32]) according to

$$u_u = \sup_{s \geq 0} \left\{ \textstyle\sum_f u\left(s_f\right) - \xi^{*T} Rs \right\} + \sup_{c \in \widetilde{C}_e} \left\{ \xi^{*T} c \right\}. \tag{6.4}$$

The lower bound (6.5) involves only the columns generated thus far, as indicated by $\mathcal{J}$, to find the best supply vector. The lower bound is given by

$$u_l = \sup_{s \geq 0} \left\{ \textstyle\sum_f u\left(s_f\right) - \xi^{*T} Rs \right\} + \sup_{c \in \widetilde{C}_e^{\mathcal{J}}} \left\{ \xi^{*T} c \right\}. \tag{6.5}$$

Finding a new link rate vector from the $\mathcal{K}$-element rate region $\widetilde{C}_e$ that maximises capacity for the given demand solves the scheduling subproblem $\sup_{c\in\widetilde{C}_e}\left\{\xi^{*T}c\right\}$. An extreme point in $\widetilde{C}_e$ will maximise capacity [32] rather than a combination of link rate vectors. This generated column does not require that all $\mathcal{K}$ elements have to be known, but the new vector can be obtained by solving a mixed integer linear programming formulation discussed in the proceeding subsection.

Optimality is reached when the new link rate vector cannot supply a greater capacity than an existing vector. The process of solving the restricted master problem and expanding $\mathcal{J}$ is continued until the difference between the optimal upper bound u_u and lower bound u_l becomes smaller than a certain threshold ε, as shown by

$$u_u - u_l = \sup_{c\in\widetilde{C}_e}\left\{\xi^{*T}c\right\} - \sup_{c\in\widetilde{C}_e^{\mathcal{J}}}\left\{\xi^{*T}c\right\} < \varepsilon. \tag{6.6}$$

The main column generation algorithm that is used to optimise a schedule, by forming $\mathcal{J}$ to maximize the global utility, is as follows:

1. Initialise the index set $\mathcal{J}$ with the link rate vectors that correspond to a simple TDMA link-assigned schedule operating at base rates only, with no spatial reuse.
2. Solve the restricted master problem to optimality with a primal-dual interior-point method [41] to obtain the optimal Lagrangian multipliers or capacity demands ξ^*.
3. Add the new link rate vector, that solves the scheduling subproblem, to $\mathcal{J}$.
4. Repeat the process until $u_u - u_l < \varepsilon$, or when the generated column is already present in $\mathcal{J}$.

6.2.2 Scheduling subproblem

The optimal Lagrangian multipliers ξ_l^* give the sensitivity of the lower optimum bound u_l at the optimal point c^*. By satisfying the links with the greatest demand for capacity as indicated by ξ_l^*, the lower bound can be improved most. By finding an extreme vertex in $c \in \widetilde{C}_e$ to maximise $\xi_l^{*T}c$ a new scheduling element is added to increase the network utility. This is termed the scheduling subproblem and for networks with temporal reuse it is formulated as finding

$$\max_{v_k\in\mathcal{V}}\Big(\xi_l^{*T}\sum_{n\in\mathcal{T}(v_k)}\sum_{l\in O(n)}\mathcal{U}_n(v_k,l)C_n(v_k,l)I_L(l)\Big). \tag{6.7}$$

A mixed integer linear program is used to determine which spatial reuse clique with extended transmission rights solves the scheduling subproblem. Let the binary variable $x_l^{(r)}$ indicate whether link l is operating at r times the base rate, then the relevant constraint for all the network links $\mathcal{L}$ is given by

$$x_l^{(r)} \in \{0, 1\}, \quad \forall l \in \mathcal{L}, \forall r. \tag{6.8}$$

The binary variable y_n specifies whether node n is transmitting or not, so the following definition is included for all the network nodes $\mathcal{N}$:

$$y_n \in \{0, 1\}, \quad \forall n \in \mathcal{N}. \tag{6.9}$$

Whenever a link is transmitting at a non-zero rate the associated node also has to be activated, so this relationship is formulated as

$$\textstyle\sum_r x_l^{(r)} = y_{\mathrm{tr}(l)}, \quad \forall l \in \mathcal{L}. \tag{6.10}$$

In the program the instantaneous maximum transmission power of a node n is given by P_n which is limited to a maximum as shown in

$$0 \leq P_n \leq P_{\max}, \quad \forall n \in \mathcal{N}. \tag{6.11}$$

To ensure that all transmitting links have a sufficiently large SINR, the following linear constraint is imposed:

$$M_l^{(r)}\left(1 - x_l^{(r)}\right) + Q_{\mathrm{tr}(l)\mathrm{re}(l)} P_{\mathrm{tr}(l)} x_l^{(r)} \geq \gamma_{\mathrm{tgt}}^{(r)}\left(\sigma_{\mathrm{re}(l)} + \textstyle\sum_{n \neq \mathrm{tr}(l)} Q_{n\mathrm{re}(l)} P_n y_n\right), \quad \forall l \in \mathcal{L}, \forall r. \tag{6.12}$$

When a link l is transmitting then the term $\left(1 - x_l^{(r)}\right)$ becomes zero, and when the link is not transmitting then the coefficient $M_l^{(r)}$ simply ensures that the constraint is met for the linear program to function correctly. By choosing a sufficiently large $M_l^{(r)}$ the above constraint will be met when the link is not transmitting, so the following value will suffice:

$$M_l^{(r)} = Q_{\mathrm{tr}(l)\mathrm{re}(l)} P_{\mathrm{tr}(l)} + \gamma_{\mathrm{tgt}}^{(r)}\left(\sigma_{\mathrm{re}(l)} + \textstyle\sum_{n \neq \mathrm{tr}(l)} Q_{n\mathrm{re}(l)} P_n\right), \quad \forall l \in \mathcal{L}, \forall r. \tag{6.13}$$

For scheduling with fixed power the node transmit powers are fixed at $P_n = P_{\max}$, $\forall n \in \mathcal{N}$, and for non-adaptive rate scheduling the rate is limited to $r \in \{0, 1\}$. The variable rate and power mixed integer linear program considers all the possible temporal reuse priority policies, and given the optimal Lagrangian multipliers the program is formulated as

$$\begin{aligned} &\text{maximise} && \textstyle\sum_{n \in \mathcal{N}} \sum_{l \in O(n)} \xi_l \beta_l \sum_r c_{\mathrm{tgt}}^{(r)} x_l^{(r)} \\ &\text{subject to} && \{\beta_l : \ l \in O(n)\} \subseteq U, \quad \forall n \in \mathcal{N} \\ & && (6.8),\ (6.9),\ (6.10),\ (6.11),\ (6.12),\ (6.13). \end{aligned}$$

By ensuring that the links with greater traffic flow $\sum_f R_{lf}$ loads are assigned higher rates r in a temporal reuse link set, the complexity can be reduced. The complexity of the scheduling subproblem, however, still remains NP-hard. The following constraint can be added to the linear program to achieve the complexity reduction:

$$\operatorname{sgn}\left(\sum_{r=a}^{r_{\max}} x_l^{(r)} - \sum_{r=a}^{r_{\max}} x_m^{(r)}\right) = \begin{cases} +1 & \text{when } \sum_f R_{lf} \geq \sum_f R_{mf}, \\ 0 & \text{when } \sum_f R_{lf} = \sum_f R_{mf}, \\ -1 & \text{when } \sum_f R_{lf} \leq \sum_f R_{mf} \end{cases}$$
$$\text{for} \quad l \neq m, \ \forall l, m \in O(n), \ \forall n \in \mathcal{T}(v_k), \ a \in [1, r_{\max}]. \quad (6.14)$$

This constraint guides the selection of link rates such that higher traffic links will have an equal or higher rate than a lower traffic link in the same temporal reuse set. A lower traffic link will thus never have a higher rate than a link with a greater flow load in the same temporal reuse set.

CHAPTER 7

SCHEDULE PERFORMANCE

The performance of link-assigned STDMA with extended transmission rights is measured in this chapter, and the benefits of the temporal reuse-aware rate region are clarified. The purpose of extending transmission rights in link-assigned scheduling is two-fold. Firstly, the increased temporal reuse improves predefined schedule usage efficiency, and secondly, it permits network coding that would otherwise not be possible. Having determined the added capacity with temporal reuse, and having optimised a transmission schedule using the temporal reuse-aware capacity, the performance of the resulting schedule needs to confirm the design goals. The schedule performance is a function of the schedule capacity, fairness and power efficiency, and is compared for a multitude of relevant schedules to indicate the various niche performance areas of each schedule.

The schedule capacity is simply the maximum uniform network load while keeping the maximum end-to-end packet delay bounded. Schedule fairness is gauged as the variance in flow loads at the maximum schedule capacity, while the power efficiency measurements pertain to the average transmitter powers used by a network over several runs of a scheduling frame. These measures track key performance metrics that summarise the goodness of each scheduling algorithm through realistic simulation, and they are thus used to present the main results of this dissertation. Since full wireless mesh network simulations are used, the aptitude of each scheduling algorithm can be accurately monitored in the presence of network coding additions and the occurrence of packet depletion.

Extensive simulation was conducted to evaluate the performance of $\widetilde{C}_e$-schedules optimised

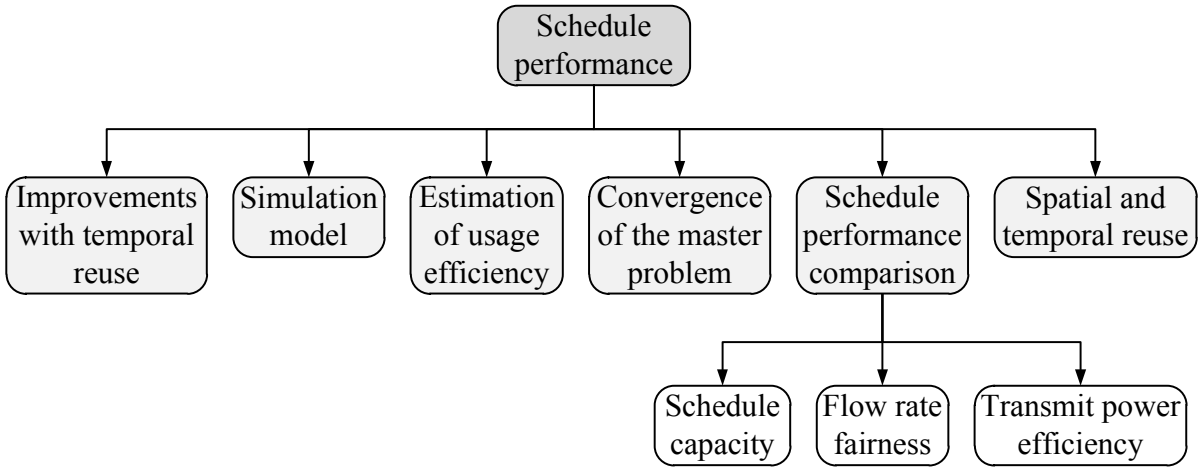

Figure 7.1: Chapter outline for the schedule performance study.

in the temporal reuse-aware rate region as compared to C-schedules optimised in the default non-aware rate region. The simulation model is expounded on and results are included that show the improvements that are gained with the addition of temporal reuse. The usage probability vector U is estimated through simulation and the process is explained and values given for networks with differing rate/power adaptivity. Schedule performance is gauged according to schedule capacity, fairness and power efficiency, and in this section the benefits of the temporal reuse-aware rate region is made clear. Finally, the relationship between spatial and temporal reuse for the various schedules is investigated. An outline of this chapter is depicted in Figure 7.1.

7.1 SIMULATION MODEL

A radio link model is used where nodes transmit omnidirectionally at a maximum possible instantaneous power of 0.1 W and experience background receiver noise power of $\sigma = 3.34 \times 10^{-12}$ W, where an absolute circuitry temperature of 290° K and a noise figure of 10 are assumed. The deterministic fading model $Q_{nm} = 10^{-4} d_{nm}^{-3}$ is used with a path loss exponent of $\chi = 3$, transmitter and receiver gains of 1 and a 1 m reference path loss ratio of $K_{nm} = 10^{-4}$. The threshold SINR for base rate transmission is set at $\gamma_{\text{tgt}}^{(1)} = 10$ dB and a shared bandwidth of $W = 83.5$ MHz is used. This model corresponds broadly to that of an indoor wireless LAN (local area network) using the entire 2.4-2.4835 GHz ISM (industrial, scientific and medical) band.

Multihop wireless mesh networks of 10 to 30 nodes are randomly generated in two dimensions where the maximum length of each dimension for 10, 15, 20, 25 and 30 node networks are set at 140 m, 160 m, 180 m, 200 m and 220 m respectively. The various square dimensions have been experimentally chosen to produce fully connected networks with a good average spatial reuse potential that increases as the number of nodes increases. Single-path minimum hop routing is used according to Dijkstra's algorithm and only networks with paths between every node pair are considered. For each data point in the results the averaged outcomes of 120 random networks are taken and each network size is analysed separately.

Schedules are determined centrally and shared with all nodes, and with the assumption of perfect synchronisation each node can operate according to the same schedule. Each data flow is communicated with packets where each packet can be relayed over one hop in one timeslot when transmitting at the base rate. The schedule capacity is determined as the maximum number of packets $\widehat{\pi}$ that can be added per timeslot to a flow randomly chosen according to a uniform distribution, such that the mean end-to-end packet delays are bounded. The numerical analysis determines the mean end-to-end packet delays, the mean flow rates and their standard deviation, and the mean transmission power per packet for the networks operating at maximum schedule capacity.

The analyses with NC use opportunistic two-way network coding [8] where a relay node XORs two packets intended for exchange between two neighbouring nodes. Neighbouring nodes do not need to communicate which packets each received, neither is opportunistic listening required with two-way coding, and the throughput gain with n-way coding is maximised when $n = 2$. First-in-first-out (FIFO) transmit buffers are employed and with NC the buffer is checked in a FIFO manner to obtain the first two packets that can be coded and transmitted over the scheduled temporal reuse set.

7.2 IMPROVEMENTS WITH TEMPORAL REUSE

The effect of temporal reuse on schedule capacity is determined for schedules optimised in the unaware rate region C with transmission rights extended afterwards. This C-optimisation does not consider the capacity changes that extended transmission rights cause and is thus temporal reuse-unaware. Every link rate vector v_k that is activated in a C-schedule has transmission rights

extended to $|\mathcal{L}_n(v_k)| - 1 = q - 1$ alternative links for $q > 0$ to see what improvements in the schedule capacity results.

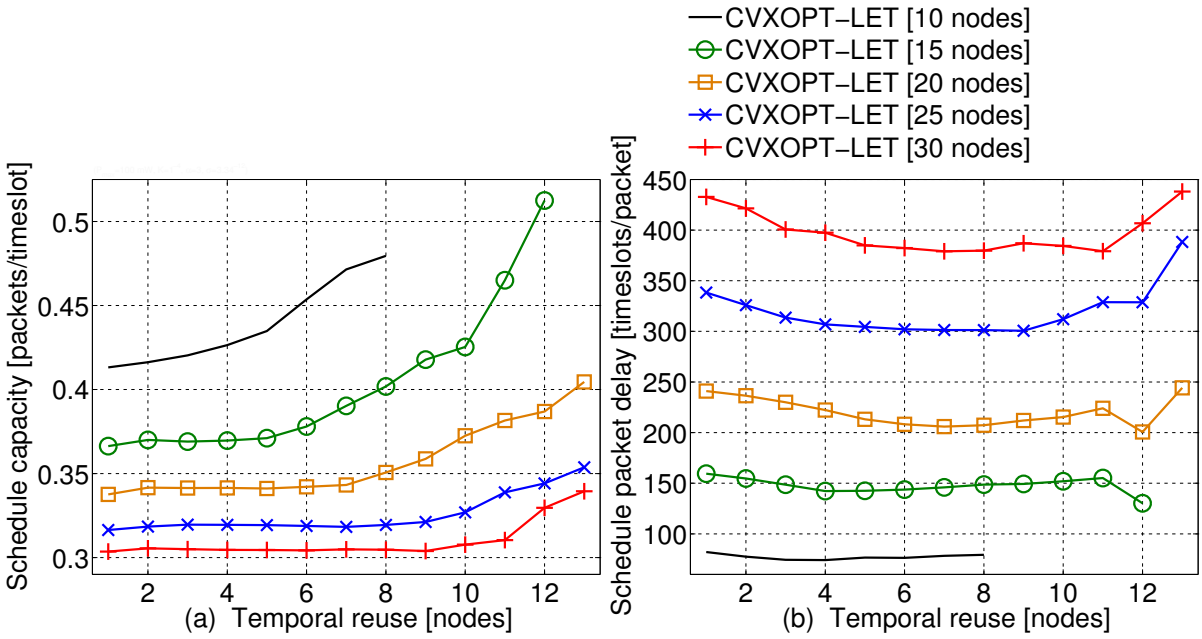

Figure 7.2: Schedule capacity (a) with extended transmission rights and corresponding mean end-to-end packet delays (b).

As the number of alternative links are increased, the schedule capacity $\widehat{\pi}$ also increases, as shown in Figure 7.2(a). So as transmission rights are extended, the added capacity $\min_{l\in\mathcal{L}} \varepsilon_l(q+n) > \min_{l\in\mathcal{L}} \varepsilon_l(q)$ expands for $n > 0$, where ε_l is a function of q, with greater improvements seen for smaller network sizes owing to smaller spatial reuse and thus better temporal reuse. The data population sizes for the large-extreme end of the x-axis are much smaller, since not all networks can achieve such large temporal reuse. This data population size inequality and the trade-off between the schedule capacity and end-to-end packet delays cause the reverse trend in the packet delay values at a large temporal reuse.

The schedule optimised in the convex rate region C is named CVXOPT-LET in Figure 7.2, where LET refers to link-assignment with extended transmission rights (full temporal reuse). The mean end-to-end packet delays for the schedule operating at capacity are given in Figure 7.2(b) and are reduced for most of the rights extension. Thus both the schedule capacity and the average end-to-end packet delays can be improved with temporal reuse.

7.3 ESTIMATION OF USAGE EFFICIENCY

Temporal reuse-unaware C-optimised schedules with full rights extension (full temporal reuse) are analysed to estimate the usage probabilities U of links in temporal reuse sets based on their assigned priorities θ. The average usage probabilities of 10 to 30 node networks are given in Table 7.1, for networks operating with schedules that have no power-rate adaptivity (CVX), power adaptivity only (Power), rate adaptivity only (Rate) and both power and rate adaptivity (Power-Rate).

Table 7.1: Prioritised usage probabilities for power-rate adaptive networks.

θ	CVX	Power	Rate	Power -Rate	Std. Dev. A	Std. Dev. B	Acc.
0	0.706	0.804	0.687	0.791	0.016	0.056	0.94
1	0.170	0.125	0.179	0.130	0.005	0.022	0.79
2	0.057	0.039	0.061	0.042	0.003	0.014	0.88
3	0.029	0.017	0.031	0.019	0.003	0.010	0.88
4	0.017	0.008	0.019	0.009	0.003	0.008	0.85
5	0.010	0.004	0.011	0.005	0.002	0.006	0.81
6	0.006	0.002	0.006	0.002	0.001	0.004	0.77

The mean (for different power-rate adaptivities) of the standard deviations due to networks having different sizes is given in the *Std. Dev. A* column. The accuracy of the given usage probabilities were determined by comparing them to those of temporal reuse-aware $\widetilde{C}_e$-schedules and is given in the *Acc.* column. The validity of the assumption that different network realisations of the same size have similar usage probabilities is measured with the mean (for different power-rate adaptivities) of the mean (for different network sizes) of the standard deviations due to different network topologies as given in the column *Std. Dev. B*. The deviations are small compared to the means for the higher priority links, so the assumption is taken as sound.

Each column displays the effect of temporal reuse, which shares capacity among the temporal reuse set to increase timeslot usage efficiency. The primary links (corresponding to $\theta = 0$) are not fully used, which indicates significant packet depletion occurring owing to unequal link capacities in proportionally fair cross-layer optimised schedules. These results

therefore show the important benefits that can be derived from temporal reuse.

7.4 CONVERGENCE OF THE MASTER PROBLEM

The number of spatial reuse groups is limited for size-constrained fixed-topology networks, and the resulting link rate vectors are all determined. The accurate temporal reuse-aware link rate vectors are also determinable and the number of vectors remains the same. The column generation must therefore end, since the number of link rate vectors is limited. Due to Carathéodory's theorem there is a high probability that the master problem will converge before all the link rate vectors have been generated. The moment no new link rate vector can increase the capacity supply, the column generation converges.

Slater's condition is met for fully connected networks, since there is a strictly feasible solution for the master problem. One such solution is given by a simple link-assigned TDMA schedule that supplies a non-zero positive capacity $\tilde{c}_l$ for each link l in the network. The network is fully connected therefore a non-zero positive flow rate $\tilde{s}_p$ can be achieved by every flow p in the network, and if a flow rate of $\min_l \left\{\tilde{c}_l / \sum_p r_{lp}\right\}$ is assigned to each flow, then the convex constraint $R\tilde{s} \preceq \tilde{c}$ is met. Since Slater's condition is met strong duality holds, and there is thus no duality gap. This means that the column generation must converge.

The convergence of the column generation for the temporal reuse-aware $\widetilde{C}_e$-schedule with extended transmission rights is depicted in Figure 7.3. The reduction in the difference between the lower and upper bounds of the master problem is shown for different network sizes. The mean convergence rate was measured for 120 random network realisations, for each network size. Since larger networks have more spatial reuse groups and data flows, the convergence rates are higher and the difference between the bounds is greater. The absence of the duality gap is confirmed, since all of the solutions converge with zero difference between the lower and upper bounds.

7.5 SCHEDULE PERFORMANCE COMPARISON

The practical superiority of schedule optimisation in the temporal reuse-aware rate region is proven through measurements of schedule capacity, flow rate fairness and transmit power

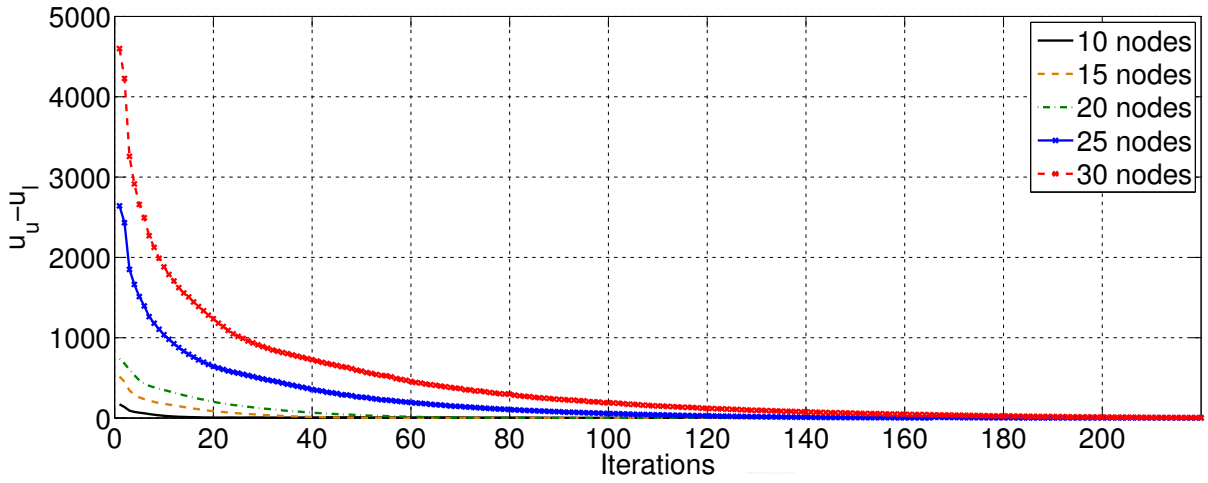

Figure 7.3: Convergence of the column generation approach to schedule optimisation.

efficiency.

7.5.1 Schedule capacity

Schedule capacity is taken as the primary schedule performance measure and it is the maximum number of packets per timeslot that can be added to a random flow so that the schedule maintains a limited mean end-to-end packet delay. The C-schedule (CVX) capacity is increased with extended transmission rights (CVX-LET) and when network coding is used (CVX-LET-NC) the capacity is increased even further, as shown in Figure 7.4(a). The temporal reuse-aware $\widetilde{C}_e$-schedule with extended transmission rights (CVXAware) has greater capacity than with CVX-LET, and the capacity improvement with NC (CVXAware-NC) is also notably larger than with CVX-LET-NC. The temporal reuse-aware rate region gives greater capacity to link rate vectors with good temporal reuse, which provides more NC opportunities for the $\widetilde{C}_e$-schedule.

Reference graphs include those of TDMA, STDMA, traffic-adaptive STDMA with temporal reuse and NC (STDMA-Adaptive-LET-NC), and traffic-adaptive node-assigned schedules with NC (Node-Assigned-NC). The STDMA schedule uses a packing heuristic [29], which packs as many links as have not yet transmitted into a timeslot, and the traffic-adaptive STDMA schedule is generated according to [30]. The node-assigned schedule lets a node choose a link with probability proportional to the number of flows that traverse the link, to achieve traffic adaptivity.

The mean end-to-end packet delays for the different schedules operating at their respective maximum capacities are given in Figure 7.4(b). Node-assigned schedules have the lowest delay, although they do not have the capacity of the cross-layer optimised link-assigned schedules. The *C*-schedule (CVX) achieves lower delays when temporal reuse (CVX-LET) is enabled, even though the delays for CVX are taken at a smaller load. The timeslot duration is a function of the packet length, which affects the quality of service if the packet delays grow large. Although, apart from the proportional fairness, the end-to-end packet delays are allowed to grow as large as possible while remaining bounded. This is warranted to obtain the maximum schedule capacity, which is a more important metric in this study than a secondary quality of service concern.

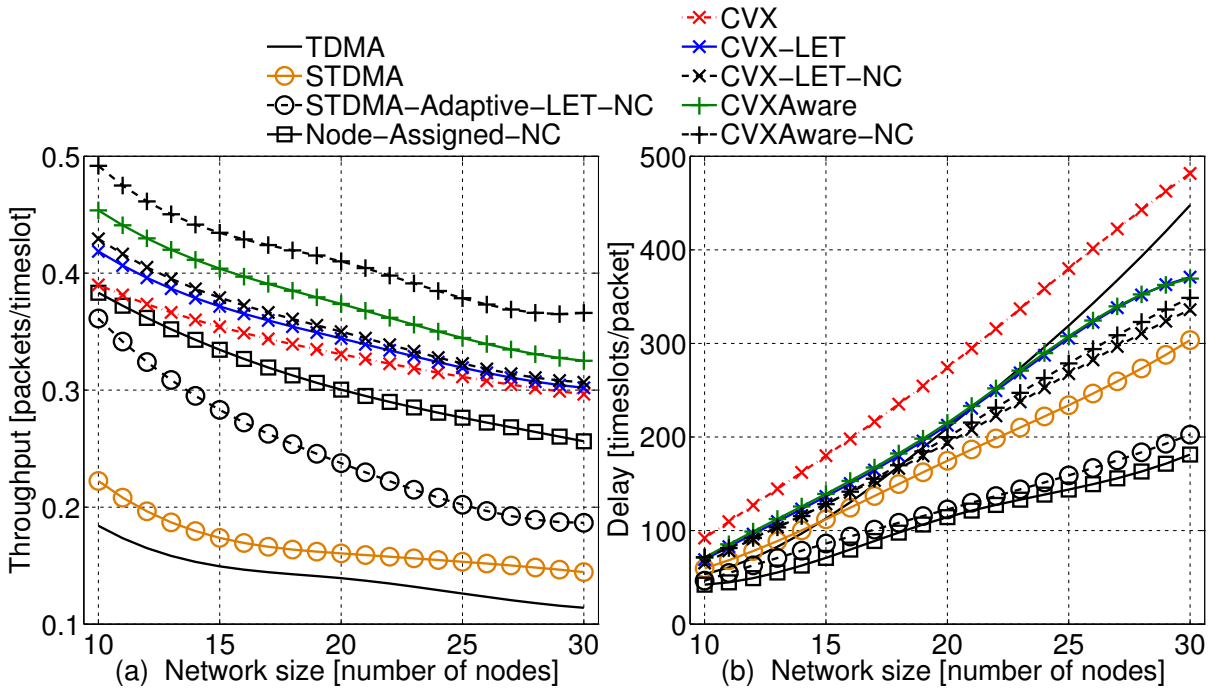

Figure 7.4: Schedule capacity (a) and corresponding end-to-end packet delay (b) comparisons.

The effect of rate and power adaptivity on the capacity of the cross-layer optimised schedules is shown in Figure 7.5. Schedules with power adaptivity (CVX-Power-LET, CVX-RatePower-LET, CVXAware-Power, CVXAware-RatePower) perform better because of more diverse spatial reuse considerations during optimisation. When NC is enabled for the temporal reuse-aware schedules (CVXAware), greater capacity increases are seen than with the *C*-schedules, as shown in Figure 7.5(b).

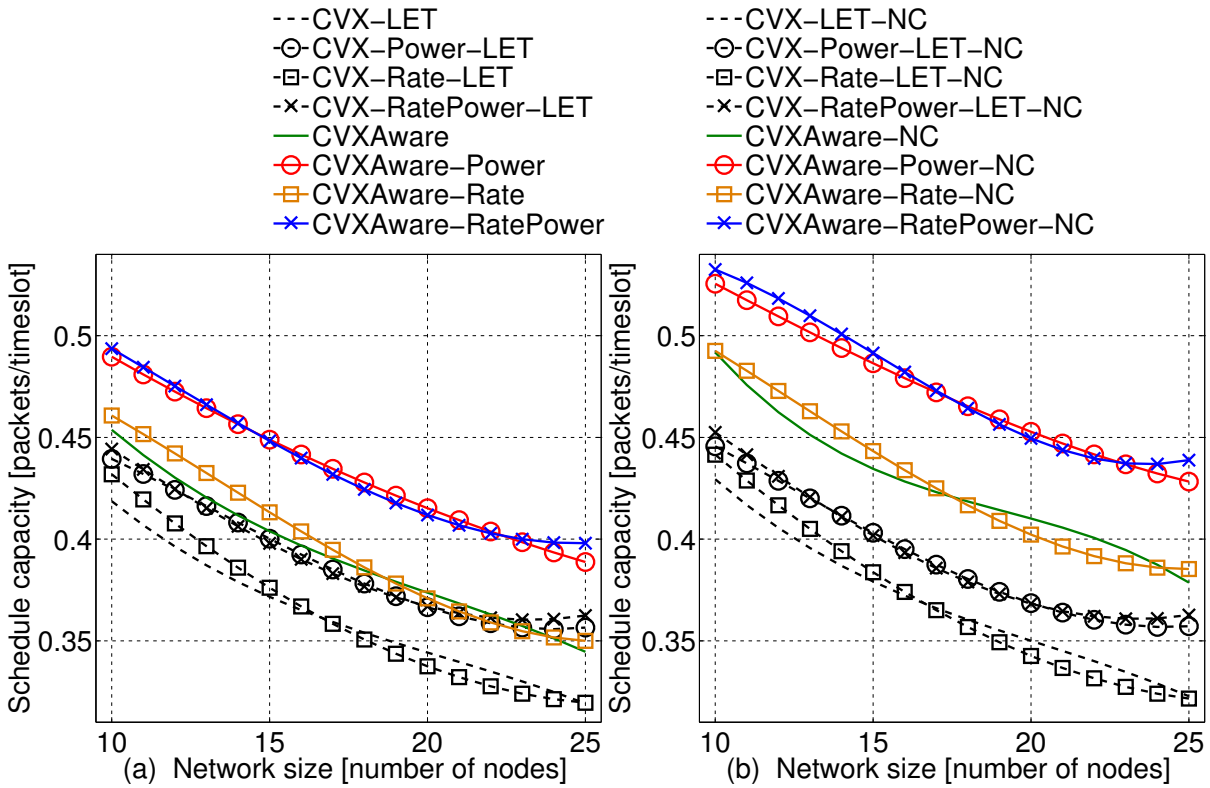

Figure 7.5: Schedule capacity comparison with (b) and without (a) NC.

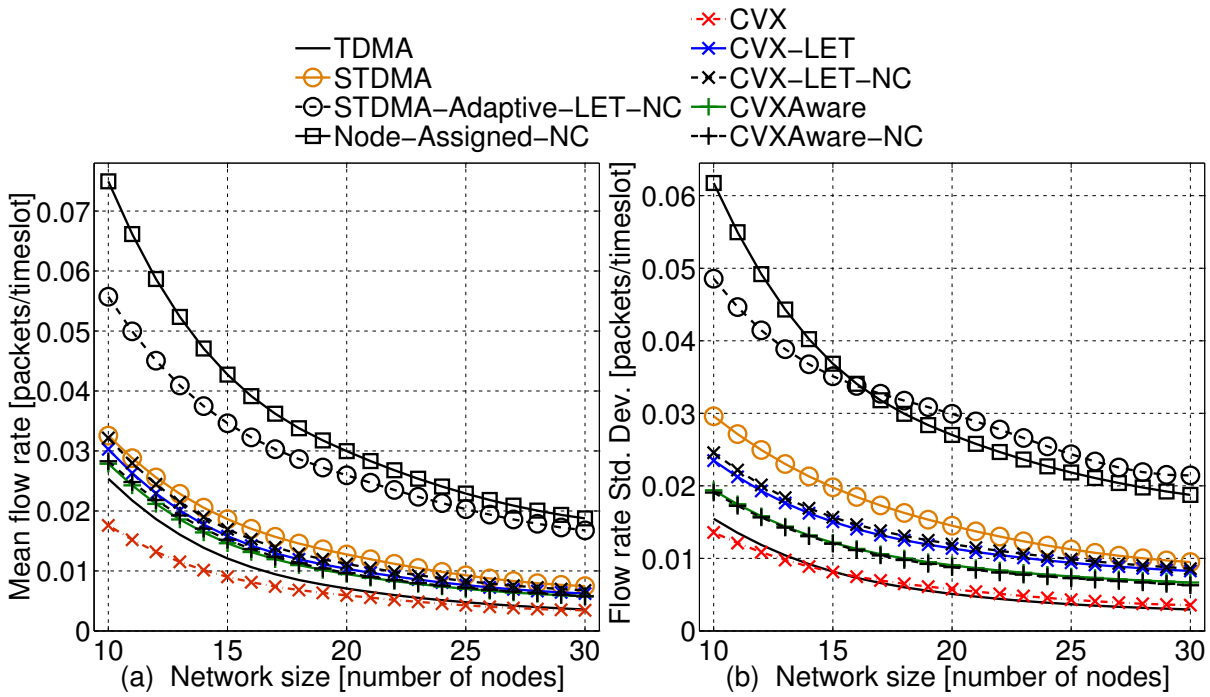

Figure 7.6: Mean flow rate (a) and fairness (b) comparison.

7.5.2 Flow rate fairness

The second important schedule performance measure is flow rate fairness, which indicates the quality of service level that can be expected with a schedule. For the schedules operating at maximum capacity the associated mean flow rates are compared in Figure 7.6(a), where node-assigned schedules have the highest rate and CVX the lowest. Node-assigned schedules achieve the highest mean flow rate at the expense of rate fairness, and the best fairness is achieved by CVX as measured by the flow rate standard deviations in Figure 7.6(b). The sum of the logarithms of the achieved flow rates during network simulation can also be used to assess proportional fairness, but the standard deviation of the achieved flow rates is calculated instead to accompany the mean achieved flow rate. The temporal reuse-aware schedule (CVXAware) achieves a better fairness than the unaware (CVX-LET) schedule, and fairness is not compromised with the use of NC for the CVXAware schedule.

For the rate-power adaptive schedules, significantly lower flow rate deviation occurs with the temporal reuse-aware schedules than with the unaware schedules, since the proportionally fair global utility is more accurately determined when taking the benefits of temporal reuse into account. The improved fairness with the $\widetilde{C}_e$-schedules is especially apparent with the power-adaptive schedules as shown in Figure 7.7(b).

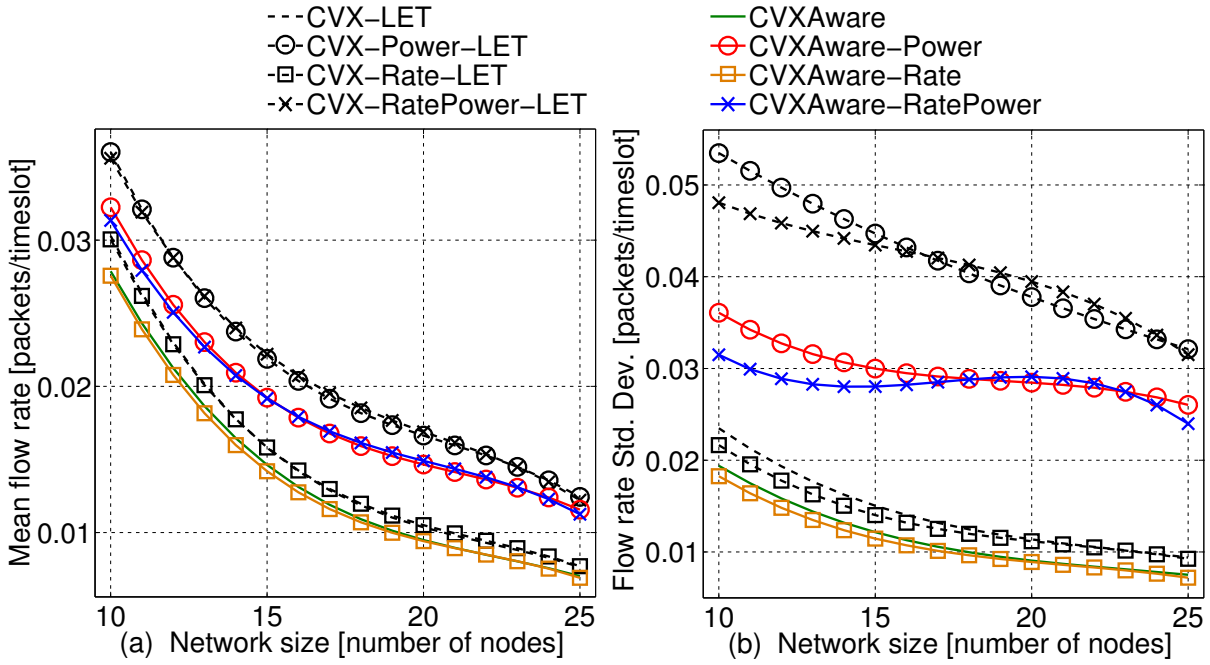

Figure 7.7: Mean flow rate (a) and fairness (b) comparison with variable rate and power control.

A network routes most of its data flows through the center of the network, so by giving a centralised link more capacity there can be more flows enjoying a higher transmission rate. This may increase the mean flow rate at the expense of reduced fairness, due to the reduced capacity experienced by flows routed across links on the edges of the network. A proportional fairness utility can balance the schedule capacity and fairness objectives explicitly, as opposed to the disregard of fairness by schedules such as node-assignment.

7.5.3 Transmit power efficiency

Power efficiency is used as the third schedule performance indicator and is related to the mean transmit power per packet. Adaptive power assignments, multi-rate transmissions and network coding can reduce the mean transmit power per packet of the full power case (CVX-LET) shown in Figure 7.8. By performing network coding (CVX-LET-NC) one transmission can relay two packets, so only half the energy is used in that case, which improves the power efficiency. Significantly less power is used with the power-adaptive schedules, and when network coding is used the temporal reuse-aware schedules achieve greater added efficiency than the non-aware schedules.

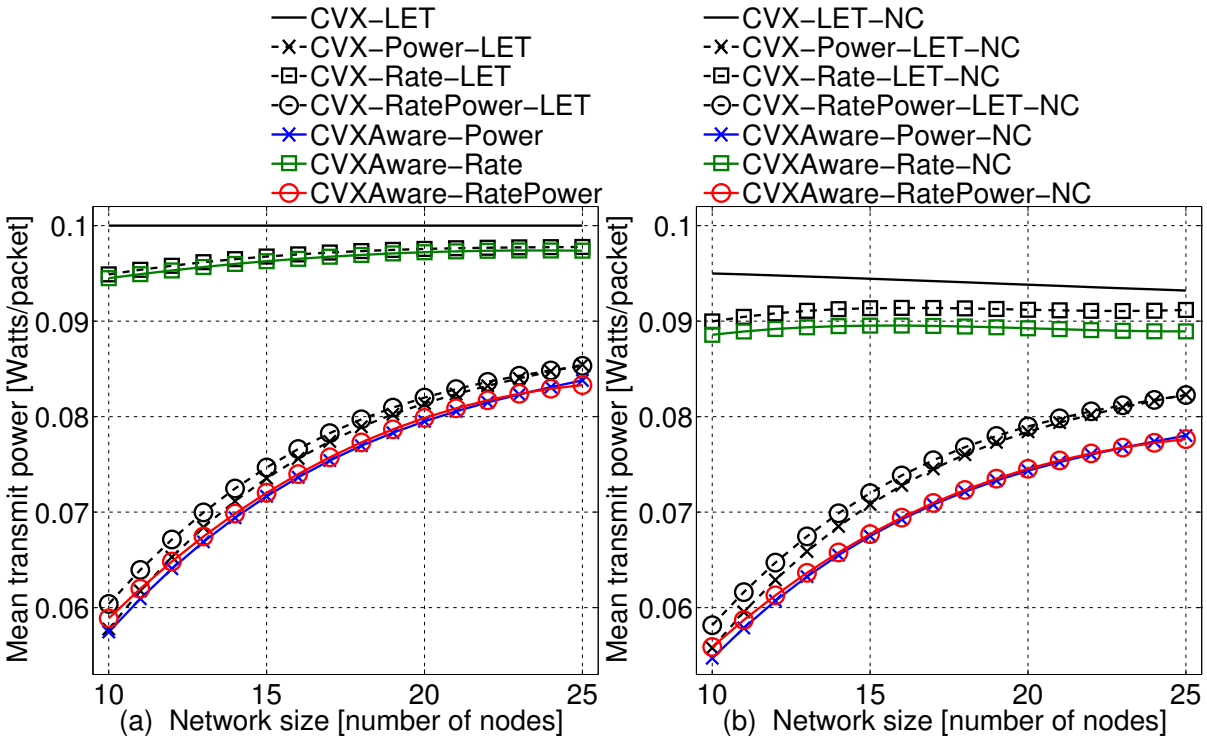

Figure 7.8: Mean transmit power comparison with (b) and without (a) NC.

7.6 SPATIAL AND TEMPORAL REUSE

There is a relationship between spatial and temporal reuse, since greater spatial reuse implies greater interference and consequently smaller temporal reuse. These results are evident in Figure 7.9, where the power-adaptive schedules have the greatest spatial reuse (a) but the smallest temporal reuse (b). Node-assigned schedules in turn achieve the highest temporal reuse, which reduces the spatial reuse possibilities so that these also achieve the smallest spatial reuse. The power-adaptive $\widetilde{C}_e$-schedules give greater preference to temporal reuse when compared to the C-schedules, which have higher spatial reuse. Thus, with temporal reuse-aware optimisation a more beneficial balance is found between spatial and temporal reuse, which results in favourable network performance.

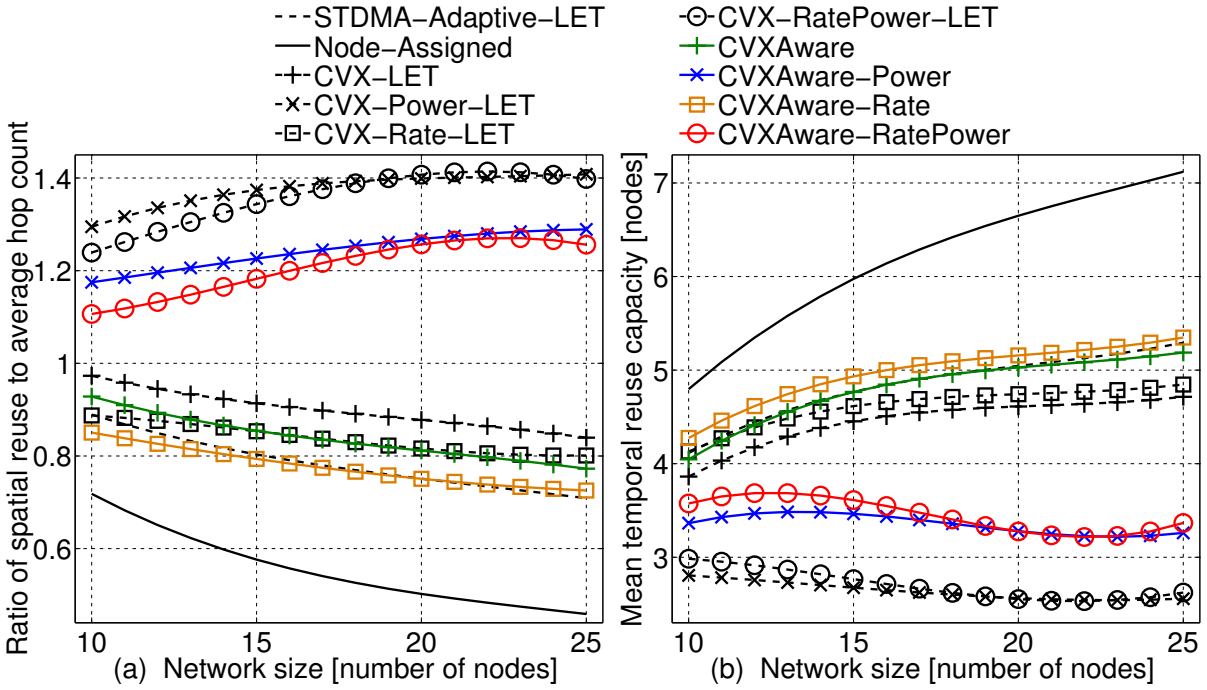

Figure 7.9: Spatial reuse (a) and temporal reuse capacity (b) comparison.

7.7 RESULTS SUMMARY

A generic transmission scheduling algorithm has been developed that produces predefined link-assigned schedules that maximise schedule capacity with proportionally fair end-to-end flow rates for stationary wireless multihop mesh networks with single-path minimum hop routing, rate and power adaptivity, both spatial and temporal reuse and network coded

forwarding. The concept of temporal reuse is newly defined in this work, and is used to re-evaluate the hybrid node-link assignment strategy of [1]. The schedules that can induce packet depletion are characterised, and it is shown how such schedules can benefit from temporal reuse.

The mesh network link rate region is refined to incorporate and account for the benefits of temporal reuse, and this temporal reuse-aware rate region is used in an updated cross-layer optimisation scheduling algorithm based on the work in [32]. It was experimentally shown that the temporal reuse-aware schedules have increased schedule capacity, better flow rate fairness, and for schedules with rate and power adaptivity, greater power efficiency than schedules optimised in the non-aware rate region of [32]. The temporal reuse-aware schedules also achieved a better balance between spatial and temporal reuse.

CHAPTER 8
FOUNTAIN CODES

The transmission scheduling has been optimised in the previous part of the document, and it has been shown to provide improved performance. The link-assigned schedules with extended transmission rights allow for network coding, and it is this aspect of the wireless mesh network operation that is focussed on for the remainder of this study. The research goal is to determine whether the integration of network coding into link channel coding and source coding can improve the network performance. Sparse graph error-correction codes are some of the most efficient and highest performance codes, so a subclass called fountain codes is employed specifically due to its rateless output property.

The purpose of the error-correcting channel code is to counteract the signal distortions caused by channel noise. Different types of channels are firstly analysed in this chapter, to determine the effects their noise have on transmission. General sparse graph codes are then introduced and specific subclasses such as low-density parity-check and fountain codes are explained. The sparse graph decoding mechanism is then formulated, as it is the key component that determines the effectivity of the channel code. This mechanism is termed belief propagation, and its behaviour is analysed with the use of density evolution. It is shown that density evolution is an important tool in specifically improving the structure of fountain codes for better error-correcting performance. An outline of the chapter is given in Figure 8.1, indicating the topics addressed regarding fountain codes.

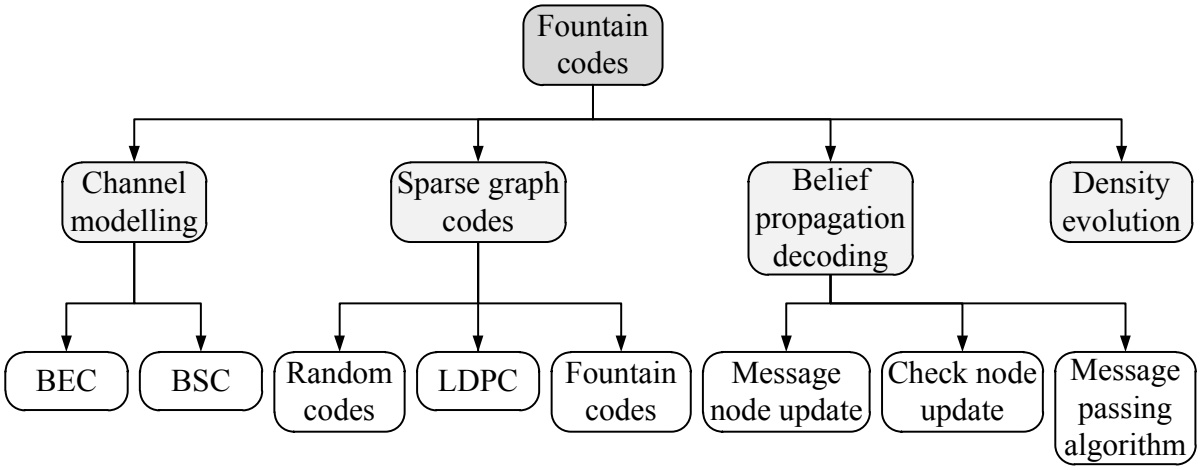

Figure 8.1: The fountain code outline covered in this chapter.

8.1 CHANNEL MODELLING

Signalling via electromagnetic waves has many benefits, such as the allowance of communication between two points that would have difficulty connecting with wires. These benefits of wireless connectivity are offset by the signal degradation caused by environmental electromagnetic disturbances, receiver circuitry noise and reduced power due to distance attenuation. When a series of signals are received and converted to binary digits, then the noise will cause some of those bits to be in error. The randomness of the noise makes it difficult to know which bits are incorrectly received, so a means of ensuring faultless reception is not immediately apparent. Claude E. Shannon [42] showed that there is maximum bound of information that can be transferred over an unreliable communication channel, termed the channel capacity. The seminal work of Shannon ushered in the age of information theory and it was finally clear that reliable data transmission is possible for rates arbitrarily close to the channel capacity.

Understanding the nature of a communication channel is instrumental in modelling the way in which it introduces errors into the received data. The error model can be used to good effect when designing a signalling strategy that can ensure reliable transmission. Two of the most important models are the binary erasure channel (BEC) and the binary symmetric channel (BSC), which serve to describe a number of real world communication channels.

8.1.1 Binary erasure channel

In some packet-based networks the checksums of the received packets are verified, and if the calculated checksum does not match the received checksum then the packet is erroneous. A faulty packet needs to be retransmitted in that case, rather than attempting to correct it. Figure 8.2(a) is an example of a binary erasure channel with parameter ε, where a symbol is received correctly with probability $1-\varepsilon$ and unknown or erased with probability ε. The value of an erased packet or symbol is simply not known, even though the exact position of the erased symbol is. Since there is a fraction of $1-\varepsilon$ of all the received symbols that are correct, the BEC capacity is $\text{BEC}(\varepsilon) = 1-\varepsilon$ if the channel parameter is ε. The BEC can be decoded in polynomial time seeing that the decoding problem can be reduced to solving a system of equations [43].

8.1.2 Binary symmetric channel

An additive white Gaussian noise (AWGN) channel distorts the transmitted signal x at the receiver by adding random noise e, which can change the symbol decision made on the observed value $y = x + e$. For binary phase-shift keying (BPSK) enough added noise in the right direction can flip a transmitted bit to its alternate, and given the symmetry of the Gaussian noise the probability p of a misread symbol is equal for either a 0 or 1. The resulting binary symmetric channel (BSC) shown in Figure 8.2(b) is more complicated than the BEC, because the receiver does not know exactly which symbol positions were received incorrectly. With the BEC the receiver knows which symbols are erased which simplifies the task of error correction, whereas with the BSC the maximum likelihood decoding complexity is NP-complete [44]. The BSC with channel parameter p receives a symbol correctly with probability $1-p$ and the channel capacity is given in Equation 8.1 in terms of the binary entropy $H_2(p) = -p\log_2 p - (1-p)\log_2(1-p)$.

$$\begin{aligned} \text{BSC}(p) &= 1 - H_2(p) \\ &= 1 + p\log_2 p + (1-p)\log_2(1-p) \end{aligned} \tag{8.1}$$

8.2 SPARSE GRAPH CODES

Reliable communication requires the implementation of a transmission strategy that can allow for the determination or the correction of received symbols in the case of the BEC or BSC respectively. A simple strategy is where transmitted data is repeated several times, so that the

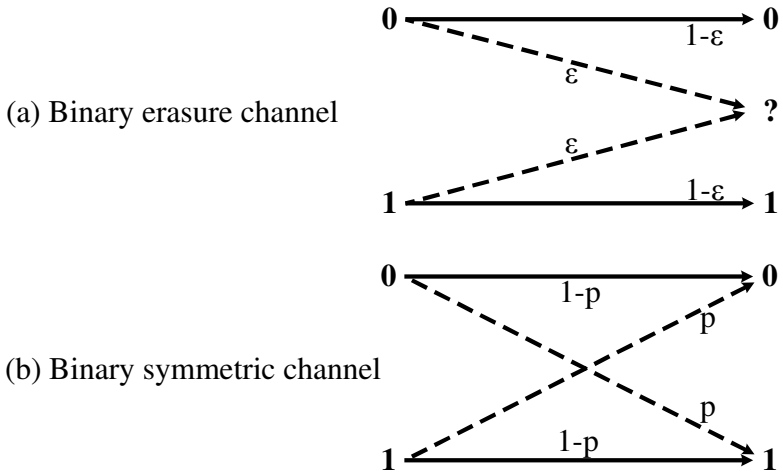

Figure 8.2: The (a) BEC(ε) and (b) BSC(p) models indicating the transition probabilities.

receiver can take a majority decision to form the most likely transmitted data sequence. There is then a need to transmit correlated redundancy to reduce the information rate below the channel capacity, which involves a strategy termed channel coding. Shannon defined [42] codes as ensembles of vectors that are to be transmitted. A code is a finite set of vectors or codewords of equal length, called the block length. The code should map or associate each vector uniquely to a k-bit input word, so there should be 2^k unique codewords of block length $n > k$. In this case, the code information rate is k/n bpc (bits per channel use) which cannot exceed the channel capacity.

8.2.1 Random codes

Capacity can be reached asymptotically in the block length $n \rightarrow \infty$ for random codes, although Shannon does not explain how to construct capacity approaching codes. Random codes of rate R are 2^{nR} random codewords of block length n over the channel input alphabet. A practical implementation of random codes requires a codebook that shows the mapping between all the random codewords and all the possible input strings. To achieve a reasonable information rate a large block length is required, often a value $n > 100$, which will produce a codebook far too large for any realistic implementation constraints.

Overcoming the practical infeasibility of a codebook-based random code necessitates a structured means of uniquely associating an input vector to a codeword. For this reason Elias [45] and Golay [46] independently introduced linear codes of block length n and dimension k

defined as subspaces of vector space $\mathbb{F}_2^n$. A linear code thus involves a basis set of k vectors of length n to give a code rate of k/n bpc (this unit is implied for the remainder of the document). Encoding is simplified from exponential to polynomial time with linear codes, where an input vector $(x_1, \ldots, x_k)$ is uniquely mapped to a codeword by taking linear combinations of the basis vectors identified by the coefficients $x_1, \ldots, x_k$. This way an explicit codebook enumeration is not required, as with random codes. Shannon showed [42] that there are sequences of linear codes with rates arbitrarily close to channel capacity, so that the maximum likelihood decoding error approaches 0 as the block length goes to infinity. Random linear codes specifically are known to achieve capacity.

8.2.2 Low-density parity-check codes

It is clear that efficient encoding is possible with linear codes, but a practical implementation also requires efficient decoding and a relatively good information rate. There is a need then for capacity achieving subclasses of linear codes for which maximum likelihood decoding can be done in polynomial time. For this reason low-density parity-check (LDPC) codes were invented in the early 1960's by Robert Gallager in his Ph.D dissertation [47]. LDPC codes have fast probabilistic encoding and decoding algorithms and a wealth of analytic and combinatorial design tools makes the codes practically and theoretically attractive.

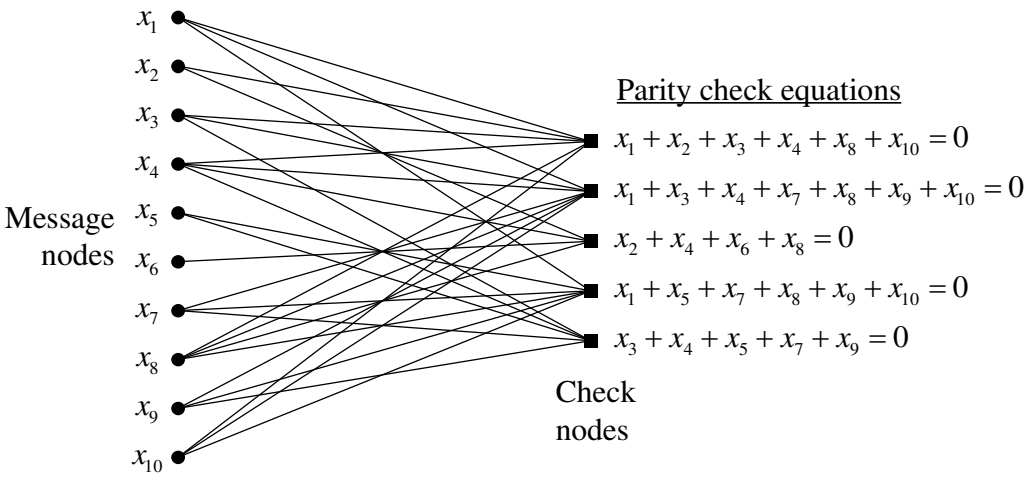

Figure 8.3: A bipartite graph representation of a linear code with parity-check equations.

LDPC codes are obtained from and decoded with bipartite graphs with n left message nodes and r right check nodes, as shown in Figure 8.3. The code block length is n and the input words are of length $k = n - r$ at least. The n coordinates of the codeword vectors are associated

with the message nodes, and the codewords are chosen such that for each check node the sum of the neighbouring message nodes are zero. The adjacency matrix of the graph is $H \in \mathbb{F}_2^{r \times n}$ where the entry $(i, j) = 1$ if the i^{th} check node is connected to the j^{th} message node. Validating the parity values of a received codeword $x = (x_1, \ldots, x_n)$ can be done according to $Hx^T = 0$, which will be zero if the received vector is a valid codeword. In the case of a distorted codeword $y = x + e$ received over an additive noise channel, the non-zero syndrome $Hy^T = H(x + e)^T = Hx^T + He^T = 0 + He^T = He^T = S$ can be computed. The decoder is tasked with finding the most likely transmitted codeword given the observation, and the bipartite graph is used in the process.

Any linear code has an associated representation as a bipartite graph, although the graph is not uniquely defined by the code. The key property of LDPC codes is the sparsity of the adjacency matrix H, which allows for algorithmic decoding efficiency. A sequence of $m \times n$ matrices is c-sparse if $mn \to \infty$ and the number of non-zero elements is less than $c \max(m, n)$. For LDPC codes each adjacency matrix H has an associated generator matrix $G \in \mathbb{F}_2^{k \times n}$ which is used to efficiently map an input word $s = (s_1, \ldots, s_k)$ uniquely to a codeword $x = (x_1, \ldots, x_n)$ via $sG = x$. The relationship between the parity-check matrix and the generator matrix is given by $HG^T = 0$, which produces a dense G for a sparse H. The burden of the dense generator matrix may be offset by exploiting cyclic construction methods or other structural design strategies to reduce the encoding complexity to an acceptable level.

The structure of LDPC bipartite graphs are often described in terms of two degree distributions $\lambda(x)$ and $\rho(x)$, one for the message nodes and the other for the check nodes respectively. The degree i of a message node is the number of parity-check equations in which the node features, and a check node degree j is the number of message nodes in the associated parity-check equation. A graph can be connected randomly and if it adheres to certain proportions of degrees, as specified by the degree distributions, then it can form a valid decoding graph. The fraction of graph edges that are connected to message nodes that have degree i is denoted by λ_i, and the fraction of edges connected to check nodes of degree j is given by ρ_j. The dual degree

distributions are thus given as in Equations (8.2) and (8.3), both from an edge perspective.

$$\text{Message degree distribution:} \quad \lambda(x) = \sum_i \lambda_i x^{i-1} \tag{8.2}$$

$$\text{Check degree distribution:} \quad \rho(x) = \sum_j \rho_j x^{j-1} \tag{8.3}$$

These degree distributions can assist in predicting the behaviour of belief propagation decoding, as they dictate how the messages sent during decoding change after each iteration. LDPC codes can thus be designed with optimised degree distributions so that certain performance guarantees can be made.

8.2.3 Fountain codes

The fixed rate of LDPC codes allows for a specific code construction that fulfils certain encoding and decoding requirements. The downside is that a different code is needed every time the channel conditions change. For this reason, fountain codes, a rateless class of sparse-graph codes, were designed [48, 49] for channels of which the noise level is not known a-priori. A fountain code produces a potentially limitless stream of output symbols for a finite given input, so that the transmitter can adaptively change the code rate if need be [50]. The key design property that makes fountain codes rateless is that every output symbol is generated independently as the sum of a certain number of randomly chosen input symbols. A synchronised pseudo-random number generator may be used at both the transmitter and receiver to allow for coherent decoding of a set of received output symbols.

One of the first classes of efficient fountain codes, called LT-codes (Luby transform-codes), was discovered by Michael Luby [48], specifically for the erasure channel. The focus in the work on joint coding is on binary fountain codes that are truncated, since the block length can be potentially infinite. An LT-code output symbol is also the sum of i independently chosen input symbols, where the probability of an output node with degree i is given by Ω_i. The output degree distribution generator polynomial is $\Omega(x) = \sum_i \Omega_i x^i$, which is a useful polynomial construct that assists in calculating for example the mean output degree $\Omega'(1) = \sum_i i\Omega_i$. An LT-code can then be described as a fountain code with parameters $(k, \Omega(x))$. The decoding graph or Tanner graph for an LT-code is also a bipartite graph with k left input nodes and n right output nodes, and the graph also serves as the direct encoding graph. In this respect the adjacency matrix H is used differently than in an LDPC code, since a different generator matrix

is employed by an LDPC code.

LT-codes are meant to be used especially in erasure environments, such as the BEC, and is designed to be hard-decoded without belief propagation. An output degree distribution has been optimised for this LT-code scenario, and it is termed the robust soliton distribution [49]. This distribution is composited from two degree distributions $w(d)$ and $t(d)$, which are each a function of the probabilities for a given degree d. The ideal soliton distribution is defined in Equation (8.4), where k is the number of input nodes or source symbols.

$$\text{Ideal solition distribution:} \quad w(d) = \begin{cases} 1/k & \text{for } d = 1 \\ 1/\left(d(d-1)\right) & \text{for } 1 < d \leq k \end{cases} \tag{8.4}$$

The second component function is given in Equation (8.5), where $S = c\sqrt{k}\log(k/\delta)$, with $c < 1$ an arbitrary positive constant and $(1-\delta)$ the probability that all k input symbols can be recovered when only kZ output symbols are available. The robust soliton distribution $\Omega(x) = \sum_i \mu(i)x^i$ is then a function of the combination of the two distributions as shown in Equation (8.6), where $Z = \sum_{d=1}^{k}(w(d) + t(d))$.

$$\text{Modifying distribution:} \quad t(d) = \begin{cases} S/(dk) & \text{for } d = 1, 2, \ldots, k/S - 1 \\ S\log(S/\delta)/k & \text{for } d = k/S \\ 0 & \text{for } d > k/S \end{cases} \tag{8.5}$$

$$\text{Robust soliton distribution:} \quad \mu(d) = \frac{w(d) + t(d)}{Z} \tag{8.6}$$

The ideal soliton distribution is designed to theoretically minimise the expected overhead, although fluctuation around the mean and lack of packet diversity can cause a deficiency of symbols of degree one. These symbols are required for hard-decoding, so the robust soliton distribution is modified to produce more symbols of degree one to ensure successful decoding. The input node degree distribution $\Psi(x)$ describes the fractions of input nodes that have certain degrees, and since input nodes are randomly connected with an average degree of $\zeta = n\Omega'(1)/k$ it can be shown through a Taylor expansion that the input node degree distribution is $\Psi(x) = e^{\zeta(x-1)}$.

8.2.4 Comparison between LDPC and fountain codes

Fountain codes were originally designed for efficient broadcasting of common content to many users connected via binary erasure channels. Even when users have different symbols erased,

the extra symbols made available by the fountain code can be used by all users to get sufficient data for lossless recovery with hard-decoding. Since fountain codes can be soft-decoded with the means of belief propagation, it has been adapted to serve on other channels such as the BSC or AWGN channels like LDPC codes.

Fountain codes have been designed so that it can produce a potentially endless amount of output symbols, and is thus fully rateless. LDPC codes, on the other hand, normally have fixed input-to-codeword rates. The performance guarantees of the LDPC code depends on the specific rate for which its degree distributions have been optimised. For fountain codes only the output degree distribution needs to be optimised, so that the code can still assume any rate with the Poisson distributed input degree distribution.

LDPC codes have a separate generator matrix with which an input is transformed into a codeword, whereas fountain codes use the parity-check matrix directly as the generator matrix for transforming an input into an output. This means that the LDPC syndrome becomes the fountain code output word, and the LDPC codeword corresponds with the fountain code input word during belief propagation decoding. The LPDC message or variable nodes is thus also the fountain code input nodes, and the LDPC check nodes is the fountain code output nodes.

The LDPC parity-check equations are calculated according to all-zero parity, while the effective fountain code syndrome/output is not all-zero. This eases the design of fountain codes, since there is no separate generator matrix that has to conform with the all-zero syndrome requirement $HG^T = 0$. Regardless of the actual syndrome value S, belief propagation remains equally effective in solving the key equation $Hy^T = S$. Table 8.1 lists a number of important distinctions between LDPC codes and fountain codes.

Table 8.1: A comparison of key characteristics between LDPC and fountain codes.

	LDPC	Fountain code
Rate	Fixed	Rateless
Encoding	$sG = x$	$Hs^T = x$
Decoding	$Hx^T = 0$	$Hx^T = S$
Message degree distribution	$\lambda(x)$	$\psi(x)$
Check degree distribution	$\rho(x)$	$\omega(x)$

8.3 BELIEF PROPAGATION DECODING

The decoder at the receiver-side is tasked with finding the most likely codeword that was sent, given the information of the observed codeword. By listing all the codewords and calculating the conditional probability for each of the codewords, given the observed values, the codeword with the maximum probability can be found. Shannon proved [42] that the maximum likelihood decoding error goes to zero exponentially fast with increases in the code block length. This maximum likelihood decoding is the best the receiver can do, since it uses all the available information to the best of its ability. Unfortunately, explicit codeword enumeration and conditional probability calculation is prohibitively complex for practical block lengths, so maximum likelihood decoding is not computationally feasible for most codes.

Basing a code on a graph, such as a bipartite graph for sparse graph codes, provides the potential for elegant and efficient encoding and especially decoding algorithms. One such decoding algorithm is belief propagation, which is a subclass of iterative message-passing algorithms. Belief propagation is also used in artificial intelligence [51]. Belief propagation sends sets of messages back and forth between the message and check nodes in the bipartite graph, where the messages are beliefs or probabilities of what each node value should be. The message sent from a message node to a directly connected check node is computed using the observed value for the message node from the channel reception and the values received from all the other directly connected check nodes. Note that the message computation does not take into account the value received from the check node for which it is calculated. This condition of not including a value from a node in a message to that node also applies for messages sent from check to message nodes.

A bipartite coding graph establishes a relationship between the message nodes involved in a parity-check equation, which is useful in helping to determine the value of a message node if for example its value is erased. Furthermore, through the coordination of value beliefs these parity-check equations can help to resolve low reliability values. It is the structure of the sparse graph code that allows for efficient message-passing that can improve value reliabilities. Working from the parity-check equation each check node c can inform a message node v of the value it believes the message node should have, without consulting the observed received value m_v associated with the message node. In Figure 8.4(b) the check node

$y_3 = x_2 + x_4 + x_6 + x_8$ calculates the perceived value $m_{y_3x_4}$ of message node x_4, by solving $y_3 + x_4 - y_3 = x_2 + x_4 + x_6 + x_8 + x_4 - y_3$. The parity-check equation is a summation in the binary Galois field, where a subtraction is effectively an addition, so that $x_4 = x_2 + x_6 + x_8 + y_3$. In this manner a message node value can be calculated at an involved check node, without requiring information from the message node in question. This is the key mechanism that belief propagation exploits to perform error-correction.

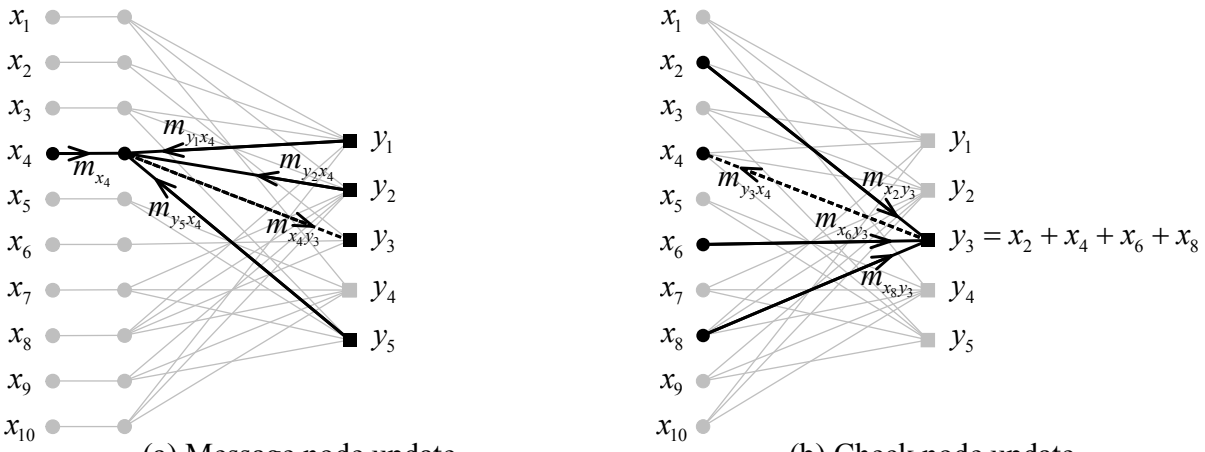

(a) Message node update (b) Check node update

Figure 8.4: Belief propagation message (a) and check node (b) updates.

8.3.1 Message node update

To formulate the exact belief propagation update equations, a mechanism is firstly required to accurately combine the channel and check node beliefs for a message node into an averaged group belief. In the case of Figure 8.4(a) the beliefs $m_{x_4}, m_{y_1x_4}, m_{y_2x_4}, m_{y_5x_4}$ must be aggregated into one belief. For this purpose each belief can be expressed as a log-likelihood, and then simply summed together to obtain the average belief. This belief ($m_{x_4y_3}$) is then sent to the non-participating check node to inform it of the value of the specific message node, which can then be used in the message node update of the following iteration. The information, previously sent from the check node to which the message node now responds, is not factored into the update to avoid intrinsic information transfer. This is an important condition, because if a check node receives its own information back then it fortifies its own beliefs, which is unwarranted. This intrinsic information cycling will happen eventually, unless the bipartite graph has no cycles and forms a tree. A cycle occurs when two or more message nodes share two or more check nodes, which causes a vice versa situation wherein a check node's belief is

cycled back to itself via an alternate message node.

The likelihood of a binary random variable x is given by $L(x) = p(x = 0)/p(x = 1)$, and its log-likelihood is $\log L(x)$. Given another binary random variable y, the conditional likelihood of x is $L(x|y) = p(x = 0|y)/p(x = 1|y)$, and the conditional log-likelihood is $\log L(x|y)$. The log-likelihood $\log L(x|y_1, \ldots, y_d)$ of a message node x needs to be determined, conditioned on its d neighbouring check nodes $y_1, \ldots, y_d$, where d is the degree of the message node. This computation needs to be written in terms of the messages $\log L(x|y_i)$ received from the neighbouring check nodes. Notice that the parity-check equations are assumed to be independent, and in the case of fountain codes should be independent. Belief propagation is built upon this independence assumption and the assumption that the message-passing equivalent graph forms a tree. If x has equiprobable outcomes then $L(x|y) = L(y|x)$, and using the chain rule and the independence assumption the message-node log-likelihood can then be written as

$$\log L(x|y_1, \ldots, y_d) = \sum_{i=1}^{d} \log L(x|y_i). \tag{8.7}$$

8.3.2 Check node update

In the check node update shown in Figure 8.4(b), each message node sends its own perceived value to an involved check node, based on its channel observation and what all the other involved check nodes say its value should be. A check node can use the log-likelihoods received from its neighbouring message nodes, together with its parity-check equation, to give a message node new information on its value. The check node can send to a message node x the calculated log-likelihood $\log L(x_1 + \ldots + x_d = 0|y_1, \ldots, y_l)$, conditioned on a subset of the check nodes which influence the log-likelihoods received from its neighbouring message nodes. The value of the message node to which the check node responds is omitted from the parity-check equation, with the purpose of obtaining an independent belief for the message node in question. To write the parity-check log-likelihood in terms of $\log L(x_i|y_1, \ldots, y_l)$, notice the relationship in Equation (8.8) due to the independence assumption and since $p(x_1 + x_2 = 0|y_1, \ldots, y_l) = p(x_1 = 0|y_1, \ldots, y_l)p(x_2 = 0|y_1, \ldots, y_l) + (1 - p(x_1 = 0|y_1, \ldots, y_l))\,(1 - p(x_2 = 0|y_1, \ldots, y_l))$.

$$2p(x_1 + x_2 = 0|y_1, \ldots, y_l) - 1 = (2p(x_1 = 0|y_1, \ldots, y_l) - 1)\,(2p(x_2 = 0|y_1, \ldots, y_l) - 1) \tag{8.8}$$

Forming a chain rule from Equation (8.8), it can be shown that the entire parity-check formulation can be included as follows:

$$2p(x_1 + ... + x_d = 0|y_1, ..., y_l) - 1 = \prod_{i=1}^{d} (2p(x_i = 0|y_1, \ldots, y_l) - 1) \tag{8.9}$$

The log-likelihood based on the parity-check equation can then be written in terms of previously received log-likelihood values $\log L(x_i|y_1, \ldots, y_l)$. First note that the definition $L(x) = \frac{p(x=0)}{p(x=1)}$ of likelihood is used to integrate Equation (8.9) into the proof so that

$$\begin{aligned}\log L(x_1 + \ldots + x_d = 0|y_1, \ldots, y_l) &= \log\left(\frac{p(x_1 + ... + x_d = 0|y_1, ..., y_l)}{1 - p(x_1 + ... + x_d = 0|y_1, ..., y_l)}\right) \\ &= \log\left(\frac{1 + (2p(x_1 + ... + x_d = 0|y_1, ..., y_l) - 1)}{1 - (2p(x_1 + ... + x_d = 0|y_1, ..., y_l) - 1)}\right) \\ &= \log\left(\frac{1 + \prod_{i=1}^{d} (2p(x_i = 0|y_1, \ldots, y_l) - 1)}{1 - \prod_{i=1}^{\ell} (2p(x_i = 0|y_1, \ldots, y_l) - 1)}\right).\end{aligned} \tag{8.10}$$

By using the identity $2\tanh^{-1} z = \log\left(\frac{1+z}{1-z}\right)$ it can then be shown that Equation (8.10) is

$$\log\left(\frac{1 + \prod_{i=1}^{d} (2p(x_i = 0|y_1, \ldots, y_l) - 1)}{1 - \prod_{i=1}^{\ell} (2p(x_i = 0|y_1, \ldots, y_l) - 1)}\right) = 2\tanh^{-1}\left(\prod_{i=1}^{d}(2p(x_i = 0|y_1, \ldots, y_l) - 1)\right). \tag{8.11}$$

Using the likelihood equality $p(x_i = 0|y_1, \ldots, y_l) = \frac{L(x_i=0|y_1,...,y_l)}{1+L(x_i=0|y_1,...,y_l)}$ it can then be shown that Equation (8.11) is

$$2\tanh^{-1}\left(\prod_{i=1}^{d}(2p(x_i = 0|y_1, \ldots, y_l) - 1)\right) = 2\tanh^{-1}\left(\prod_{i=1}^{d}\frac{L(x_i = 0|y_1, \ldots, y_l) - 1}{L(x_i = 0|y_1, \ldots, y_l) + 1}\right). \tag{8.12}$$

Finally, the identity $\tanh z = \frac{e^{2z}-1}{e^{2z}+1}$ can be used to prove that the parity-check log-likelihood $\log L(x_1 + \ldots + x_d = 0|y_1, \ldots, y_l)$ can be written in terms of the received log-likelihood values $\log L(x_i = 0|y_1, \ldots, y_l)$ as

$$\begin{aligned}\log L(x_1 + \ldots + x_d = 0|y_1, \ldots, y_l) &= 2\tanh^{-1}\left(\prod_{i=1}^{d}\frac{L(x_i = 0|y_1, \ldots, y_l) - 1}{L(x_i = 0|y_1, \ldots, y_l) + 1}\right) \\ &= 2\tanh^{-1}\left(\prod_{i=1}^{d}\tanh(0.5\log L(x_i = 0|y_1, \ldots, y_l))\right).\end{aligned} \tag{8.13}$$

8.3.3 Message-passing algorithm

In round 0 of belief propagation each message node v sends its log-likelihood ratio $m_{vc}^{(0)}$ to neighbouring check nodes c based on the channel observations, which for a BSC(p)

channel would be $\log((1-p)/p)$. During further rounds each message node v will send its log-likelihood ratio $m_{vc}^{(\ell)}$ conditioned on its channel observations and the beliefs of neighbouring check nodes, without cycling back intrinsic information directly. Each check node c will send a value $m_{cv}^{(\ell)}$ to each of its message nodes v so that their parity-check equations are fulfilled. The belief update equations are thus given in Equations (8.14) and (8.15), and are executed iteratively for a maximum number of iterations, or until the least reliable likelihoods exceed a threshold.

$$m_{vc}^{(\ell)} = \begin{cases} m_v, & \text{if } \ell = 0, \\ m_v + \sum_{c' \in C_v \setminus \{c\}} m_{c'v}^{(\ell-1)}, & \text{if } \ell \geq 1. \end{cases} \tag{8.14}$$

$$m_{cv}^{(\ell)} = 2 \tanh^{-1} \left(\prod_{v' \in V_c \setminus \{v\}} \tanh(\frac{1}{2} m_{v'c}^{(\ell)}) \right) \tag{8.15}$$

With LDPC codes the received codeword is mapped to the message nodes via m_v, but this differs from a fountain code since its codeword is mapped to the check nodes instead. Where an LDPC code uses a separate generator matrix to produce a codeword from an input source, the fountain code uses the parity-check matrix to encode and decode. For this reason the check update equation needs to include the received log-likelihood m_c of every codeword symbol as mapped to a check node. The message node log-likelihoods m_v will in most cases then revert to zero, unless the receiver has information of an input bias $p_s \neq \frac{1}{2}$. The message-passing algorithm update equations for fountain codes, or LDPC codes that are used for compression, are given in Equations (8.16) and (8.17).

$$m_{vc}^{(\ell)} = \begin{cases} m_v, & \text{if } \ell = 0, \\ m_v + \sum_{c' \in C_v \setminus \{c\}} m_{c'v}^{(\ell-1)}, & \text{if } \ell \geq 1. \end{cases} \tag{8.16}$$

$$m_{cv}^{(\ell)} = 2 \tanh^{-1} \left(\tanh(\frac{1}{2} m_c) \prod_{v' \in V_c \setminus \{v\}} \tanh(\frac{1}{2} m_{v'c}^{(\ell)}) \right) \tag{8.17}$$

In the Equations of (8.14) and (8.15) the set of check nodes incident to message node v is C_v, and the set of message nodes incident to check node c is given by V_c. In belief propagation each graph edge is traversed a constant number of times for a constant number of belief propagation iterations, which makes the number of operations linear in the number of message nodes for a sparse graph. The algorithm is independent of the channel and the specific messages passed is dependent on the channel. The benefit of belief propagation is mainly its efficiency, since maximum likelihood decoding can be more optimal as in the case of biregular bipartite graphs of a large common message node degree.

8.4 DENSITY EVOLUTION

The messages sent along the Tanner graph edges during belief propagation are considered to be random variables, and under the independence assumption the messages are statistically independent during every round. This assumption is however only correct for the first ℓ rounds if the message neighbourhood of each message node forms a tree. With Martingale arguments and under the tree assumption it can be shown that the behaviour of the message-passing algorithm can be analysed with asymptotical correctness [52–54]. This is the task of density evolution, which groups the log-likelihood messages sent from all the message nodes into a common log-likelihood probability density, and the same for messages sent from check nodes. Tracking the change due to the update equations in only one common density neatly summarises the behaviour of the message-passing algorithm, without having to work with individual messages.

8.4.1 Message node updates

To illustrate that all the outgoing messages from one side of the graph can be described by one common log-likelihood ratio probability density, consider the first channel-conditioned messages m_v sent from the message nodes to the check nodes at the start of the algorithm. The noise experienced for each received codeword symbol was sampled randomly from the channel noise probability density, and so m_v can be described by the channel noise density if the added assumption is made that the all-zero codeword was sent. The all-zero codeword assumption maintains the accuracy of density evolution for symmetric channels, since the additive noise is independent of the exact symbols being sent. Since the message-passing algorithm works directly with log-likelihoods, density evolution also requires an L-density, which is a probability density a wherein the probability of a message with a certain log-likelihood ratio is specified. The channel L-densities for the BEC and BSC are given in Equations (8.18) and (8.19) respectively, where Δ_z is the Dirac delta functional at point z.

$$\mathsf{a}_{\mathrm{BEC}(\varepsilon)}(y) = \varepsilon\Delta_0(y) + (1-\varepsilon)\Delta_{+\infty}(y) \tag{8.18}$$

$$\mathsf{a}_{\mathrm{BSC}(p)}(y) = p\Delta_{-\log\frac{1-p}{p}}(y) + (1-p)\Delta_{\log\frac{1-p}{p}}(y) \tag{8.19}$$

The messages that can be received at a node during a specific round is described by the L-density of the incoming message. The incident node would then perform an update calculation to form a new message to be sent to neighbouring nodes. In the case of message nodes during the later rounds $\ell \geq 1$, the incoming messages are added together according to $m_{vc}^{(\ell)} = m_v + \sum_{c' \in C_v \setminus \{c\}} m_{c'v}^{(\ell-1)}$

featuring in Equation (8.14). If the channel-conditioned messages m_v are described by density a_0 and the received messages by common density a, then the density-equivalent calculation would be $\mathsf{a}_0 \star \mathsf{a}^{\star(d-1)}$ for a message node of degree d. The $(d-1)$-fold convolution $\mathsf{a}^{\star(d-1)}$ of the real density a gives the density of the summation of $(d-1)$ random variables of density a. The multi-fold convolution can be divided logarithmically into pairwise convolutions (shown in Equation (8.20)) to efficiently compute the new density. A convolution in the time domain is equivalent to a multiplication in the Fourier domain, so by converting the densities to and remaining in the Fourier domain the convolutions can be performed faster.

$$\mathsf{a}^{\star 2} = \mathsf{a} \star \mathsf{a}, \quad \mathsf{a}^{\star 3} = \mathsf{a} \star \mathsf{a}^{\star 2}, \quad \mathsf{a}^{\star 5} = \mathsf{a}^{\star 2} \star \mathsf{a}^{\star 3}, \quad \mathsf{a}^{\star 6} = \mathsf{a}^{\star 3} \star \mathsf{a}^{\star 3} \tag{8.20}$$

The message nodes typically have different degrees, as determined by the message node degree distribution, so to determine the common density of the messages sent from the message nodes to the check nodes the degree distribution has to be taken into account. For LDPC codes the fraction of edges relaying a message from a degree i message node is given by λ_i, and so that fraction of the new computed density $\mathsf{a}^{\star(i-1)}$ at degree i message nodes will feature in the final common message density given in Equation (8.21).

$$\mathsf{a}_0 \star \lambda(\mathsf{a}) = \mathsf{a}_0 \star \left(\sum_i \lambda_i \mathsf{a}^{\star(i-1)} \right) \tag{8.21}$$

8.4.2 Check node updates

Similarly, the check nodes will receive messages from the message nodes during each round according to a common density. Each check node will calculate a belief of a message node log-likelihood according to the update $m_{cv} = 2\tanh^{-1}\left(\prod_{v' \in V_c \setminus \{v\}} \tanh(0.5 \log m_{v'c})\right)$ featuring in Equation (8.15). This computation can also be segmented into pairwise calculations given by Equation (8.22) due to the implication of Equation (8.23) in a chain rule.

$$2\tanh^{-1}(\tanh(\frac{1}{2}i)\tanh(\frac{1}{2}j)) \tag{8.22}$$

$$2\tanh^{-1}\left(\tanh(\frac{1}{2}i)\tanh(\frac{1}{2}j)\tanh(\frac{1}{2}k)\right) = 2\tanh^{-1}\left(\tanh\left(\frac{1}{2}\cdot 2\tanh^{-1}(\tanh(\frac{1}{2}i)\tanh(\frac{1}{2}j))\right)\tanh(\frac{1}{2}k)\right) \tag{8.23}$$

Using the table method in [55], every combination of two messages i and j that gives the result of Equation (8.22) is determined and the probability of the combination is added to the

probability density for that point. With messages i and j sampled from a log-likelihood density a, let the new density calculated according to Equation (8.22) be denoted by $\mathsf{a}^{*2} = \mathsf{a} * \mathsf{a}$. A check node of degree i will thus calculate the message $\mathsf{a}^{*(i-1)}$ if the most recent messages received from the neighbouring message nodes had L-density a. As with the message nodes, the edge degree distribution defines how messages of different degrees contribute to the final common message density. The fraction of edges that relay a message of degree i is given by ρ_i, and the complete L-density of the messages sent from the check nodes to the variable nodes are given in Equation (8.24).

$$\rho(\mathsf{a}) = \sum_i \rho_i \mathsf{a}^{*(i-1)} \tag{8.24}$$

8.4.3 Degree distribution optimisation

The log-likelihood density of the messages sent by the message nodes are tracked for each round of belief propagation, according to Equation (8.25). The first density a_0 is determined solely by the channel noise density, which then evolves as the message-passing algorithm resolves the information. Assuming that the all-zero codeword was sent, then it will mean that the larger part of a_0 will be in the positive domain for a reasonable BSC noise level. This is the case since $\log\left(\frac{1-p}{p}\right)$ would be positive for a zero symbol, where the probability of the symbol being one is a small p. With this antipodal mapping the negative part of the message density a_ℓ is associated with an incorrect symbol decoding decision, since a negative log-likelihood would mean the symbol is a one. This decoding error $\int_{x<0} \mathsf{a}_\ell(x)dx$ should decrease round after round with belief propagation, until the error becomes negligible.

$$\mathsf{a}_\ell = \mathsf{a}_0 \star \lambda(\rho(\mathsf{a}_{\ell-1})) \tag{8.25}$$

The role of density evolution is then to analyse the error of a code, and to provide a fitness measure specifically for the degree distributions which define the code. By having a tool to easily measure the utility of a code, the degree distributions can be readily optimised. Notice that under the independence and tree assumption the behaviour of a code is completely determined by the message and check degree distributions. By changing the degree distributions, the rate of error decrease and the error floor values are also changed. In practice small changes are made to one of the degree distributions, and a fitness measure then guides the degree distribution changes in the right direction.

In order to write Equation (8.25) of density evolution in terms of fountain code degree

distributions, first note that the calculation is made in terms of edge degree distributions and not node degree distributions. The message node degree distribution $\Psi(x) = \Psi_i x^i$ and the check node degree distribution $\Omega(x) = \Omega_i x^i$ for fountain codes then need to be used in edge degree distribution formulations, which are given by $\psi(x) = \psi_i x^{i-1}$ and $\omega(x) = \omega_i x^{i-1}$ in Equations (8.26) and (8.27). The fraction ω_i of edges are connected to output nodes of degree i, and the probability that a randomly chosen edge is connected to an input node of degree i is given by ψ_i. The output degree distributions do not depend on the number of output nodes, while the input degree distributions do.

$$\psi(x) = \psi_i x^{i-1} = \frac{\Psi'(x)}{\Psi'(1)} \tag{8.26}$$

$$\omega(x) = \omega_i x^{i-1} = \frac{\Omega'(x)}{\Omega'(1)} \tag{8.27}$$

The edge degree distributions for fountain codes can be used to characterise the belief propagation algorithm, as shown in the fountain code density evolution Equation (8.28). Since LDPC codes and fountain codes use the exact same message-passing algorithm and bipartite graph type, density evolution can be performed for both where $\lambda(x)$ and $\psi(x)$, as well as $\rho(x)$ and $\omega(x)$ are describing the same edge degree distributions. Density evolution then predicts the behaviour of belief propagation for soft-decoded fountain codes.

$$\mathsf{a}_\ell = \mathsf{a}_0 \star \psi(\omega(\mathsf{a}_{\ell-1})) \tag{8.28}$$

The density evolution formula in Equation (8.28) correspond with the LDPC decoding update Equations (8.14) and (8.15). However, with fountain codes the codeword is received at the check nodes, so the formula has to reflect the starting log-likelihoods a_m and a_c of both the input or message nodes and the output or check nodes, respectively. Normally the message node starting log-likelihoods will be zero ($a_m = \Delta_0$), and the check node starting log-likelihoods will reflect the density of the channel over which the codeword was received. The updated density evolution formula is thus given in Equation (8.29), which correspond to the update Equations (8.16) and (8.17).

$$\mathsf{a}_\ell = \mathsf{a}_m \star \psi(\mathsf{a}_c * \omega(\mathsf{a}_{\ell-1})) \tag{8.29}$$

Considering the important influence of the degree distributions on the performance of decoding on a Tanner graph, an optimised distribution should be used. For fountain codes the equivalent node degree distribution in (8.30) has been designed for the BEC, but it has been shown to produce good performance for binary symmetric channels [56–58]. The message node degree

distribution $\Psi(x)$ still remains a Poisson distribution, as the input nodes are sampled randomly for connection to the check or output nodes. The optimised output degree distribution used for fountain codes is given by

$$\Omega(x) = 0.008x + 0.494x^2 + 0.166x^3 + 0.073x^4 + 0.083x^5 + 0.056x^8 + 0.037x^9 + 0.056x^{19} + 0.025x^{65} + 0.003x^{66} \quad (8.30)$$

CHAPTER 9

JOINT SOURCE -CHANNEL CODING

Traditional data compression methods are mostly not suitable for use over noisy channels, so it is made evident in this chapter that error-correction codes such as sparse graph fountain codes are more appropriate for such scenarios. The earliest attempts at compression with channel codes are discussed and an outline of the history of compression with error-correction codes is given. The use of sparse graph codes in source compression is revealed and it is indicated how fountain codes can compress data in a natural manner. It is shown in this chapter how the efficiency of belief propagation decoding can be harnessed to allow for source coding with channel codes. The basic approaches to source compression with fountain codes specifically are discussed, including decremental and incremental redundancy schemes that ensure lossless compression at the best rates possible.

The main benefit of a channel code based compressor is that it has much higher resilience to the typical catastrophic error propagation experienced with conventional compressors. By subsuming the source coder and the channel coder into one operation, greater noise-robustness can be achieved. In this chapter an overview is given of how a fountain code compressor can be used as a true joint source-channel code. Experimental results are reviewed to display the robustness of the compression scheme against the noise of binary symmetric channels such as the BSC and AWGN channel. The goal of this chapter is to introduce the concept of joint coding, where after the schemes will be expanded to include network coding in chapter ten. The factors that are included in this chapter on joint coding are given in the outline of Figure 9.1.

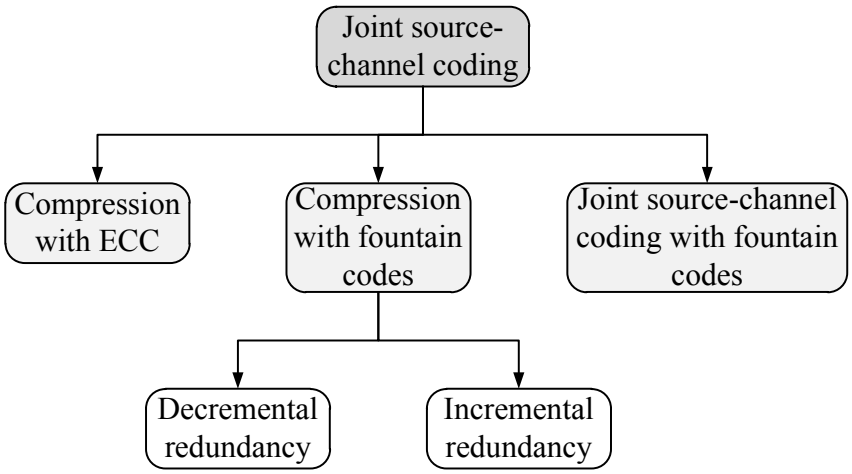

Figure 9.1: An outline of the chapter content and topics on joint coding.

9.1 COMPRESSION WITH ERROR-CORRECTION CODES

Conventional data compression algorithms, such as Huffman, Lempel-Ziv, Run-length, Tunstall and arithmetic coding, describe compressed data in terms of variable-length symbols. This makes traditional compressors especially vulnerable to catastrophic error propagation when their compressed data is transmitted over wireless communication channels with residual channel errors and noise [59]. Catastrophic error propagation can be minimised by limiting the compression block length, but this results in poorer compression performance.

Channel error-correction codes that are bespoke for symmetric channels such as the BSC, can correct a certain fraction of symbol errors wherever they might occur. The graph structure used in belief propagation decoding alludes to the lack of the propagation of errors, since the graph connections remain essentially the same regardless of the order of the nodes or errors. For this reason the use of error-correction codes as data compressors have been considered ever since Weiss [60] used a c-correcting (n, k)-binary linear channel code for compression. Here the channel code uses n-length codewords, inputs of k symbols and syndromes of length $n - k$. The idea is that if you know the base codeword x and the syndrome $S = H(x + e)^T = Hx^T + He^T = He^T$ calculated when an error pattern e is imposed on x, then the error pattern e can be determined. This scheme can then compress an n-length error pattern, of Hamming weight less or equal to c, into an $n - k$ length syndrome by assuming the zero codeword was sent.

The compression approach of Weiss was then extended [61, 62] to a variable-to-fixed length scheme, where 0-symbols are appended to shorter input sequences to extend it to the required codeword n-length. Ancheta [63] implemented a fixed-to-fixed length linear source coder using BCH (Bose Chaudhuri Hocquenghem) codes. These initial linear lossless codes (including [64]) were non-universal, limited to memoryless sources and were not competitive with the traditional compressors of the day. Punctured Turbo codes were employed [65] much later, where knowledge of the source bias was used to improve compression. At about the same time LDPC codes were harnessed [66–68] to achieve universal lossless data compression with linear encoding and decoding complexity. This approach exploited source memory and was shown to have performance that can compete with traditional compression algorithms.

Fountain codes are decoded on the same principles as LDPC codes, but since fountain codes are rateless they are more amenable to universal compression. The issue with an LDPC compressor implementation is that a different code is needed for every different compression ratio, seeing that the code rate is fixed. Fountain codes replaced LDPC codes in [69] for use in compression due to the natural support of variable compression rates. The use of sparse graph block codes is necessary since syndrome forming has quadratic complexity and maximum likelihood has exponential complexity in the block length for general linear codes. Linear fixed-length coding achieves the minimum achievable compression rate asymptotically in the block length, for memoryless and arbitrary sources [70]. Specifically the Shannon-MacMillan theorem [42, 71] states that there are fixed-length n-to-m compression codes of rate $m/n > C + \delta$ with vanishing block error probability as the block length goes to infinity. A standard random coding argument [72] can be used to show that asymptotical optimality for memoryless sources is not lost by making a fixed-length source code linear.

9.2 SOURCE COMPRESSION WITH FOUNTAIN CODES

During the decoding of fountain codes no syndrome is calculated, unlike LDPC codes where a syndrome $S = Hy^T$ is calculated from a received codeword y. With fountain codes the codeword itself is the syndrome as it is defined for LDPC codes. This shows that fountain codes are even more suitable for use in compression, where the syndrome forms the compressed data. A very simple compression implementation would involve the calculation of $m > nH_2(p_s)$ output symbols, for a binary input source s with Bernoulli source constant of p_s. An important

aspect of this implementation is the possibility of decompressing at the compressor, so that lossless compression can be ensured.

When the fountain code output symbols have been generated, and the compressor finds that the compression was not lossless, then information can be added. If the compressor finds that lossless decompression is possible, then it can remove data to improve the compression ratio. Some of these information addition and removal strategies are explained in this section, and the compression algorithms are formulated.

9.2.1 LT-code compressor with decremental redundancy

The basic algorithm setup for source compression with an LT-code is reviewed [69, 73, 74] in this subsection, and a simple random puncturing approach is applied to improve the compression rate. It is also shown how the puncturing scheme can be changed to be low-degree biased for improved compression performance [73]. The code elements and operation blocks required are the robust soliton output degree distribution, the bipartite encoding/decoding graph and the belief propagation message passing algorithm. The compression scheme is functionally illustrated in Figure 9.2.

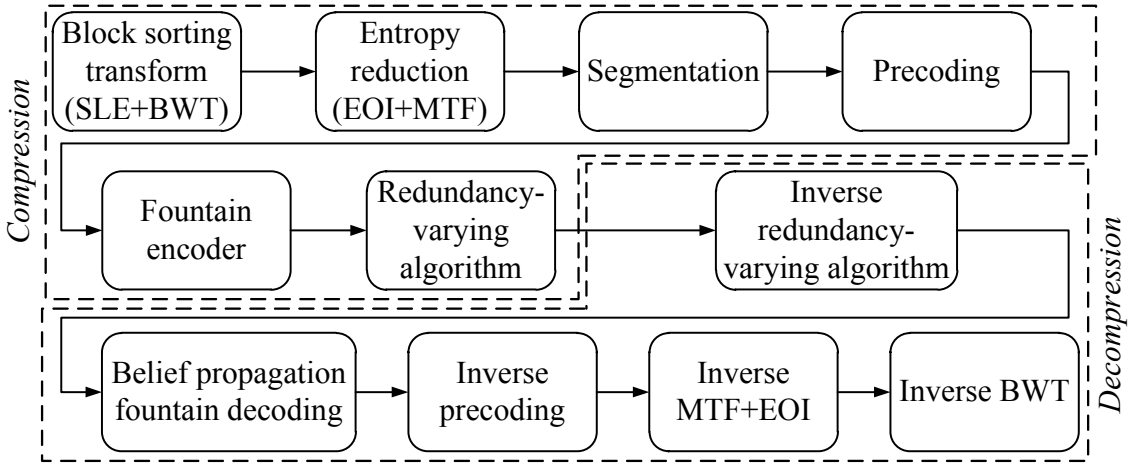

Figure 9.2: Universal compression with fountain codes.

9.2.1.1 Input preprocessing

A binary fountain code can only remove binary redundancy when applied to the task of compression, so it must be ensured that the input source has the lowest binary entropy possible.

Most real world data sources have redundancy in terms of higher level symbols, like eight bits or 24 bits, so these sources will have to be preprocessed to move that memory into its binary form. The Burrows-Wheeler transform (BWT) [75] can accomplish this, as it outputs an asymptotically piecewise i.i.d. (independent and identically distributed) form (for stationary ergodic tree sources) that can be processed by a MTF (move-to-front) transform and an EOI (entropy ordered indices) transformation to render a binary compressible source. The BWT is a one-to-one transform, where all cyclic shifts of the input string are sorted lexicographically. The last column of the resulting matrix forms the BWT output, and the original string can be recovered with the BWT output and the index of the original sequence in the lexicographically sorted matrix.

9.2.1.2 Output encoding

For a decremental redundancy approach enough output symbols need to be generated, so that some can be removed or punctured to improve the compression ratio. A compression rate of $\frac{m}{n} > 1.1$ should ensure that the original input (of length n) can be recovered from the m available output symbols. Each output symbol S_k can be generated by sampling an output degree i randomly from the robust soliton degree distribution, and then summing i randomly chosen input symbols in GF(2), according to Equation (9.1) where $f(\cdot)$ refers to the random index sampling.

$$S_k = \sum_{j=1}^{i} x_{f(j)} \tag{9.1}$$

As each output symbol is added, the associated bipartite graph also gets a new check node. This new check node has connections to the subset of message or input nodes which feature in its sum as given in Equation (9.1). The bipartite graph can then be used as a Tanner graph for belief propagation decoding during decompression.

9.2.1.3 Decremental redundancy

The goal of the compressor is to minimise the compression ratio, and to ensure lossless decoding. The compressor can test for lossless decompression by attempting to decode the original input from the available output symbols and the log-likelihood value of the input. For a binary input source with a Bernoulli constant or 1-bias of p_s, a compression rate of $H_2(p_s)$ can be achieved. For such an input the message node starting log-likelihood ratios $m_v = \log \frac{1-p_s}{p_s}$ will be set to the associated bias log-likelihood. This is a key piece of information which

helps the entropy coder to achieve a good compression ratio. The decompressor will also have available the syndrome or output symbols $\{S_k\}$, where the starting log-likelihood $m_c = \pm\infty$ of each associated check node will be set either to $+\infty$ for $S_k = 0$ or $-\infty$ for $S_k = 1$. The decoder now has all the required values to start belief propagation on the Tanner graph created during output encoding.

By using synchronised pseudo-random number generators at the compressor and decompressor, the same bipartite graph can be generated when the decompressor knows the generator seed and graph length. This method is also used to inform the decompressor of the sequence of symbol locations that are randomly punctured, as in the case of decremental redundancy. When the compressor attempts decompression and finds it was lossless, then it can remove random output symbols to reduce the compression ratio. The compressor will keep testing until it cannot remove any more symbols while the decompression remains lossless. In practice the number of punctured symbols is adjusted with adaptive successive rate refinement [76], which is a binary search algorithm moving between two extreme compression rates $\frac{m}{n} = 0.9$ and $\frac{m}{n} = 2.0$ in order to find the smallest lossless rate.

The simplest decremental redundancy scheme involves random puncturing of output symbols, such that the effective output degree distribution remains the same. As was established in Chapter 8, the code degree distribution largely determines the code performance. This observation led to a modified puncturing scheme called LT-IDP (LT-code with incremental degree puncturing) [73], where the lowest degree unpunctured output symbols are chosen to be punctured. This effectively shifts the output degree distribution into a higher average degree. It was shown that such a puncturing approach can improve compression over the entire binary entropy range, when compared to basic random puncturing.

9.2.2 LT-code compressor with incremental redundancy

The compressor tests whether lossless decompression is possible with a certain number of output symbols, and when it finds that the recovered input has errors it increases the compression ratio. The compressor can either add extra output symbols, according to adaptive successive rate refinement, or it can exploit specific information available during belief propagation decoding of the inadequate compressed data. In an attempt to minimise the

compression ratio, the compressor seeks to include the most information with the fewest number of symbols. During belief propagation specific log-likelihood ratio values are kept for each message or input node, and they are calculated according to Equation (9.2) where p_{sv} is the probability that the symbol has value 1.

$$\log \frac{1 - p_{sv}^{(\ell)}}{p_{sv}^{(\ell)}} = m_v + \sum_{c \in C_v} m_{cv}^{(\ell-1)} \tag{9.2}$$

The message node with the least reliability needs the most information to be recovered losslessly, so with the strategy called CLID (closed-loop iterative doping) [69] the original value associated with the message node that has the smallest log-likelihood ratio $\min_{v \in V} \left| \log \frac{1-p_{sv}^{(\ell)}}{p_{sv}^{(\ell)}} \right|$ is appended to the compressed data. This single symbol then adds the most information possible, and the reliability of the associated message node can then be made infinite for improved belief propagation decoding. These high-information symbols appended to the compressed data makes the scheme more vulnerable to noise, since the possible symmetric flip of the symbol value can degrade the belief propagation decoding.

The compressor can start to generate output symbols in the same fashion as described for decremental redundancy, from a robust soliton or other optimised output degree distribution. The focus with incremental redundancy is to start with a lossy compressed dataset and add information according to CLID. As the compressor runs the decoding algorithm, it may decide to start appending CLID symbols after a certain number of initial iterations. The compressor can decide at what frequency to add symbols, and the belief propagation algorithm is informed as the symbols are added to ensure a duplicate process at the decompressor.

9.2.3 Performance comparison of compression methods

The binary compression performance of the random puncturing, LT-IDP and LT-CLID compressors are reviewed [73] in this subsection, to illustrate the capability of fountain codes to compress data. The performance comparison considers the useful binary entropy range for Bernoulli constants up to 0.3. Input blocks of $n = 10000$ are used throughout, and the robust soliton parameters are $c = 0.05$ and $\delta = 0.4$. The starting compression rate of $\frac{m}{n} = 1.1$ is used for decremental redundancy, and the maximum log-likelihood ratio is set at 25.0. The belief propagation algorithm uses a maximum of 40 iterations and 300 iterations for the decremental and incremental redundancy approaches, respectively. The LT-CLID algorithm starts doping

every iteration after 10 iterations until lossless compression can be ensured. The results are shown in Figure 9.3, where the incremental degree puncturing scheme outperforms both a simple random puncturing scheme and the LT-CLID algorithm.

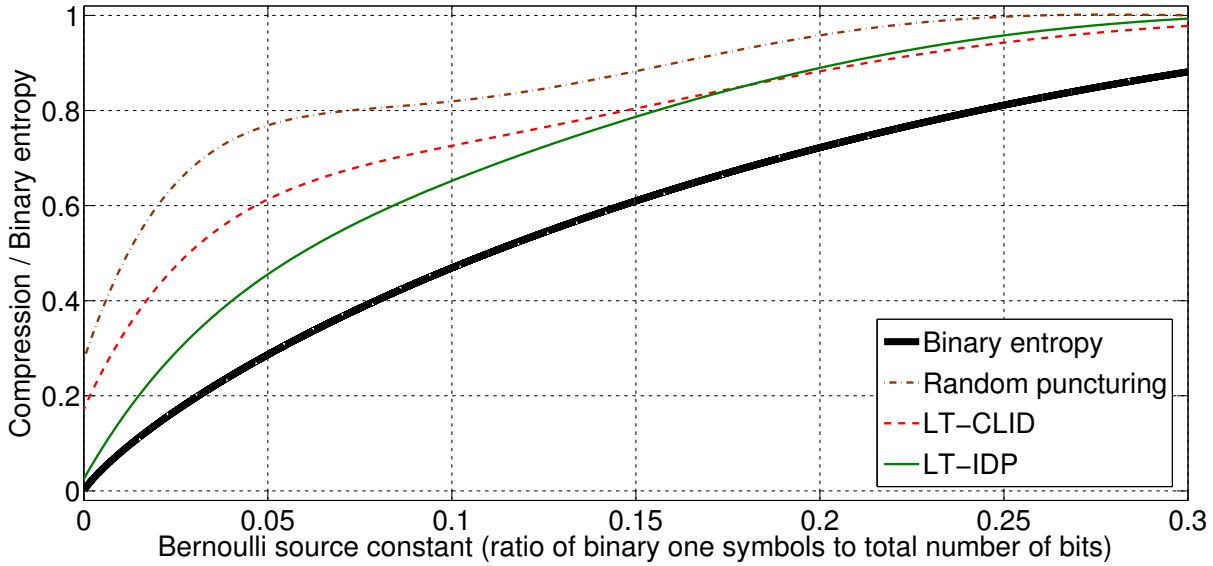

Figure 9.3: Comparative memoryless source compression performance comparison.

9.3 JOINT SOURCE-CHANNEL CODING WITH FOUNTAIN CODES

Compression based on error-correction codes is less susceptible to noise and catastrophic error propagation than traditional compression algorithms. An error-correction code is normally used for channel coding, although it has a dual purpose since it can do source compression as well. Joint source-channel coding integrates a separate source coder or compressor and a channel coder into one coder that encodes and decodes data on one graph to effectively compress a channel input and protect it against errors. The difference between a compressor and a joint source-channel coder will be seen in the errors introduced in compressed data that is mapped to the output or check nodes when the compressed data is transmitted over a noisy channel. The starting log-likelihood ratios m_c associated with every check node will thus be set individually to $\pm \log \frac{1-p}{p}$ for a BSC(p) channel depending on the received symbol estimates. The source bias p_s will be transmitted with the compressed data in its log-likelihood form, and belief propagation will be run as normal with all the information mapped to the graph.

The noise robustness of the fountain joint coders with decremental and incremental redundancy

is shown [73] in this section. An input source with segments over the useful binary entropy range was compressed by both the LT-IDP and LT-CLID compressors, before being transmitted over a BSC and binary AWGN channel, where after the payload was decompressed. The header was not corrupted, as it is not protected against noise. The decompressed output was compared to the original input, and the bit error rate was measured for different channel noise intensities. The results are shown for the BSC and the AWGN channel in Figures 9.4 and 9.5 respectively. It is shown that the CLID approach makes the payload more prone to errors after decompression.

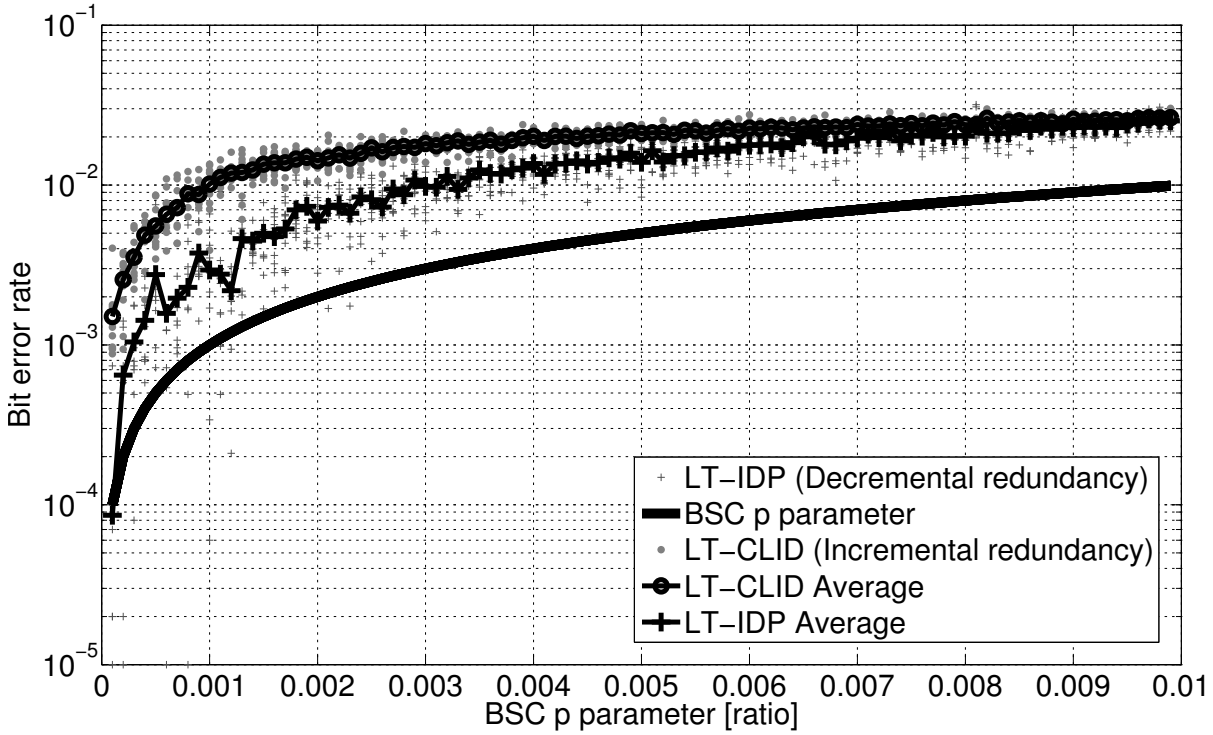

Figure 9.4: A noise robustness comparison on the BSC.

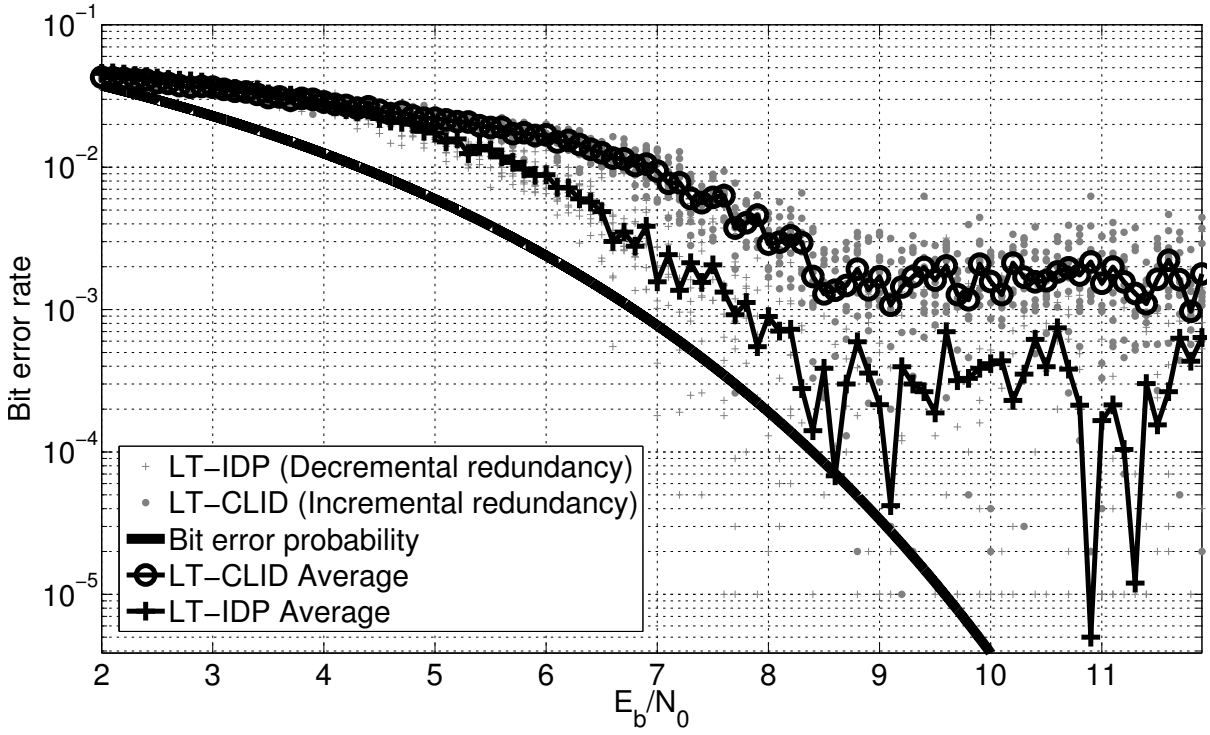

Figure 9.5: Noise robustness comparison on a flat fading BI-AWGN channel.

CHAPTER 10

JOINT SOURCE -CHANNEL -NETWORK CODING

The main 'arteries' of wireless mesh networks are replete with two-way network coding opportunities, where a centrally located relay can combine two packets intended for exchange between two of its neighbouring nodes into one transmission. Additionally no opportunistic listening or buffer content synchronisation is required, and compared to extended n-way network coding throughput gain is maximised with two-way network coding. Deploying this type of network coding can contribute significantly to network throughput without requiring drastic changes in network operation or a large additional overhead. Most joint channel-network coding techniques improve throughput and in [77] the linear property of the channel code is used to reduce the computational complexity during network decoding. A joint channel-network parity-check matrix is constructed in [78] where random network coding is done. In [79] the relay forwards the XORed combination of the parity-check bits of the source messages, and joint channel-network turbo decoding is done at the destination node. A joint channel-network message passing decoding algorithm is given [80] for the destination node.

Motivated to develop a true joint source-channel-network code that compresses, adds robustness against channel noise and network codes two input packets on a single bipartite graph and iteratively decodes the intended packet on the same Tanner graph, an adaptation of the fountain code of [81] is presented in this chapter. The proposed code (JSCNC) is shown through extensive experimental analysis to outperform a separated joint source-channel and network code (SSCNC), which is used in the traditional two-way network coding sense, in high source entropy and high channel noise regions. The system model is firstly introduced, where the

capacity of the joint source-channel-network coding scenario is given. The two-stage fountain code implementation [81] of a joint source-channel code is revisited, where a computationally efficient subroutine is contributed, as well as an analysis of how the intermediate error rate translates to the system error rate. The joint source-channel-network code adaptation is also discussed, and the separate and joint codes are experimentally compared. An outline of the chapter is depicted in Figure 10.1.

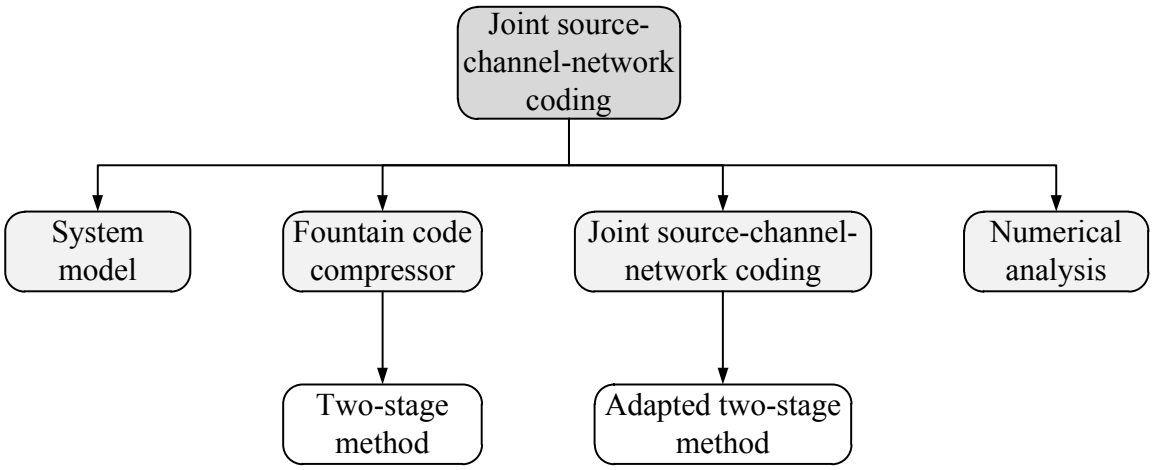

Figure 10.1: The chapter outline showing the topics that are covered.

10.1 SYSTEM MODEL

The bidirectional wireless relays that are considered, broadcast the sum of two packets received from nodes A and B, so that A (respectively B) can discern the packet sent from B (resp. A) by subtracting its own packet from the broadcast sum [8]. As seen in Figure 10.2, by transmitting combined information the relay can exchange information between sources A and B in one timeslot, instead of a separate timeslot for each of the two packets to be forwarded. No direct communication link is assumed between nodes A and B.

The decode-recode-forward strategy employed by the relay must take into account the symbol 1-biased source entropies p_A and p_B of both packets A and B, the transmission channel noise ε and the network coding required to combine both packets into one. For the network operating in GF(2) and the relay-source channel being BSC(ε), the joint source-channel-network coding

capacity C for the system is given in Equation (10.1).

$$C = \frac{1 - H_2(\varepsilon)}{\max\left(H_2(p_A), H_2(p_B)\right)} = \frac{1 - H_2(\varepsilon)}{H_2(p)} \tag{10.1}$$

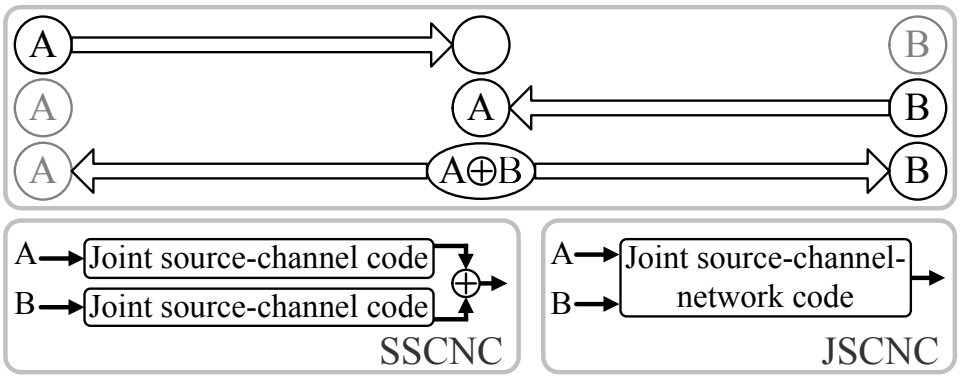

Figure 10.2: Two-way wireless network coding, and separate and joint source-channel and network coding.

The binary entropy function is given by $H_2(\cdot)$ and there is assumed to be no correlation between the information in the two packets, or between the packets and the channel. In fact, the packets and channel are independently generated as Bernoulli processes with the respective parameters. The packet entropies are made equal in this study to simplify the analysis, in other words $p_A = p_B = p$. Coding performance is gauged in terms of the mean of the bit error rates experienced at nodes A and B after they have decoded their intended packets. Both packets A and B consist of K bits, and the relay transmits $N = \upsilon K/C$ coded bits to nodes A and B, where $\upsilon > 1$ is the coding overhead. After decoding packet B (resp. A) at node A (resp. B), the BER (bit error rate) is measured as $\delta_A = K'_B/K$ (resp. $\delta_B = K'_A/K$) where K'_B (resp. K'_A) is the number of errors in the recovered packet when compared to the correct one. The system BER δ is then taken as the mean $\delta = (\delta_A + \delta_B)/2$.

A joint source-channel code, with a XOR-based network code, and a joint source-channel-network code (Figure 10.2) are evaluated in terms of the system BER. The following section expounds on the implementation of the joint codes, which are based on fountain codes.

10.2 FOUNTAIN CODE COMPRESSOR

The two-stage fountain code compressor of [81] displayed in Figure 10.3, which utilises an LT-code [48], is reviewed in this section. Fountain codes can produce an output stream of varying length, which makes it more suitable for employment as a joint source-channel code than LDPC or turbo codes.

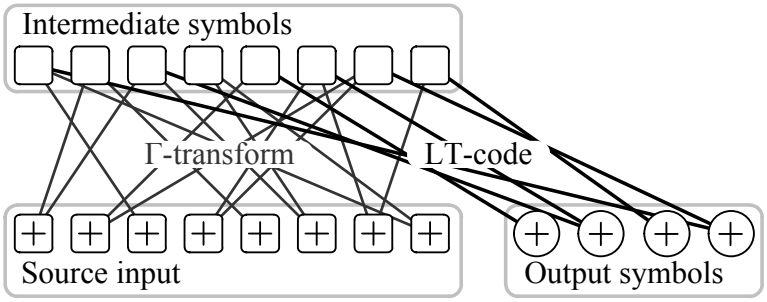

Figure 10.3: Two-stage approach to joint source-channel coding with an LT-code.

In the two-stage compressor, a source input of K symbols $(x_1, \ldots, x_K)$ is mapped to K intermediate symbols $(y_1, \ldots, y_K)^T = \Gamma^{-1}(x_1, \ldots, x_K)^T$ via a linearly invertible $K \times K$ matrix Γ. This ensures that every input symbol participates in the resulting bipartite graph, unlike the direct approach [73] where the probability of an unconnected input symbol is relatively high. For the LT-code output degree distribution $\Omega(x) = \sum_{d=1}^{K} \Omega_d x^d$, the average input degree is $\zeta = \upsilon\Omega'(1)/C$. Then with the input degree distribution $\Psi(x) = (\zeta x/N + 1 - \zeta/N)^N$, the fraction of unrepresented input symbols with the direct approach is strongly dependent on the source entropy and channel noise as shown by:

$$\Psi(0) = \left(1 - \frac{\zeta}{N}\right)^N = \left(1 - \frac{\Omega'(1)}{K}\right)^{\upsilon K/C} \tag{10.2}$$

The Hamming weights of the rows of Γ are sampled according to $\Omega(x)$, so that with the additional N output symbols $(x_{K+1}, \ldots, x_{K+N})$ the final Tanner graph can be interpreted as a $(K, \Omega(x))$ LT-code with input $(y_1, \ldots, y_K)$ and output $(x_1, \ldots, x_{K+N})$. Through Belief Propagation (BP) decoding $(y_1, \ldots, y_K)$ can be recovered, and consequently the original source $(x_1, \ldots, x_K)^T = \Gamma(y_1, \ldots, y_K)^T$ as well. The a-priori entropies for the intermediate symbols are set to 0.5, for the input source symbols it is set to $H_2(p)$ and the reliabilities of the received output symbols are set to be dependent on $H_2(\varepsilon)$.

A computationally efficient method of rendering a singular Γ invertible in GF(2), is to

firstly calculate the row echelon form of $[\Gamma\ I]$. Here the last $K - \text{Rank}(\Gamma)$ rows will point to the constituent rows of Γ that contribute to the corresponding zero sum. Separately, for each zero-sum row in the row echelon form, one of its constituent rows of Γ must be changed so that the zero-sum row now sums to one of the $K - \text{Rank}(\Gamma)$ absent variables in the echelon form. The row echelon form must be re-evaluated until $\text{Rank}(\Gamma) = K$. In this manner the initial matrix is reconditioned to achieve a fully sufficient row echelon form and thus be linearly invertible.

If an error rate of δ_y is experienced in the decoded intermediate symbols $(y_1, \ldots, y_K)$ after BP decoding, then the resulting error rate δ of $(x_1, \ldots, x_K)$ can be approximated as in (10.3). In practice this error rate translation has proven to be a surprisingly accurate upper bound as shown in Figure 10.4.

$$\delta\left(\delta_y, \Omega\right) = \sum_{d=1}^{K} \Omega_d \sum_{j=1}^{\lfloor \frac{d+1}{2} \rfloor} \binom{d}{2j-1} \delta_y^{2j-1} (1-\delta_y)^{d-2j+1} \tag{10.3}$$

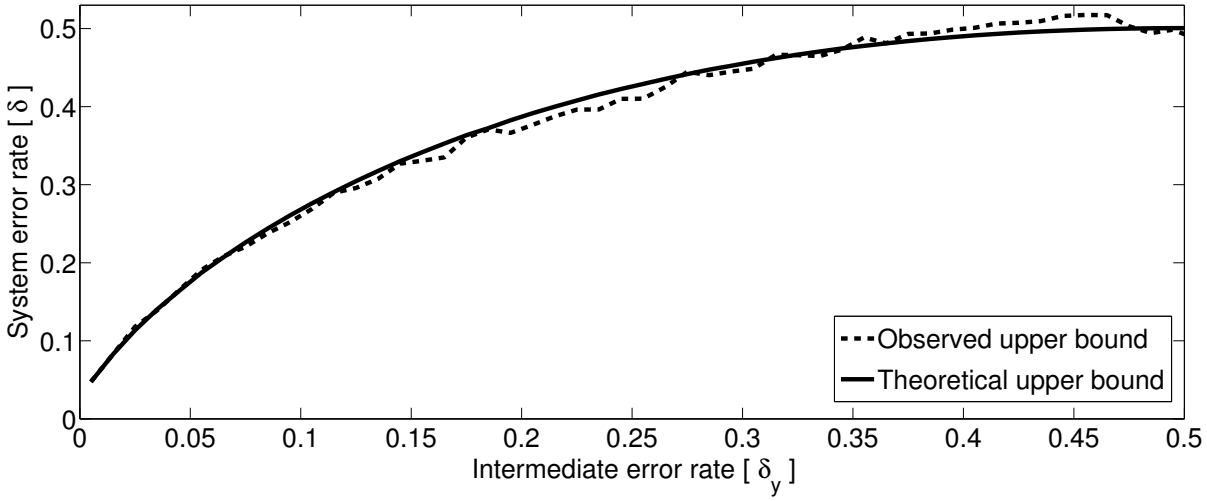

Figure 10.4: System error rate upper bound comparison.

The output symbols $(x_{K+1}, \ldots, x_{K+N})$ are transmitted, in conjunction with the input source entropy $H_2(p)$, and BP decoding is run on the reconstructed graph at the receiver side. When used in the network coding scenario, the two sets of output symbols $(x^A_{K+1}, \ldots, x^A_{K+N})$ and $(x^B_{K+1}, \ldots, x^B_{K+N})$ generated by the joint source-channel coder for packets A and B are summed together to $(x^A_{K+1} + x^B_{K+1}, \ldots, x^A_{K+N} + x^B_{K+N})$. Node A (resp. B) generates the same output symbols $(x^A_{K+1}, \ldots, x^A_{K+N})$ (resp. $(x^B_{K+1}, \ldots, x^B_{K+N})$) with packet A (resp. B) and subtracts it from the received symbols A+B, the resulting packet is then decoded to recover the unknown

packet $(x^B_{K+1}, \ldots, x^B_{K+N})$ (resp. $(x^A_{K+1}, \ldots, x^A_{K+N})$). The implementation of an alternative joint source-channel-network coder follows.

10.3 JOINT SOURCE-CHANNEL-NETWORK CODING

The network coding summation can be integrated into the joint code by inputting the concatenation of packets A and B (Figure 10.5), which requires a new $2K \times 2K$ matrix Γ to map $2K$ input symbols $(x_1, \ldots, x_K, x_{K+1}, \ldots, x_{2K})$ to $2K$ intermediate symbols $(y_1, \ldots, y_{2K})$. The motivation of this approach is to evaluate the potential benefit that is gained by operating on a Tanner graph of twice the size. The trade-off is higher complexity in BP decoding and determining Γ^{-1} (in principle quadratic in K).

With the JSCNC (joint source-channel-network code) the same amount $\upsilon K/C$ of output symbols are generated as with the SSCNC (separate source-channel and network code), but from twice the amount of intermediate symbols. In practice the output symbols are augmented with the values of the intermediate symbols with the lowest reliability according to the performed BP decoding (CLID [81]). The relay will perform this augmentation in a lossless coding scenario with its estimate of the channel noise, and in the case of this enlarged code two checks will be performed. The relay will append CLID symbols until it is reasonably certain that both nodes A and B will be able to recover their respective packets. The number of required CLID symbols can be estimated by δ_y.

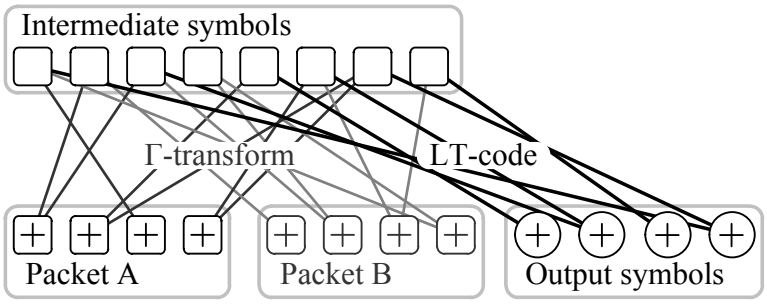

Figure 10.5: Joint source-channel-network coding with a two-stage LT-code.

Node A (resp. B) will map the fully reliable symbols $(x_1, \ldots, x_K)$ (resp. $(x_{K+1}, \ldots, x_{2K})$) of packet A (resp. B) to the Tanner graph for BP decoding, and also the likelihood ratio $\ln((1-p_B)/p_B)$ (resp. $\ln((1-p_A)/p_A)$) of packet B (resp. A) to the appropriate input nodes $(x_{K+1}, \ldots, x_{2K})$ (resp. $(x_1, \ldots, x_K)$) and the received channel output estimate LLRs

(log-likelihood ratios) $\ln(\varepsilon/(1-\varepsilon)) \cdot (z_1^A, \ldots, z_N^A)$ (resp. $\ln(\varepsilon/(1-\varepsilon)) \cdot (z_1^B, \ldots, z_N^B)$) to the output nodes $(x_{2K+1}, \ldots, x_{2K+N})$. Here the relay hard output bits received by node A and B are given by $(z_1^A, \ldots, z_N^A)$ and $(z_1^B, \ldots, z_N^B)$ respectively. The CLID symbols can be used during the BP decoding to ensure lossless decoding with high probability. The experimental results are analysed in the next section.

10.4 NUMERICAL ANALYSIS

The system error rates δ of the separate and joint codes (SSCNC and JSCNC) for all combinations of source entropies p and channel noise ε are compared in this section. Independent Mersenne twisters were used to produce 100 different code, source and channel realisations for every (p, ε) pair coded by both codes, so that high quality error rate estimations could be obtained through averaging. The receivers were assumed to have perfect knowledge of the channel noise level ε.

A good joint source-channel code has to perform well simultaneously on the BEC (binary erasure channel) and BSC channels, so that it can compress and protect data sufficiently. Therefore an LT-code output degree distribution of $\Omega(x) = 0.008x + 0.494x^2 + 0.166x^3 + 0.073x^4 + 0.083x^5 + 0.056x^8 + 0.037x^9 + 0.056x^{19} + 0.025x^{65} + 0.003x^{66}$ is chosen, which was shown to perform satisfactory on the aforementioned channels (see [81]).
The source length was set as $K = 5000$ and a coding overhead of $\upsilon = 1.2$ was chosen throughout for every (p, ε) and both joint codes, which means that the codes are operating at $83.\dot{3}\%$ of system capacity. BP decoding was limited to 100 iterations and a maximum LLR of 25 was adopted. CLID was not performed for any of the joint codes, so that the code performance could be directly determined.

The mean bit error rates of the decoded packets are compared for the two joint codes for different source entropies and channel noises in Figures 10.6 and 10.7. In the high source and channel entropy regions, the joint code (JSCNC) outperforms the separated joint source-channel and network code (SSCNC), at the expense of notably poor performance for $\varepsilon \leq 0.1$ and $p \leq 0.05$. The separated coding performs well under the entire range of (p, ε), but is outperformed in the high entropy and noise regions by the joint code.
The proposed joint source-channel-network code effectively doubles the code block length

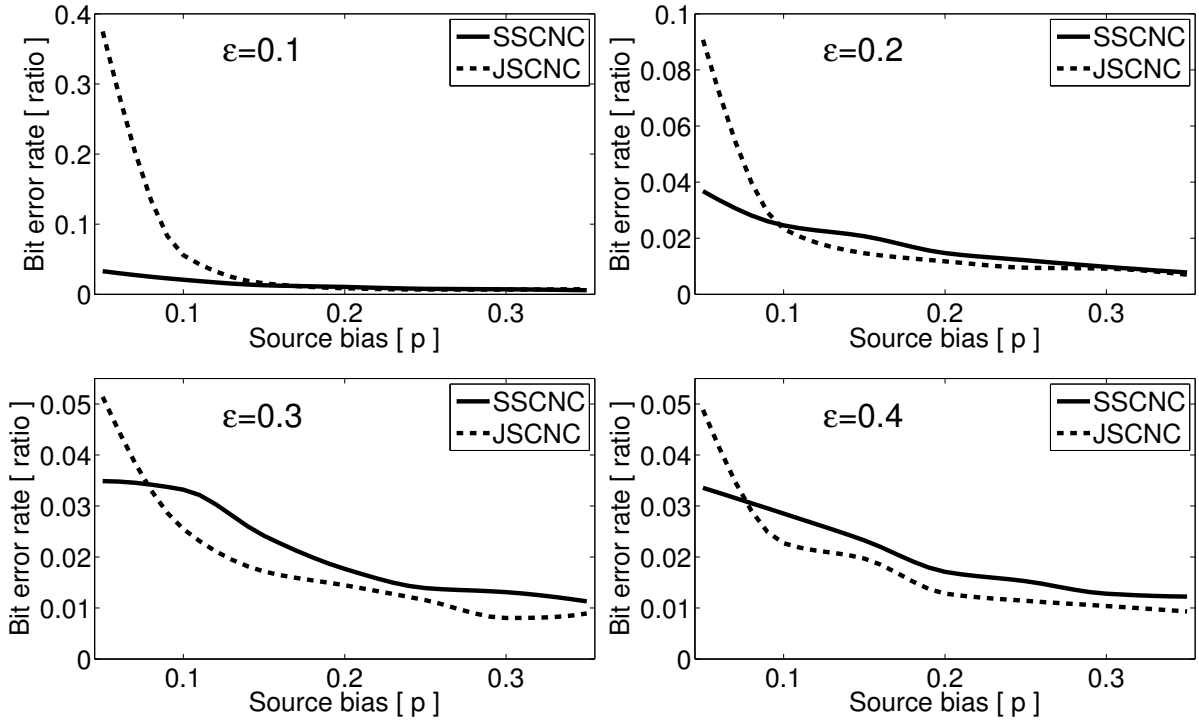

Figure 10.6: System error rates δ vs. source entropy p for different channel noises ε.

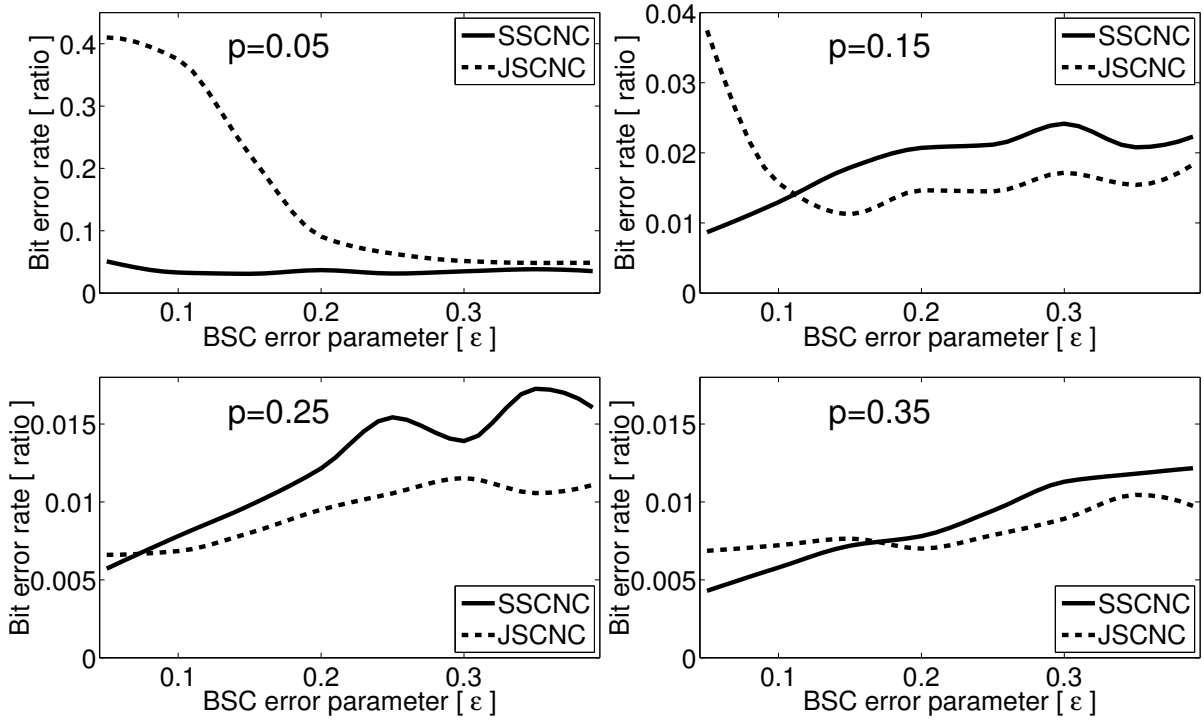

Figure 10.7: System error rates δ vs. channel noise ε for different source entropies p.

which benefits performance for high source entropies and channel noise realisations, when compared to the separated code. The astute reader would have recognised the opportunity to artificially increase the Tanner graph length with predetermined data at both the relay and source nodes, to harness a bigger code for improving performance in the high entropy-noise regions, similar to what is achieved by the joint source-channel-network code presented in this chapter. Furthermore, the joint source-channel code itself can be artificially lengthened for high entropy-noise performance, although at the expense of an increased error rate in the low entropy-noise region.

CHAPTER 11

CONCLUSIONS AND FUTURE RESEARCH

11.1 CONCLUSION

A temporal reuse-aware cross-layer optimisation framework for multihop wireless mesh networks was designed in this dissertation, as well as a truly joint three-way source-channel-network code. The research questions that guided the investigations are reviewed and the contributions and conclusions are discussed for each of the two featured topics.

11.1.1 Cross-layer optimisation of wireless networks with temporal reuse

The first research question that has been addressed in this study is as follows: What generic transmission scheduling algorithm can produce predefined link-assigned schedules that maximise schedule capacity with proportionally fair end-to-end flow rates for quasi-stationary multihop mesh networks with single-path minimum hop routing, rate and power adaptivity, both spatial and temporal reuse and network coding?

The following contributions were made in answering this question:

1. The hybrid node-link assignment strategy of [1] was re-evaluated in terms of a new concept that is defined here, namely temporal reuse, which is recognised as the time-domain analogue of spatial reuse.

2. A specific characterisation of the schedules that could induce packet depletion was given, and it was then shown that optimal schedules can potentially benefit from higher usage

efficiency afforded by temporal reuse.

3. A new achievable rate region was formulated that provides better estimates of the increased link capacities due to temporal reuse. The rate region was derived to be generic, meaning that only information on the network topology and data flows are needed to calculate its capacity without having to simulate the network in question.

4. A cross-layer optimisation scheduling algorithm was given that uses the newly proposed rate region and solves the scheduling subproblem with temporal reuse in mind.

Firstly, it was experimentally shown that by optimising schedules with temporal reuse in the temporal reuse-aware rate region the schedule capacity is increased when compared to optimisation in the non-aware rate region of [32]. In addition, flow rate fairness is also improved with the proposed scheduler and the benefit derived from network coding is also greater. For schedules with rate and power adaptivity it was shown that the proposed scheduler achieves better power efficiency.

The relationship between spatial and temporal reuse was analysed and the temporal reuse-aware scheduler managed a more effective balance for the different rate and power adaptivities. The trade-off between schedule capacity and fairness was affirmed and it was shown that the proposed class of optimised link-assigned schedules outperforms node-assigned schedules in that respect.

11.1.2 Joint source-channel-network coding

The second research question was: Can a truly joint three-way source-channel-network coding algorithm, based on fountain codes outperform a separated joint source-channel and network code (joint source-channel code and separate network code) in a high noise and high entropy coding region?

A number of contributions were made in answering this research question, some of which are as follows:

1. A structural comparison was made between sparse graph LDPC codes and fountain codes, where the relationship between the degree distributions of the codes were made evident.

2. It was shown how density evolution could be used to optimise the degree distributions of fountain codes, for its uses in channel coding, joint source-channel coding and joint source-channel-network coding.

3. An efficient algorithm for rendering singular matrices in GF(2) invertible was explained to facilitate the design of a two-stage joint coding approach with fountain codes.

4. An error-translation analysis was done for the two-stage joint source-channel coding algorithm based on fountain codes.

5. A scheme was explained for a truly joint source-channel-network code based on the two-stage joint source-channel coding approach with fountain codes.

The novel adaptation of the two-stage fountain code compressor [81] for use in a joint source-channel-network code effectively doubles the code block length, and it was experimentally shown that this approach outperforms a separated source-channel and network code in the high noise and high entropy coding regions.

11.2 FUTURE RESEARCH

The possible avenues of extended or additional research in the topics addressed in this study are listed and discussed in this section. The future research that deserves attention is handled separately for cross-layer optimisation of wireless mesh networks with temporal reuse and joint source-channel-network coding.

11.2.1 Cross-layer optimisation of wireless networks with temporal reuse

Possible extensions of the network methods to which the study is limited include multipath routing, cooperative coding and more complex n-way ($n > 2$) network coding.

11.2.1.1 Multipath routing

Changing the routing from single-path minimum hop routing to multipath routing has the potential to reduce congestion in a multihop mesh network, amongst other benefits. Usually the path decisions depend on the current network state and traffic for multipath routing, which complicates the scheduling optimisation. Methods may be studied to reliably calculate network capacity regions for networks with multipath routing and temporal reuse.

11.2.1.2 Cooperative coding

Network coding presents a very basic form of cooperative coding, where neighbouring nodes work together to accomplish a non-standard coding effect. More complicated forms of cooperative coding exist and these may be incorporated into a simulation environment to test the temporal reuse-aware optimised scheduling. Possible amendments can improve the schedule optimisation for networks with cooperative coding.

11.2.1.3 Multi-way network coding

This study focuses on the most efficient case of network coding, namely two-way network coding, in the absence of opportunistic listening. The optimisation framework contributed in this dissertation could be re-evaluated to give improved results in the presence of opportunistic listening and more complex n-way ($n > 2$) network coding.

11.2.2 Joint source-channel-network coding

Some of the areas of improvement for the joint coding investigated in this dissertation include degree distribution optimisation, implementation in wireless mesh networks, low entropy-noise region performance increases and the study of other channel models. Extensions of the joint code for multi-way network coding is also a possible research outlet.

11.2.2.1 Degree distribution optimisation

While the density evolution methods for fountain codes were discussed in this study, they were not used to optimise the output degree distribution for the joint source-channel-network codes. The degree distribution optimisation tools given in this dissertation can be used to optimise the joint source-channel-network codes proposed in this work.

11.2.2.2 Implementation in wireless networks

The various ways in which a joint code can be integrated in wireless mesh network operation could be investigated, in order to synthesize the complete implementation details. This dissertation presented one of many approaches to enable network coding support for a network, but there is scope for further detailed investigation of the actual implementation of joint coding.

11.2.2.3 Low entropy-noise region performance

Future research could investigate modifications to the proposed joint source-channel-network code to improve its low entropy-noise performance to equal that of the separated joint source-channel and network code. This could produce a joint code that is fit for any source-channel environment.

11.2.2.4 Channel models

The joint codes in this study has been designed for binary symmetric noise channels, but the codes could be redesigned for other channel models and the performance can be measured to determine if there are some channels that are more appropriate for these codes.

REFERENCES

[1] J. Grönkvist, "Novel assignment strategies for spatial reuse TDMA in wireless ad hoc networks," *Wireless Networks*, vol. 12, no. 2, pp. 255–265, March 2006.

[2] J. Jubin and J. Tornow, "The DARPA packet radio network protocols," in *Proc. of the IEEE 75 (1)*, January 1987.

[3] M. Matsumoto and T. Nishimura, "Mersenne twister: a 623-dimensionally equidistributed uniform pseudo-random number generator," *ACM Trans. on Modeling and Computer Simulation*, vol. 8, no. 1, pp. 3–30, 1998.

[4] P. Gupta and P. Kumar, "The capacity of wireless networks," *IEEE Trans. Inf. Theory*, vol. 46, pp. 388–404, March 2000.

[5] E. W. Dijkstra, "A note on two problems in connexion with graphs," *Numerische Mathematik*, vol. 1, pp. 269–271, 1959.

[6] R. Bellman, *Dynamic Programming*, isbn 0486428095 ed. Princeton University Press, Princeton, NJ (Republished 2003: Dover), 1957.

[7] R. Ahlswede, N. Cai, S.-Y. Li, and R. Yeung, "Network information flow," *IEEE Trans. Inf. Theory*, vol. 46, no. 4, pp. 1204 –1216, Jul. 2000.

[8] S. Katti, H. Rahul, W. Hu, D. Katabi, M. Medard, and J. Crowcroft, "XORs in the air: Practical wireless network coding," *IEEE/ACM Trans. Netw.*, vol. 16, no. 2, pp. 497–510, 2008.

[9] C. Fragouli, J. L. Boudec, and J. Widmer, "Network coding: An instant primer," *ACM SIGCOMM Comput. Commun. Rev.*, vol. 36, no. 1, pp. 63–68, January 2006.

[10] K. Menger, "Zur allgemeinen Kurventheorie," *Fund. Math.*, vol. 10, pp. 95–115, 1927.

[11] S. Li, R. Yeung, and N. Cai, "Linear network coding," *IEEE Trans. Inf. Theory*, vol. 49, no. 2, pp. 371–381, February 2003.

[12] R. Koetter and M. Medard, "An algebraic approach to network coding," *IEEE/ACM Trans. Netw.*, vol. 11, no. 5, pp. 782–795, October 2003.

[13] T. Ho, M. Medard, R. Koetter, D. Karger, M. Effros, J. Shi, and B. Leong, "A random linear network coding approach to multicast," *IEEE Trans. Inf. Theory*, vol. 52, no. 10, pp. 4413–4430, October 2006.

[14] P. Chou, Y. Wu, and K. Jain, "Practical network coding," in *Proc. 41st Annu. Allerton Conf. Communication, Control and Computing*, October 2003, Monticello, IL.

[15] S. Biswas and R. Morris, "Opportunistic routing in multi-hop wireless networks," in *Proc. ACM SIGCOMM*, August 2005, pp. 133–144.

[16] C. Gkantsidis and P. Rodriguez, "Network coding for large scale content distribution," in *INFOCOM 2005. 24th Annu. Joint Conf. of the IEEE Computer and Communications Societies.*, vol. 4, March 2005, pp. 2235 – 2245 vol. 4.

[17] M. Wang and B. Li, "R2: Random push with random network coding in live peer-to-peer streaming," *IEEE J. Sel. Areas in Commun.*, vol. 25, no. 9, pp. 1655 –1666, December 2007.

[18] S. Zhang, S.-C. Liew, and P. P. Lam, "Physical-layer network coding," in *ACM Mobicom 06*, 2006.

[19] P. Karn, "MACA: A new channel access method for packet radio," in *Proc. of the ARRL/CRRL Amateur Radio 9th Computer Netw. Conf.*, 1990, pp. 134–140.

[20] V. Bharghavan, A. Demers, S. Shenker, and L. Zhang, "MACAW: Media access protocol for wireless LANs," in *Proc. of the ACM SIGCOMM Conf.*, 1994.

[21] J. Garcia-Luna-Aceves and C. L. Fullmer, "Floor acquisition multiple access (FAMA) in single-channel wireless networks," in *Mobile Networks and Applications (Springer)*, 1998, pp. 262–273.

[22] F. Talucci, M. Gerla, and L. Fratta, "MACA-BI (MACA by invitation) - A receiver oriented access protocol for wireless multihop networks," in *Proc. IEEE PIMRC*, 1997.

[23] J. Garcia-Luna-Aceves and A. Tzamaloukas, "Reversing the collision-avoidance handshake in wireless networks," in *Proc. of ACM/IEEE Mobicom*, 1999.

[24] I. Cidon and M. Sidi, "Distributed assignment algorithms for multihop packet radio network," *IEEE Trans. Comput.*, vol. 38, no. 4, pp. 456–460, 1990.

[25] I. Chlamtac and S. Kutten, "A spatial reuse tdma/fdma for mobile multi-hop radio networks," in *IEEE InfoCom '85*, vol. 1, 1985, pp. 389–394.

[26] B. Hajek and G. Sasaki, "Link scheduling in polynomial time," *IEEE Trans. Inf. Theory*, vol. 35, no. 5, pp. 910–917, 1988.

[27] I. Chlamtac and A. Lerner, "A link allocation protocol for mobile multi-hop radio networks," in *IEEE GlobeCom '85*, vol. 1, 1985, pp. 238–242.

[28] L. Pond and V. Li, "A distributed time-slot assignment protocol for multi-hop broadcast packet radio networks," in *IEEE MilCom*, vol. 1, October 1989, pp. 70–74.

[29] K. Papadaki and V. Friderikos, "Approximate dynamic programming for link scheduling in wireless mesh networks," *Computers & Operations Research*, vol. 35, no. 12, December 2007.

[30] J. Grönkvist, "Traffic controlled spatial reuse TDMA in multi-hop radio networks," in *PIMRC*, 1998, pp. 1203–1207.

[31] F. Luus and B. Maharaj, "Cross-layer optimization of wireless networks with extended transmission rights," in *GLOBECOM 2010, 2010 IEEE Global Telecommun. Conf.*, December 2010, pp. 1 –5.

[32] M. Johansson and L. Xiao, "Cross-layer optimization of wireless networks using nonlinear column generation," *IEEE Trans. on Wireless Commun.*, vol. 5, no. 2, Feb. 2006.

[33] S. Toumpis and A. Goldsmith, "Capacity regions for wireless ad hoc wireless networks," *IEEE Trans. on Wireless Commun.*, vol. 2, no. 4, pp. 736–748, 2003.

[34] C. Carathéodory, "Über den variabilitätsbereich der fourierschen konstanten von positiven harmonischen funktionen," *Rend. Circ. Mat. Palermo*, vol. 32, pp. 193–217, 1911.

[35] B. Radunovic and J.-Y. Boudec, "Rate performance objectives of multihop wireless networks," *IEEE Trans. on Mobile Computing*, vol. 3, no. 4, pp. 334–349, Oct.-Dec. 2004.

[36] ——, "Joint scheduling, power control and routing in symmetric one-dimensional, multi-hop wireless networks," in *WiOpt'03*, Sophia Antipolis, France, 2003, pp. 31–42.

[37] F. Kelly, A. Malulloo, and D. Tan, "Rate control in communications networks: shadow prices, proportional fairness and stability," *J. Operational Research Society*, vol. 49, pp. 237–252, 1998.

[38] P. Värbrand, P. Björklund, and D. Yuan, "Resource optimization of spatial TDMA in ad hoc radio networks: A column generation approach," in *IEEE InfoCom 2003*, San Francisco, March 2003.

[39] P. Soldati, B. Johansson, and M. Johansson, "Proportionally fair allocation of end-to-end bandwidth in STDMA wireless networks," in *ACM MobiHoc '06*, Florence, Italy, May 2006.

[40] S. Low and D. Lapsley, "Optimization flow control - I:Basic algorithm and convergence," *IEEE/ACM Trans. Netw.*, vol. 7, no. 6, pp. 861–874, December 1999.

[41] A. Wächter and L. Biegler, "On the implementation of a primal-dual interior point filter line search algorithm for large-scale nonlinear programming," *Mathematical Programming*, vol. 106, no. 1, pp. 25–57, 2006.

[42] C. Shannon, "A mathematical theory of communication," *Bell Systems Technical Journal*, vol. 27, pp. 623–656, 1948.

[43] P. Elias, "Coding for two noisy channels," in *Inform. Theory, Third London Symposium*, 1955, pp. 61–76.

[44] E. Berlekamp, R. McEliece, and H. van Tilborg, "On the inherent intractability of certain coding problems," *IEEE Trans. Inf. Theory*, vol. 24, pp. 384–386, 1978.

[45] P. Elias, "Coding for noisy channels," in *IRE Conv. Record*, 1955, pp. 37–47.

[46] M. J. E. Golay, "Notes on digital coding," in *Proc. IEEE*, vol. 36, 1949, p. 657.

[47] R. G. Gallager, "Low density parity-check codes," Ph.D. dissertation, MIT Press, Cambridge, MA, 1963.

[48] M. Luby, "LT-codes," in *Proc. 43rd Annu. IEEE Symp. Foundations of Comp. Science*, Nov. 2002, pp. 271–280.

[49] D. MacKay, *Information Theory, Inference, and Learning Algorithms*. Cambridge University Press, 2003.

[50] M. G. Luby, M. Mitzenmacher, M. A. Shokrollahi, and D. A. Spielman, "Efficient erasure correcting codes," *IEEE Trans. Inf. Theory*, vol. 47, pp. 569–584, February 2001.

[51] J. Pearl, *Probabilistic Reasoning in Intelligent Systems: Networks of Plausible Inference*. Morgan Kaufmann Publishers, Inc., 1988.

[52] M. Luby, M. Mitzenmacher, A. Shokrollahi, and D. Spielman, "Analysis of low density codes and improved designs using irregular graphs," *IEEE Trans. Inf. Theory*, vol. 47, pp. 585–598, 2001.

[53] T. Richardson and R. Urbanke, "The capacity of low-density parity-check codes under message-passing decoding," *IEEE Trans. Inf. Theory*, vol. 47, no. 2, pp. 599–618, Feb 2001.

[54] T. Richardson, A. Shokrollahi, and R. Urbanke, "Design of capacity-approaching irregular low- density parity-check codes," *IEEE Trans. Inf. Theory*, vol. 47, pp. 619–637, 2001.

[55] T. Richardson and R. Urbanke, *Modern Coding Theory*. Cambridge University Press, 2008.

[56] O. Etesami and A. Shokrollahi, "Raptor codes on binary memoryless symmetric channels," *IEEE Trans. Inf. Theory*, vol. 52, no. 5, pp. 2033–2051, May 2006.

[57] O. Etesami, M. Molkaraie, and A. Shokrollahi, "Raptor codes on symmetric channels," in *IEEE Int. Symp. Inform. Theory*, June 2004, p. 38.

[58] R. Palanki and J. Yedidia, "Rateless codes on noiseless channels," in *IEEE Int. Symp. on Inform. Theory*, June 2004, p. 37.

[59] P. Mitran and J. Bajcsy, "Turbo source coding: A noise-robust approach to data compression," in *Proc. DCC'02*, April 2002, pp. 465–465.

[60] E. Weiss, "Compression and coding," *IRE Trans. on Inform. Theory*, pp. 256–257, April 1962.

[61] P. E. Allard and A. W. Bridgewater, "A source encoding technique using algebraic codes," in *1972 Canadian Computer Conf.*, June 1972, pp. 201–213.

[62] K. C. Fung, S. Tavares, and J. M. Stein, "A comparison of data compression schemes using block codes," in *IEEE Int. Electrical and Electronics Conf.*, October 1973, pp. 60–61.

[63] T. Ancheta, "Syndrome source coding and its universal generalization," *IEEE Trans. Inf. Theory*, vol. 22, no. 4, pp. 432–436, July 1976.

[64] H. Ohnsorge, "Data compression system for the transmission of digitalized signals," in *IEEE Int. Conf. on Commun.*, vol. 2, June 1973, pp. 485–488.

[65] J. Garcia-Frias and Y. Zhao, "Compression of binary memoryless sources using punctured turbo codes," *IEEE Commun. Lett.*, vol. 6, pp. 394–396, September 2002.

[66] G. Caire, S. Shamai, and S. Verdú, "A new data compression algorithm for sources with memory based on error correcting codes," in *2003 IEEE Workshop on Inform. Theory*, April 2003, pp. 291–295.

[67] ——, "Lossless data compression with error correction codes," in *2003 IEEE Int. Symp. on Inform. Theory*, July 2003, p. 22.

[68] G. Caire, S. Shamai, and Verdú, "Universal data compression with LDPC codes," in *Proc. of Third Int. Symp. On Turbo Codes and Related Topics*, Sept. 2003, pp. 55–58, Brest, France.

[69] G. Caire, S. Shamai, A. Shokrollahi, and S.Verdú, "Fountain codes for lossless data compression," *DIMACS Series in Discrete Mathematics and Theoretical Computer Science*, 2005.

[70] G. Caire, S. Shamai, and S. Verdú, "Noiseless data compression with low density parity check codes," *DIMACS Series in Discrete Mathematics and Theoretical Computer Science*, vol. 66, pp. 263–284, 2004.

[71] B. McMillan, "The basic theorems of information theory," *Ann. Math. Statist.*, vol. 24, pp. 196–219, June 1953.

[72] I. Csiszar and J. Korner, *Information theory: Coding theorems for discrete memoryless systems*. New York: Academic, 1981.

[73] B. Maharaj and F. Luus, "Decremental redundancy compression with fountain codes," in *Netw. and Commun., 2008. WIMOB '08. IEEE Int. Conf. on Wireless and Mobile Computing,*, 2008, pp. 328–332.

[74] F. Luus, A. McDonald, and B. Maharaj, "Universal decremental redundancy compression with fountain codes," *SAIEE Africa Research Journal*, vol. 101, no. 2, pp. 68–77, June 2010.

[75] M. Burrows and D. J. Wheeler, "A block-sorting lossless data compression algorithm," in *Tech. Rep. SRC 124*, May 1994.

[76] N. Dütsch, "Code optimisation for lossless compression of binary memoryless sources based on fec codes," *Euro. Trans. Telecomms*, vol. 17, pp. 219–229, 2006.

[77] S. Zhang, Y. Zhu, S.-C. Liew, and K. Letaief, "Joint design of network coding and channel decoding for wireless networks," in *Proc. of IEEE WCNC 2007*, March 2007, pp. 779–784, Hong Kong.

[78] D. Bing and Z. Jun, "Design and optimisation of joint network-channel LDPC code for wireless cooperative communications," in *Proc. 11th IEEE Singapore Int. Conf. on Commun. Systems (ICCS 2008)*, 2008, pp. 1625–1629.

[79] S. Tang, J. Cheng, C. Sun, R. Suzuki, and S. Obana, "Turbo network coding for efficient and reliable relay," in *Proc. ICCS 2008*, 2008, pp. 1603–1608.

[80] X. Xu, M. Flanagan, and N. Goertz, "A shared-relay cooperative diversity scheme based on joint channel and network coding in the multiple access channel," in *Proc. 5th Int. Symp. on Turbo Codes and Related Topics*, 2008, pp. 243–248.

[81] G. Caire, S. Shamai, A. Shokrollahi, and S. Verdú, "Universal variable-length data compression of binary sources using fountain codes," in *Proc. of IEEE Inform. Theory Workshop*, 2004, pp. 123–128.